UNIVERSITY OF OKLAHOMA

GRADUATE COLLEGE

SOLGEL SILICATES: THICKNESS CONTROL AND INTERACTIONS WITH

CUCURBIT[7]URIL/DYE COMPLEXES

A DISSERTATION

SUBMITTED TO THE GRADUATE FACULTY

in partial fulfillment of the requirements for the

Degree of

DOCTOR OF PHILOSOPHY

By

TAMI ANNETTE MARTYN
Norman, Oklahoma
2009

SOLGEL SILICATES: THICKNESS CONTROL AND INTERACTIONS WITH
CUCURBIT[7]URIL/DYE COMPLEXES

A DISSERTATION APPROVED FOR THE
DEPARTMENT OF CHEMISTRY AND BIOCHEMISTRY

BY

<div style="text-align: right;">

_____
Dr. Wai Tak Yip, Chair

_____
Dr. Roger E. Frech

_____
Dr. Ralph A. Wheeler

_____
Dr. Ann West

_____
Dr. Lloyd A. Bumm

</div>

To those who supported me through the years, though they did not know what I

would do with the guidance they gave;

To those whose varying levels of formally and informally gained scientific expertise

have encouraged me to understand both the limitations of the information available

and to seek the possibilities of information not yet gained;

To the community and friends that have shared passions and cared for my children;

To the family that has loved and supported me throughout the years;

I thank you.

ACKNOWLEDGEMENTS

TABLE OF CONTENTS

VII. Comparison of R6G and R6G/CB7 Complex Photostability in Solution Phase, Alcogel Monolith and Hydrogel Monolith at Bulk Concentrations

LIST OF TABLES

LIST OF FIGURES

ABSTRACT

This work reports the progress made in investigating the versatility of solgel silicate thickness control and hosting capabilities for use in sensor and optical material technologies. Thickness control of the solgel silicate was obtained by absorbing the silicate into a biocompatible polyelectrolyte multilayer thin film scaffold. The composite structure is capable of maintaining its porosity, which allows external stimuli to access the interior of the film. In hopes of improving upon dye survival lifetime and brightness, complexation of cucurbit[7]urils (CB7) with the cationic dye molecules, rhodamine 6G (R6G) and pyronin Y (PyY), was investigated. Favorable results found with the R6G/CB7 and PyY/CB7 complexes led to the introduction of the complexes to the optical material.

Since CB7 complexation enhances the emission intensity and photostability of R6G in solution, CB7-complexed R6G was analyzed using single molecule fluorescence spectroscopy in an effort to better understand how CB7 interacts with R6G, and the related molecule Pyronin Y, to enhance emission intensity and photostability. Electrostatic attraction between CB7 and cationic dye molecules, R6G and PyY, give the complexes high association constants in solution. The barrel shape of CB7 has an electronegative ring of oxygens at the cavity portal, which attract the positive charge of the dye molecules. However, R6G, a well-known and commonly used laser dye, is too large to be fully included into the CB7 cavity. Single-molecule measurements showed a wide distribution of emission intensities from individual R6G/CB7 complexes. The concurrent changes in polarization and

intensity indicate the R6G molecule is moving in relation to the CB7 cavity, causing a reduction in emission intensity as R6G leaves the CB7 cavity. Furthermore, the changing emission intensity of individual R6G/CB7 complexes demonstrates the broad intensity distribution is not merely a collection of different static intensities, but includes complexes with dynamic motion which leads to different emission intensities for each complex.

The incorporation of CB7-complexed R6G into a solgel silicate matrix was intended to combine the photostability enhancement that solgel silicates can provide with the intensity enhancement dye to complexation with CB7. However, R6G/CB7 and PyY/CB7 complexes had substantially different emission properties with the immobilization matrices used than they possessed when spincoated without a matrix. R6G/CB7 in an alcogel thin film emitted similarly to R6G alone in the alcogel thin film, both in emission intensity and survival lifetime. PyY/CB7 on a PAH monolayer emitted midway between the PyY on PAH and PyY/CB7 without a matrix. Both dye molecules had the highest emission intensity and survival lifetime when complexed by CB7 and without a matrix. Complexation by CB7 seems to be interrupted by the matrices, possibly due to a competition for complexation of the dye molecules. Both the solgel silicate and PAH monolayer possess some negatively charged portions, which may be the cause of the reduced complexation effects with the matrices present.

The research described in this thesis demonstrated a novel method of thickness control for solgel silicates. Additionally, investigations into the relationship between

CB7 and two xanthene dye molecules revealed the interactions between CB7 and

R6G and PyY are not static. Incorporating dynamic complexes based on

electrostatic attraction into solgel silicates changes the emission properties of the dye

molecules as the silicate surface and CB7 portals have similar attractions for the dye

molecules.

Chapter I

Introduction

The solgel process is a simple procedure that has shown its worth in many areas of sensor and material development. Producing materials in a variety of thicknesses that can be optically transparent and hold a wide variety of guest molecules, solgel materials are adaptable for many purposes. The solgel process involves two chemical reactions that occur as a one-pot synthesis to produce porous glass. The first step is hydrolysis of a metal alkoxide to the alcohol, Reaction 1.

$$(RO)_3 \text{ M-OR} \rightarrow (RO)_3 \text{ M-OH} \qquad \text{(Reaction 1)}$$

The second process is condensation of the metal alcohols (Reaction 2) which proceeds three-dimensionally to yield a porous network.

$$(RO)_3 \text{ M-OH} + (RO)_3 \text{ M-OH} \rightarrow (RO)_3 \text{ M-O-M (OR)}_3 + H_2O \text{ (Reaction 2)}$$
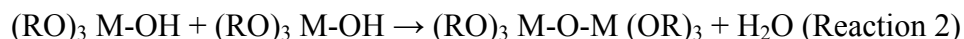
In developing the silicate network, the difference of using an acid-catalyzed sol precursor solution or a reaction catalyzed by a basic environment yields an extended network, or discrete nanoparticles, respectively. Besides the adaptability of the shape, the characteristics of the silica solgel that directly affect interactions with guest molecules are also adaptable. Both the pore size[1-3] and charge on the pores[4, 5] can be adjusted during the preparation of the solgel by adjusting the ratio of reactants.[6] This allows silica solgel materials to adopt a range of microstructures and to interact with the guest molecules by physically constraining motion with strong electrostatic interactions[7] or through hydrophobic interactions.[8]

A variety of metals have been used as part of the solgel process, including silicon, titanium, zirconium,[9, 10] antimony and tin[11] leading to the development of antireflective coatings,[12] catalyst substrates, screening technology, protective coatings for living cells,[13] chromatography columns,[14] and heat-insulating materials.[15] These projects have sought to improve many features of the solgel and its interactions with host molecules, including cracking,[16, 17] controlling microstructure,[18] organically modifying the pore surfaces,[19, 20] and improving biocompatibility by reducing the amount of alcohol produced during solgel formation (Reaction 1).[21-23] This thesis will focus on the use of silica for solgel material development.

The availability and ease of use of silicon has led to a great number of developments with silicon as the metal of choice in solgel glasses. Development of silica solgel materials for applications has included optical sensors for copper ions in solution by silicate thin films,[24] magnetic drug targeting by Fe/SiO_2 particles that deliver the drug.[25] Over the past decade, dye-doped silica solgel sensors have been developed to yield oxygen sensors,[26, 27] acid indicators,[28] liquid and solid-state dye lasers.[29] Through the development of these materials several features of the sensors have been addressed including dye leaching, photostability,[26, 29] drying conditions,[30] resistance to delamination[31] and diffusion of both guest molecules[32, 33] and analytes into the matrix.[34] The photostability and brightness of the dye molecules, as well as thickness control of the solgel matrix to improve response time to external stimuli, are the focuses of this thesis.

2

Recent developments incorporating silica solgel materials with polymers have focused mostly on forming hybrid materials, where the polymer and sol precursor solution are mixed together before gelation occurs.[35, 36] However, performing the two solgel reactions within a polymer film has also been used to form a hybrid film where the polymer and solgel were bonded during condensation of the silicate.[37] In this case, swelling of the polymer was noticeable and harsh conditions were necessary to impregnate the polymer with the solgel components. Silica solgel has also been used as an intermediate layer between a hydrogel and polymer coating to produce ceramic spheres with a polymer coating as a possible biocatalytic membrane.[38] With nanoparticles, solgel silicates have been used to coat silver nanoparticles,[39] or provide nanoparticles to be coated by polymers.[40] In clay/solgel hybrid materials, solgel can attach to the clay and the combined material presents properties of both materials.[41] Our approach more closely resembles the intercalation of solgel silicates into clay, though these preparations also introduce the solgel reactants to the clay before solgel formation.[42]

THICKNESS CONTROL OF SILICA SOLGEL

In order to control the thickness of the solgel silicate, we have employed polyelectrolyte multilayer (PEM) thin films as a scaffold system. Absorbing the solgel into PEM films using capillary action is a new way to combine polymer films with silica solgel, which has the opportunity to realize the advantages of both materials.

Thin films require fewer guest molecules to achieve a specific concentration. Thin films also allow faster response by the guest molecules to diffusing external solutions. The common ways to control thickness for solgel silicates are by spincoating[17, 43, 44] and dipcoating,[16, 45] both of which have limited applications to biomolecules as the coating methods do not provide a solid structure to maintain the water content of silica hydrogels most commonly used with biological guest molecules. Alcogels have a greater proportion of silicate content in the solgel network as compared to hydrogels, so alcogels are better able to maintain their structure without external support.

Dipcoating silica solgels involves putting a substrate into the sol precursor solution and drawing the substrate out of the solution with controlled force and speed, allowing the solgel silicate to adhere to the substrate.[45] Spincoating solgel silicates is accomplished by pipetting the solgel precursor solution onto a coverglass and spinning the solgel to the required thickness by controlling the speed, usually between 3000 rpm and 6000 rpm.[43, 46] Spincoating can also denature proteins, rendering them unable to maintain their bioactivity. Limitations of dipcoating and spincoating are inherent in the forces required to achieve thickness control. The force applied to the silicate when it is spincoated would be too great for a protein to maintain its structure and functionality. Dipcoating includes a spatial resolution of the changes in silicate formation, with drying occurring by solvent evaporation and gravitational draining. Both dipcoating and spincoating rely on solvent evaporation

as the silicate gels to a solid structure. This drying is the source of the problem for solgel silicates as a host for biological molecules.

However, neither dipcoating nor spincoating has been used for hydrogels, solgel silicates with a high buffer content that reduces the alcohol concentration produced during reactions forming the silicate network, thus making the hydrogels much more biocompatible. Current hydrogels are formed as monoliths to fit the containers available and have been successful in retaining the bioactivity of enzymes.[47-50] Using polyelectrolyte thin films as a scaffold provides a structural framework with adjustable thickness on the nanometer scale through a layer-by-layer deposition. PEMs are a porous material that have already been developed into biocompatible materials.[51-55] In a thin film, fewer guest molecules are used, which conserves materials. However, to have the same output from fewer dye molecules requires the guest molecules to emit at high levels without the assistance of a high number of molecules.

HIGH-OUTPUT FLUORESCENT MOLECULES

Another focus of this thesis is development of long-lived, highly fluorescing molecules necessary for optical materials, especially for the field of solid-state lasers and organic light emitting devices (OLEDs).[56] The lifetime of solid-state lasers is determined by how long the emitting dye can be used. The new option we are exploring is incorporation of CB7 to protect the dye molecules. CB7 can form non-covalent complexes with cationic organic molecules,[57, 58] as has been studied in

solutions. When dye molecules are complexed by CB7, the photophysical properties of the dye molecules are altered.[59-61] The interactions of CB7 with the complexed dye molecule have not been fully characterized. Part of the work presented in this thesis will be a more complete understanding of the ability of CB7 to complex cationic xanthene dye molecules, rhodamine 6G (R6G) and pyronin Y (PyY). The changing interactions between R6G and CB7 have been noted on a single-molecule level through enhancement of emission intensity and survival lifetime upon complexation. These interactions are strongly affected by the local environment and geometry of the complex as noted by reduction of the complexation enhancement. This expands on the understanding gained through ensemble measurements that CB7 complexation affects photobleaching kinetics to different extents in different container materials (quartz vs. polystyrene cuvettes).[60, 62] From studies of organic dye molecules, complexation by CB7 showed [57, 60, 61] increase in fluorescence intensity, shift in dye emission wavelength, either hypsochromic or bathochromic shifts, and high association constants with cationic dye molecules. Since association constants are descriptive of dynamic equilibria, an attempt to gain insight into the dynamic relationship between CB7 and complexed dye molecules is presented.
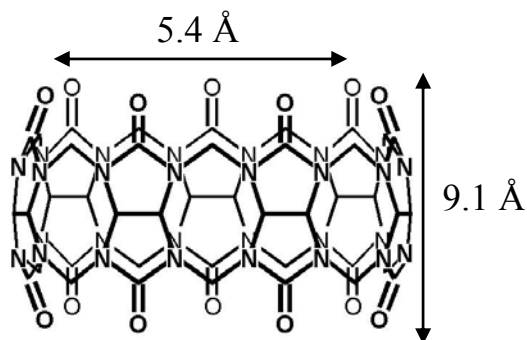
Features of the R6G/CB7 complex that encourage movement include the non-covalent complexation and the relative sizes of the CB7 cavity and R6G. The

cavity of CB7 is 5.4 Å wide at the portal openings and 9.1 Å deep.[63] The xanthene

moiety of R6G and PyY is ~12 Å long. R6G also has a side group that likely

expands its girth to ~10 Å wide from the ~ 3.5 Å wide xanthene of PyY. The

mismatch in sizes reduces the K_a of CB7-complexation and increases the number of

conformations available to the complexes.[64] Understanding how CB7-complexation

is affected by its environment and how the complexed molecules interact will further

the incorporation of CB7 into new materials development. CB7-complexation will

be used to help maintain the fluorescence of dye molecules in a limited space[65] and

therefore improve the incorporation of CB7-complexed dyes into other materials.

In summary, the two features being improved with the work presented in this

thesis are: (1) the ability to have controlled thickness silicates by impregnating PEM

thin films and (2) a brighter, longer lasting dye molecule using CB7-complexation.

This thesis reports an effective way of forming solgel thin films to a desired

thickness by soaking an alcogel precursor solution into a preformed polyelectrolyte

film. Utilizing the PEM film as a scaffold may lead to development of other

composite materials, such as a PEM/hydrogel system. The dynamic nature of CB7-

complexation within thin film and monolith solgel environments shows how

important environment may be to incorporating non-covalent complexes into new

materials. A new method of solgel thickness control and incorporation of CB7 into

solgel materials both aim to expand on the current applications available to silica

solgel in the areas of sensor technology and new optical materials.

REFERENCES

1.   Kanamori, K.; Nakanishi, K.; Hirao, K.; Jinnai, H., Three-dimensional observation of phase-separated siloxane sol–gel structures in confined spaces using laser scanning confocal microscopy (LSCM). *Colloids Surf., A* **2004,** 241, (1-3), 215-224.

2.   Kanamori, K.; Yonezawa, H.; Nakanishi, K.; Hirao, K.; Jinnai, H., Structural formation of hybrid siloxane-based polymer monolith in confined spaces. *J. Sep. Sci.* **2004,** 27, (10-11), 874-886.

3.   Shrinivasan, S.; Breadmore, M. C.; Hosticka, B.; Landers, J. P.; Norris, P. M., Toward optimization of macroporous silica gels for application to capillary or microchip-based CEC and LC *J. Non-Cryst. Solids* **2004,** 350, 391-396.

4.   Aylward, W. M.; Pickup, P. G., Ion-exchange and ion-transport in silica and sulphonated-silica (ormosil) hydrogels. *Electrochim. Acta* **2008,** 53, (11), 3897-3902.

5.   Higgins, D. A.; Collinson, M. M.; Saroja, G.; Bardo, A. M., Single-Molecule Spectroscopic Studies of Nanoscale Heterogeneity in Organically Modified Silicate Thin Films. *Chem. Mater.* **2002,** 14, (9), 3734-3744.

6.   Kumar, R.; Roy, I.; Ohulchanskyy, T. Y.; Goswami, L. N.; Bonoiu, A. C.; Bergey, E. J.; Tramposch, K. M.; Maitra, A.; Prasad, P. N., Covalently Dye-Linked, Surface-Controlled, and Bioconjugated Organically Modified Silica Nanoparticles as Targeted Probes for Optical Imaging. *ACS Nano* **2008,** 2, (3), 449-456.

7.   Gilliland, J. W.; Yokoyama, K.; Yip, W. T., Effect of Coulombic Interactions on Rotational Mobility of Guests in Sol-Gel Silicate Thin Films. *Chem. Mater.* **2004,** 16, (20), 3949-3954.

8.   Zhou, Y.; Yip, W. T., Balance between Coulombic Interactions and Physical Confinement in Silica Hydrogel Encapsulation. *J. Phys. Chem. B* **2009,** 113, (17), 5720-5727.

9.   Seshadri, K. S.; Selvaraj, M.; Kesavamoorthy, R.; Srinivasan, M. P.; Varatharajan, K.; Lal, K. B.; Krishnasamy, V., Estimation and comparison of pore charge on titania and zirconia membranes prepared by sol-gel route using zeta potential measurement. *J. Sol.-Gel Sci. Technol.* **2003,** 28, (3), 327-333.

10.   Sakka, S.; Kozuka, H., Sol-Gel Preparation of Coating Films Containing Noble Metal Colloids. *J. Sol.-Gel Sci. Technol.* **1998,** 13, (1-3), 701-705.

11.   Sadeh, A.; Sladkevich, S.; Gelman, F.; Prikhodchenko, P.; Baumberg, I.; Berezin, O.; Lev, O., Sol-Gel-Derived Composite Antimony-Doped, Tin Oxide-Coated Clay-Silicate Semitransparent and Conductive Electrodes. *Anal. Chem.* **2007,** 79, (14), 5188-5198.

12.   Schulz, U., Review of modern techniques to generate antireflective properties on thermoplastic polymers. *Appl. Opt.* **2006,** 45, (7), 1608-1618.

13.   Ciriminna, R.; Pagliaro, M., Recent Uses of Sol-Gel Doped Catalysts in the Fine Chemicals and Pharmaceutical Industry. *Org. Process Res. Dev.* **2006,** 10, (2), 320-326.

14.   Kato, M.; Sakai-Kato, K.; Toyo'oka, T., Silica sol-gel monolithic materials and their use in a variety of applications. *J. Sep. Sci.* **2005,** 28, (15), 1893-1908.

15.   Sakka, S., Current sol-gel activities in Japan. *J. Sol.-Gel Sci. Technol.* **2006,** 37, 135-140.

16.   Kozuka, H.; Hirano, M., Single-Step Dip Coating of Crack-Free BaTiO$_3$ Films >1 mm Thick: Effect of Poly(vinylpyrrolidone) on Critical Thickness *J. Am. Ceram. Soc.* **2000,** 83, (5), 1056-1062.

17.   Kozuka, H.; Hirano, M., Radiative Striations and Surface Roughness of Alkoxide-Derived Spin Coating Films. *J. Sol.-Gel Sci. Technol.* **2000,** 19, (1-3), 501-504.

18.   Yamashita, H.; Yoko, T.; Sakka, S., Preparation of $Li_2B_4O_7$ Films with Preferential Orientation by Sol–Gel Method. *J. Am. Ceram. Soc.* **1992,** 74, (7), 1668-1674.

19.   Gancitano, P.; Ciriminna, R.; Testa, M. L.; Fidalgo, A.; Ilharcob, L. M.; Pagliaro, M., Enhancing selectivity in oxidation catalysis with sol-gel nanocomposites. *Org. Biomol. Chem.* **2005,** 3, (13), 2389-2392.

20.   Pagliaro, M.; Ciriminna, R.; Man, M. W. C.; Campestrini, S., Better Chemistry through Ceramics: The Physical Bases of the Outstanding Chemistry of ORMOSIL. *J. Phys. Chem. B* **2006,** 110, (5), 1976-1988.

21.   Brook, M. A.; Chen, Y.; Guo, K.; Zhang, Z.; Brennan, J. D., Sugar-modified silanes: precursors for silica monoliths. *J. Mater. Chem.* **2004,** 14, (9), 1469-1479.

22.   Sui, X.; Cruz-Aguado, J. A.; Chen, Y.; Zhang, Z.; Brook, M. A.; Brennan, J. D., Properties of Human Serum Albumin Entrapped in Sol−Gel-Derived Silica Bearing Covalently Tethered Sugars. *Chem. Mater.* **2005,** 17, (5), 1174-1182.

23.   Ellerby, L. M.; Nishida, C. R.; Nishida, F.; Yamanaka, S. A.; Dunn, B.; Valentine, J. S.; Zink, J. I., Encapsulation of Proteins in Transparent Porous Silicate Glasses Prepared by the Sol-Gel Method. *Science* **1992,** 255, (5048), 1113-1115.

24.   Miled, O. B.; Boissiere, C.; Sanchez, C.; Livage, J., Spectro-ellipsometric studies of activated sol-gel thin films to detect Cu^{2+} ions in aqueous solutions. *J. Phys. Chem. Solids* **2006,** 67, 1775-1780.

25.   Kim, H.-J.; Ahn, J.-E.; Haam, S.; Shul, Y.-G.; Song, S.-Y.; Tatsumi, T., Synthesis and characterization of mesoporous Fe/SiO_2 for magnetic drug targeting. *J. Mater. Chem.* **2006,** 16, (17), 1617-1621.

26.   McDonagh, C. M.; Shields, A. M.; McEvoy, A. K.; MacCraith, B. D.; Gouin, J. F., Optical Sol-Gel-Based Dissolved Oxygen Sensor: Progress Towards a Commercial Instrument. *J. Sol.-Gel Sci. Technol.* **1998,** 13, 207-211.

27.   Jorge, P. A. S.; Mayeh, M.; Benrashid, R.; Caldas, P.; Santos, J. L.; Farahi, F., Applications of quantum dots in optical fiber luminescent oxygen sensors. *Appl. Opt.* **2006,** 45, (16), 3760-3767.

28.   John, M. S.; Kishen, A.; Sing, L. C.; Asundi, A., Determination of bacterial activity by use of an evanescent-wave fiber-optic sensor. *Appl. Opt.* **2002,** 41, (34), 7334-7338.

29.   Rahn, M. D.; King, T. A.; Gorman, A. A.; Hamblett, I., Photostability enhancement of Pyrromethene 567 and Perylene Orange in oxygen-free liquid and solid dye lasers. *Appl. Opt.* **1997,** 36, (24), 5862-5871.

30.   Mei, E.; Bardo, A. M.; Collinson, M. M.; Higgins, D. A., Single-Molecule Studies of Sol-Gel-Derived Silicate Films. Microenvironments and Film-Drying Conditions. *J. Phys. Chem. B* **2000,** 104, (43), 9973-9980.

31.   Villegas, M. A.; Pascual, L., Chemical and optical properties of dye-doped sol-gel films. *J. Mater. Sci.* **2000,** 35, 4615-4619.

32.   Hellriegel, C.; Kirstein, J.; Brauchle, C.; Latour, V.; Pigot, T.; Olivier, R.; Lacombe, S.; Brown, R.; Guieu, V.; Payrastre, C.; Izqueirdo, A.; Mocho, P., Diffusion of Single Streptocyanine Molecules in the Nanoporous Network of Sol-Gel Glasses. *J. Phys. Chem. B* **2004,** 2004, (38), 14699-14709.

33.   Kanungo, M.; Collinson, M. M., Controlling Diffusion in Sol-Gel Derived Monoliths. *Langmuir* **2005,** 21, (3), 827-829.

34.   McKiernan, J.; Simoni, E.; Dunn, B.; Zink, J. I., Proton Diffusion in the Pores of Silicate Sol-Gel Glasses. *J. Phys. Chem.* **1994,** 98, (3), 1006-1009.

35.   Hsiao, C. N.; Huang, K. S., Synthesis, characterization, and applications of polyvinylpyrrolidone/SiO2 hybrid materials. *J. Appl.Polym. Sci.* **2005,** 96, (5), 1936-1942.

36.   Doherty, W. J., III; Armstrong, N. R.; Saavedra, S. S., Conducting polymer growth in porous sol-gel thin films: formation of nanoelectrode arrays and mediated electron transfer to sequestered macromolecules. *Chem. Mater.* **2005,** 17, (14), 3652-3660.

37.   Sun, D.; Zhang, R.; Liu, Z.; Huang, Y.; Wang, Y.; He, J.; Han, B.; Yang, G., Polypropylene/silica nanocomposites prepared by in-situ sol-gel reaction with the aid of CO_2. *Macromolecules* **2005,** 38, (13), 5617-5624.

38.   Ruckenstein, E.; Hong, L., Coating water-swellable polymer latexes by interfacial polymerization. *J. Appl. Polym. Sci.* **1995,** 55, (7), 1081-92.

39.   Liu, S.; Zhang, Z.; Han, M., Gram-scale synthesis and biofunctionalization of silica-coated silver nanoparticles for fast colorimetric DNA detection. *Anal. Chem.* **2005,** 77, (8), 2595-2600.

40.   Costantini, A.; Luciani, G.; Annunziata, G.; Silvestri, B.; Branda, F., Swelling properties and bioactivity of silica gel/pHEMA nanocomposites. *J. Mater. Sci.: Mater. Med.* **2006,** 17, (4), 319-325.

41.   Qian, Z.; Hu, G.; Zhang, S.; Yang, M., Preparation and characterization of montmorillonite– silica nanocomposites: A sol– gel approach to modifying clay surfaces. *Physica B* **2008,** 403, 3231-3238.

42.   Letaief, S.; Ruiz-Hitzky, E., Silica–clay nanocomposites. *Chem. Commun.* **2003,** 2003, (24), 2996-2997.

43.   Chang, S.-m.; Doong, R.-a., ZrO_2 thin films with controllable morphology and thickness by spin-coated sol-gel method. *Thin Solid Films* **2005,** 489, (1-2), 17-22.

44.   Gorman, B. P.; Anderson, H. U., Processing of composite thin film solid oxide fuel cell structures. *J. Am. Ceram. Soc.* **2005,** 88, (7), 1747-1753.

45.   Huang, M. H.; Dunn, B. S.; Zink, J. I., In Situ Luminescence Probing of the Chemical and Structural Changes during Formation of Dip-Coated Lamellar Phase Sodium Dodecyl Sulfate Sol-Gel Thin Films. *J. Am. Chem. Soc.* **2000,** 122, (15), 3739-3745.

46.   Gilliland, J. W.; Yokoyama, K.; Yip, W. T., Comparative Study of Guest Charge-Charge Interactions within Silica Sol-Gel. *J. Phys. Chem. B* **2005,** 109, (11), 4816-4823.

47.   Lan, E. H.; Dave, B. C.; Fukuto, J. M.; Dunn, B.; Zink, J. I.; Valentine, J. S., Synthesis of sol-gel encapsulated heme proteins with chemical sensing properties. *J. Mater. Chem.* **1999,** 9, 45-53.

48.   Nguyen, D. T.; Smit, M.; Dunn, B.; Zink, J. I., Stabilization of Creatine Kinase Encapsulated in Silicate Sol-Gel Materials and Unusual Temperature Effects on Its Activity. *Chem. Mater.* **2002,** 14, (10), 4300-4306.

49.   Badjic, J. D.; Kostic, N. M., Effects of Encapsulation in Sol-Gel Silica Glass on Esterase Activity, Conformational Stability, and Unfolding of Bovine Carbonic Anhydrase II. *Chem. Mater.* **1999,** 11, (12), 3671-3679.

50.   Lloyd, C. R.; Eyring, E. M., Protecting Heme Enzyme Peroxidase Activity from H_2O_2 Inactivation by Sol-Gel Encapsulation. *Langmuir* **2000,** 16, (23), 9092-9094.

51.   Mendelsohn, J. D.; Barrett, C. J.; Chan, V. V.; Pal, A. J.; Mayes, A. M.; Rubner, M. F., Fabrication of Microporous Thin Films from Polyelectrolyte Multilayers. *Langmuir* **2000,** 16, (11), 5017-5023.

52.   Yu, A.; Caruso, F., Thin Films of Polyelectrolyte-Encapsulated Catalase Microcrystals for Biosensing. *Anal. Chem.* **2003,** 75, (13), 3031-3037.

53.   Wiemann, L. O.; Buthe, A.; Klein, M.; van den Wittenboer, A.; Daehne, L.; Ansorge-Schumacher, M. B., Encapsulation of Synthetically Valuable Biocatalysts into Polyelectrolyte Multilayer Systems. *Langmuir* **2009,** 25, (1), 618-623.

54.   Dimitrova, M.; Affolter, C.; Meyer, F.; Nguyen, I.; Richard, D. G.; Schuster, C.; Bartenschlager, R.; Voegel, J.-C.; Ogier, J.; Baumert, T. F., Sustained delivery of siRNAs targeting viral infection by cell-degradable multilayered polyelectrolyte films. *Proc. Natl. Acad. Sci. U.S.A.* **2008,** 105, (42), 16320-16325.

55.   Chung, A. J.; Rubner, M. F., Methods of Loading and Releasing Low Molecular Weight Cationic Molecules in Weak Polyelectrolyte Multilayer Films. *Langmuir* **2002,** 18, (4), 1176-1183.

56.   Rudmann, H.; Shimada, S.; Rubner, M. F., Solid-State Light-Emitting Devices Based on the Tris-Chelated Ruthenium(II) Complex. 4. High-Efficiency Light-Emitting Devices Based on Derivatives of the Tris(2,2'-bipyridyl) Ruthenium(II) Complex. *J. Am. Chem. Soc.* **2002,** 124, (17), 4918-4921.

57.   Koner, A. L.; Nau, W. M., Cucurbituril Encapsulation of Fluorescent Dyes. *Supramol. Chem.* **2007,** 19, (1-2), 55-66.

58.   Ong, W.; Gomez-Kaifer, M.; Kaifer, A. E., Cucurbit[7]uril: A Very Effective Host for Viologens and Their Cation Radicals. *Org. Lett.* **2002,** 4, (10), 1791-1794.

59.   Wagner, B. D.; Stojanovic, N.; Day, A. I.; Blanch, R. J., Host Properties of Cucurbit[7]uril: Fluorescence Enhancement of Anilinonaphthalene Sulfonates. *J. Phys. Chem. B* **2003,** 107, (39), 10741-10746.

60.   Mohanty, J.; Nau, W. M., Ultrastable rhodamine with cucurbituril. *Angew. Chem., Int. Ed. Engl.* **2005,** 44, (24), 3750-3754.

61.   Nau, W. M.; Mohanty, J., Taming fluorescent dyes with cucurbituril. *Int. J. Photoenergy* **2005,** 07, 133-141.

62.   Moore, J. L. Host-Guest Complexation of Cationic Xanthene Dyes with Cucurbit[7]uril. University of Oklahoma, Norman, 2008.

63.   Kim, J.; Jung, I.-S.; Kim, S.-Y.; Lee, E.; Kang, J.-K.; Sakamoto, S.; Yamaguchi, K.; Kim, K., New Cucurbituril Homologues: Syntheses, Isolation, Characterization, and X-ray Crystal Structures of Cucurbit[n]uril (n = 5, 7, and 8). *J. Am. Chem. Soc.* **2000,** 122, (3), 540-541.

64.   Liu, Y.; Li, C.-J.; Guo, D.-S.; Pan, Z.-H.; Li, Z., A Comparative Study of Complexation of b-Cyclodextrin, Calix[4]arenesulfonate and Cucurbit[7]uril with Dye Guests: Fluorescence Behavior and Binding Affinity. *Supramol. Chem.* **2007,** 19, (7), 517-523.

65.   Halterman, R. L.; Moore, J. L.; Mannel, L. M., Disrupting aggregation of tethered rhodamine B dyads through inclusion in cucurbit[7]uril. *J. Org. Chem.* **2008,** 73, (8), 3266-3269.

Chapter II

Experimental Methods

2.1 CHAPTER ABSTRACT

This chapter details many of the solgel sample preparations used for this thesis, as well as how the data were collected and analyzed. Both silica alcogels and silica hydrogels were used to encapsulate the dye molecules and dye complexes. Fluorescence measurements of dye properties within the solution, thin film and monolith samples allowed the effect of the environment to be discerned from the data. Further measurements of porosity size and film thicknesses were conducted to enable an accurate assessment of film characteristics.

2.2 INTRODUCTION

The methods and materials described in this chapter are meant to clarify common methods that have been used in this work. These methods will be referred to in the following chapters where their application applies. Different fluorescence microscopy techniques were used to gather absorption and emission data about dye molecules within different solgel materials or macromolecular complexes to be incorporated into solgel silicates. Fluorescence microscopy is a versatile tool commonly used to probe the intrinsic properties of materials.

By combining ensemble measurements and single molecule measurements, this thesis aims to give a more complete explanation of the heterogeneity of the systems as well as how the variations between molecules affect ensemble

measurements. Solgel silicates are known to form heterogeneous networks with pore sizes that can be defined by the guest molecules.[1] However, whether the porosity of the silicate is maintained when the solgel silicate is also a guest within another framework has not been fully explored. The effects of a heterogeneous silicate on a non-covalent macromolecular complex are also of interest. The combination of ensemble and single-molecule measurements to these systems will help to understand the extent of material influence on guest molecule properties.

2.3 MATERIALS

Solgel silicates have been used in novel ways in this thesis in the development of new materials. Solgel silicate makes up the majority of the structure in some cases, but can also be absorbed into other structures. As will be detailed here and in later chapters, dye molecules and dye complexes were used to probe the ability of silica solgels to host guest molecules and complexes in solgel thin films, monoliths and in the hybrid film composed of the silica matrix absorbed into polyelectrolyte multilayer scaffolds.

2.3.1 Solgel Silicates

The solgel solutions for both TEOS alcogels and TMOS hydrogels were used as in the literature.[2-4] The TEOS alcogel preparation included a solgel precursor solution of TEOS, H_2O, and ethanol at a ratio of 3.5:2:7 by volume with catalytic phosphoric acid, sonicated for 2 hours, and was used for the PEM/solgel composite material (Chapter 3), the R6G thin film samples (Chapters 4 and 5), and the alcogel monoliths (Chapter 7). In each case, the volume was tailored to fit the application.

Thin film samples used 60 μL from stock sol solutions of 630.4 μL. Absorbing

solgel into PEM films for the composite films required a larger quantity, 5 mL, of

precursor solution, to slow gelation and fill the conical base of the centrifuge tubes

used to hold the samples. The alcogel monoliths were made to fill the cuvettes, 2

mL, to make sure the sample was the correct height for fluorometry measurements.

The TMOS hydrogel preparation included a solgel precursor solution of

TMOS and H_2O at a ratio of 4.7:1 with catalytic hydrochloric acid, sonicated for 20

minutes in an ice bath to slow gelation, and was used for the hydrogel monoliths at

the same volume, 2 mL, as the alcogel monoliths (Chapter 7).

2.3.2 Spincoating

Many groups have used spincoated polyelectrolyte structures on ITO glass,[5-7]

silver coated glass,[8] bare glass, or on silicon[9] or have combined spincoating with

dipcoated PEM layers[10] for many applications, including fuel cells and developing

more dense, less porous, polymer films.[11] In these applications and for the purposes

of this thesis work, spincoating provides a fast, simple, reproducible method of

producing silicate thin films with thickness control and reproducible morphology.

The spincoated samples included in this thesis utilized silica alcogels

containing R6G molecules and R6G/CB7 complexes. In Chapters 4 and 5, these

spincoated samples provide a means to compare the dye molecule properties to the

CB7/dye complex. Spincoating was also used to deposit the Pyronin Y samples of

Chapter 6 to further develop an understanding of complexation with CB7, however

the PyY and PyY/CB7 solutions were spincoated onto clean coverglasses or a layer of polyallylamine hydrochloride (PAH) without the use of solgel materials.

2.3.3 PEM Film Deposition

The novel absorption of silica solgel into PEM thin films was a two-part procedure. First, the 5.5-bilayer PEM film was deposited on a substrate. Then, the silica solgel precursor solution is absorbed from one end of the PEM film. The PEM thin films used for this work used the polyelectrolytes, polyacrylic acid (PAA) and polyallylamine hydrochloride (PAH). PAA and PAH were diluted with Millipore water to 0.02 M by monomer concentration and adjusted to pH 3.5 and pH 7.5, respectively, prior to deposition using NaOH and HCl. For each monolayer, the substrate, either a coverglass or silicon wafer, was set into the polyelectrolyte solution, PAA or PAH, for 15 min., placed in deionized water for three separate rinses of 2 min., 1 min. and 1 min. as initially detailed by Decher,[12] and blown dry with nitrogen. One bilayer consists of one layer each of PAA and PAH. The initial priming monolayer of PAH gives the extra half bilayer for each film. Films were stored as formed at constant humidity and characterized within 3 months of deposition, though longer storage should not have harmed the films.

Six cm long coverglasses were immersed in polyelectrolyte and rinse solutions using polystyrene holders in glass beakers, whereas silicon wafers (approximately 3 cm long) were narrower (approximately 1 – 1.5 cm wide) and were immersed in solutions in conical-tipped polypropylene centrifuge tubes without added support.

In order to reduce background fluorescence due to the PEM films, transparent tape was adhered to one side of the coverglasses during PEM deposition. After the deposition was complete, the tape was removed with minimal residue remaining on the sample. This method removed the majority of the polyelectrolytes deposited on the back of the coverglass substrates. More information, including fluorescent images, about the use of tape may be found in Appendix A.

2.4 INSTRUMENTATION

The instruments used to collect single molecule and ensemble data were available either through the laboratory of Dr. Wai Tak Yip, or other faculty members of the Chemistry and Biochemistry Department at the University of Oklahoma. Ellipsometry was performed in the Homer L. Dodge Physics and Astronomy Department. Scanning Electron Microscopy was performed by the staff at the Electron Microscopy Facility.

All single molecule measurements were acquired using the laser setup described in section 2.4.1. Bulk Measurements were made using several instruments. Bulk measurements include fluorescence measurements of dyes that had a concentration greater than 100 nM as well as non-fluorescent measurements of material characteristics, such as size and porosity, described in sections 2.4.4 and 2.4.5.

2.4.1 Laser Setup

Using an argon ion laser as a light source, Figure 2.1, a prism spatially resolved the light to allow use of single wavelength excitation. 514 nm light and 488

nm light were used during different experiments. A ½ - waveplate and ¼ - waveplate were used to increase the circular polarization of the source light to excite all molecules equally, regardless of the orientation of their molecular dipoles. Several neutral density filters were used to attenuate the light and increase control of consistent laser power to the samples. The excitation light was coupled into an optical fiber by a 10x objective. The light from the optical fiber was then collimated by another 10x objective and entered the inverted microscope (Nikon, TE-200) through the epi-illumination port.

Within the microscope, a wavelength specific dichroic beam splitter (Chroma Technology) in the microscope directed the source light to the sample through a 100x microscope objective (Nikon, CFI Achromat oil immersion 1.25 N.A.). The sample was positioned on the microscope with a nanopositioning stage (Queensgate or Melles Griot, NanoBlock). Emission from the samples that went through the bottom of the microscope passed through the dichroic beam splitter to a mirror that directed the emission light out of the microscope to the detectors. Between the microscope and detectors the emission light was filtered with long pass filters (Omega Optical, ALPHA Technology) to reduce the amount of source light and scattered light measured. Some measurements then utilized a polarization beam splitter cube to separate the emission light by polarization where it was focused to two avalanche photodiode (APD) detectors (Perkin-Elmer, SPCM-AQR).
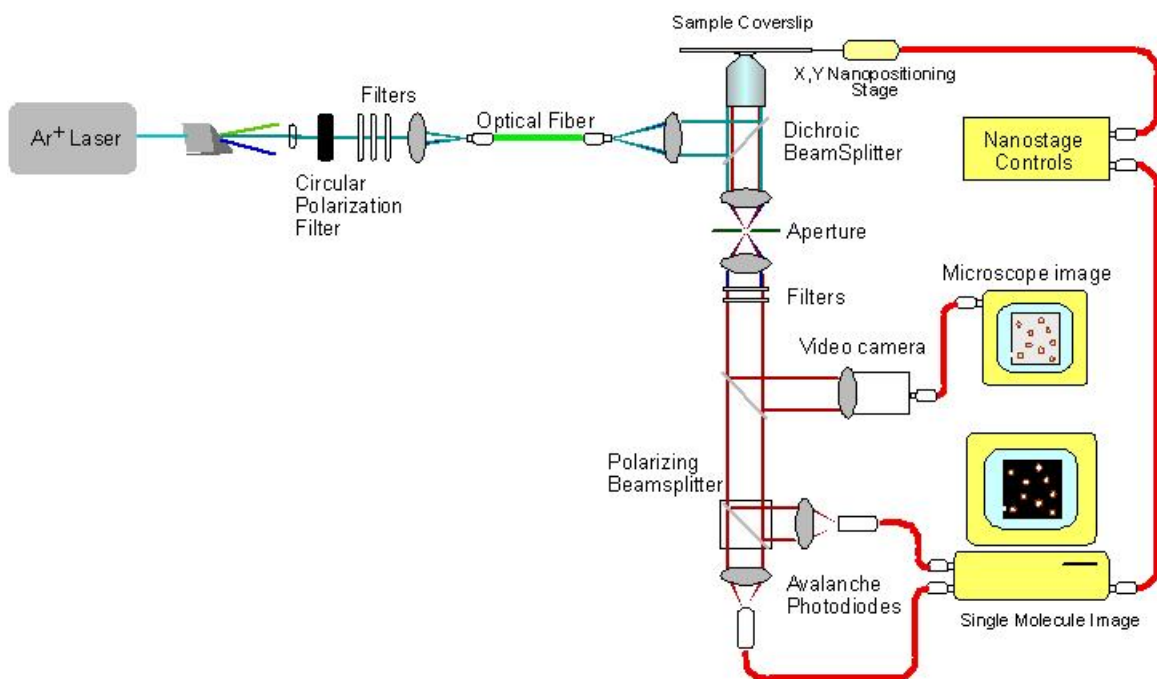
Figure 2.1 – Schematic of home-built confocal microscope (Figure based on diagram by J. W. Gilliland[13])

Visualization of the sample and focusing the sample were done using a video camera situated after the microscope and long pass filter, but before the polarization beam splitter. The video camera was not used for any data collection.

2.4.1.1. Imaging

Fluorescent images were acquired for all samples where single-molecule data or thin film emission spectra were collected, chapters 3, 4, 5 and 6. Imaging used a rastor scan of the 10 μm x 10 μm region accessed by the nanopositioning stage as controlled by the computer interface (LabView©). The images were used to screen samples that would be useful for photobleaching studies as well as to make sure the fluorescence was consistently high for bulk emission measurements. During imaging, diffusing molecules appear as streaks of light, while immobilized dye

molecules appear as round spots, Figure 2.2. Photobleaching studies, described in more detail in section 2.4.1.3, used in this thesis utilized only stationary dye molecules, so dye concentrations near 5 nM were optimized to yield approximately 30 round fluorescent dye signals per 100 μm^2 image, which allowed for appropriate separation between molecules and reduced the likelihood of dye aggregation effects.
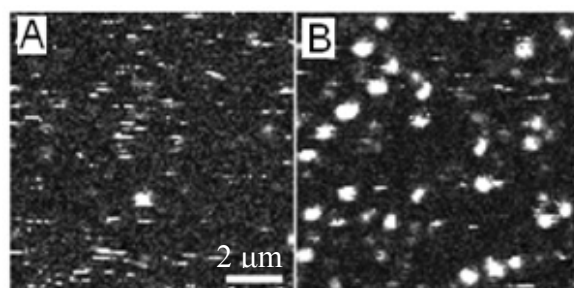
Figure 2.2 – Fluorescent images of predominately diffusing, mobile R6G dye molecules (a), or stationary R6G/CB7 complexes (b).

2.4.1.2 Survival lifetime

Once the fluorescent image of a sample had been acquired, single-molecule data was collected by photobleaching, or bleaching under continuous excitation, each individual molecule. The time required for the molecule to undergo a change that causes it to no longer emit light is referred to as the survival lifetime, Figure 2.3.
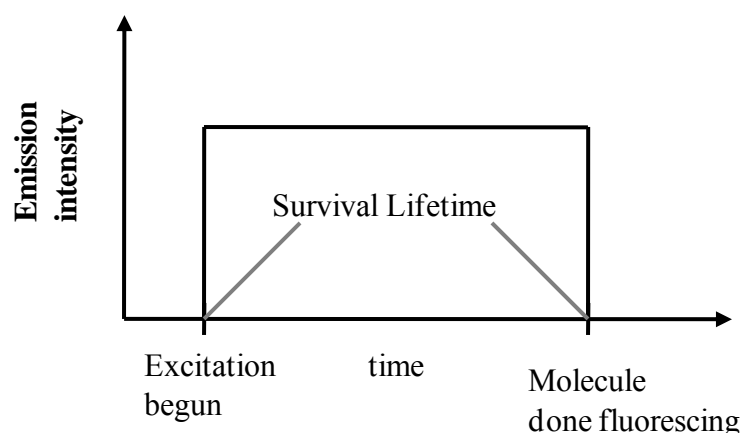
Figure 2.3 – Survival lifetime schematic

The survival lifetime can be an indication of vulnerability of a dye molecule to interactions with its surroundings. Possible causes of photobleaching are discussed in more detail in chapters 4-7 as multiple factors have been used with some success to extend the survival lifetime, such as encapsulation and complexation, in both solgel thin films and monoliths.

2.4.1.3 Dye Mobility

During photobleaching studies, polarization-resolved emission data was collected by the two APD detectors. The relative intensities detected allowed calculation of the polarization of emitted light using Equation 2.1.

$$Polarization = \frac{I_p - I_s}{I_p + I_s} \qquad \text{(E2.1)}$$

The polarization of emitted light for single molecules was then used to characterize the molecules as fixed, tumbling or intermediate for the composite film work in chapter 3. The classification scheme considered the average polarization and whether the average stayed within the standard deviation. Fixed molecules have constant, non-zero polarization as determined by the average polarization being greater than one standard deviation away from zero. Tumbling molecules have constant polarization, the average polarization for the molecule less than a standard deviation away from zero. Intermediate molecules demonstrate different polarizations throughout their lifetime.

Error in the number of molecules categorized as fixed, intermediate or tumbling was calculated using Equation 2.2:

$$\text{Error} = \sqrt{p(1 - p)n} \qquad \text{(E2.2)}$$

where p is the percent in the particular category and n is the total number of molecules in the sample. The percent of molecules not in the particular category has been represented by *1-p*. Though the R6G/CB7 complexes were not classified with the fixed, tumbling, intermediate designations, the emission polarization of the complexes was used to better understand how the molecules may be moving.

2.4.1.4 Emission Spectra

An ensemble measurement acquired for the PEM/silica composite thin films in chapter 3 was the emission spectra of oregon green 514 (ORG) molecules, collected using a CCD camera (Roper Scientific, SpectruMM). Though single molecule emission spectra are possible with the instrument, an ensemble measurement of the thin films allowed a different perspective on the heterogeneity of the system. The composite films also had a higher level of noise than spincoated silica solgel films, decreasing the signal-to-noise ratio. By monitoring the changing emission spectra of ORG, a measure of the porosity and ability of external buffer solutions to access the interior of the film was obtained.

2.4.2 Ensemble Fluorescence

Ensemble measurements of emission spectra in bulk materials were acquired from monolithic alcogels and hydrogels as well as solution samples, chapter 7. Using a fluorometer (Shimadzu RF-5301 PC Spectrofluorophotometer) allowed an adjustable emission wavelength range to be monitored as well as the ability to select the excitation wavelength. The ability to adjust the excitation wavelength was imperative to obtaining well-resolved spectra, due to the amount of scattered light

from the monoliths, chapter 7. The monolith and solution samples monitored by ensemble fluorometry allowed a measurement of a larger scale version of the solgel silicates in a way that minimized the time required for data collection while taking full advantage of the instrument capabilities.

2.4.3 Absorbance Spectra

Primarily employed as a fast, qualitative means to acquire absorption spectra, a UV-Vis spectrophotometer was utilized to determine the experimental protocol for photobleaching the monolith samples, chapter 7. In order to photobleach the samples through a closed container, the container must not absorb the light used for photobleaching. Quartz slides do not absorb significantly at the wavelength of the UV light source used to photobleach the monolith and solution samples, 275 nm.

In addition, verifying λ_{max}^{abs} of the CB7-complexed dye molecules found in literature sources was most readily achieved through the use of the UV-Vis spectrophotometer. This was assurance that both R6G and PyY and their respective complexes with CB7 were excited with appropriate wavelengths for single-molecule and ensemble measurements.

2.4.4 Thin Film Thickness

Thickness measurements of PEM films and PEM/silica composite films, chapter 3, were obtained to verify growth patterns with deposition of additional layers. As a method to determine the thickness of a thin film on a silicon wafer, ellipsometry was performed using a Gaertner Ellipsometer with a HeNe light source. Since ellipsometry is a non-destructive measurement technique, it allowed repeated

measurements of samples before and after treatments with acid or absorption of a solgel precursor solution. Therefore, changes in thickness could be correlated directly with the additional treatment without requiring considerations of differences between films. The reported error of thickness measurements was determined by repeating the measurement a minimum of three times and calculating a standard deviation.

2.4.5 Surface Morphology

Scanning electron microscopy images were obtained for the polyelectrolyte multilayer (PEM) thin films of chapter 3. Using a JEOL JSM-880 scanning microscope, at 15 kV, SEM images were obtained for 5.5- and 8.5-bilayer PAA/PAH films on coverglasses. The images were obtained at multiple resolutions and allow visualization of the surface pore sizes as well as what appear to be pores inside other pores. These images support the understanding of PEM thin films as a solid structure that contains a porous network. It is this network that is being utilized as a scaffold in the work presented in chapter 3.
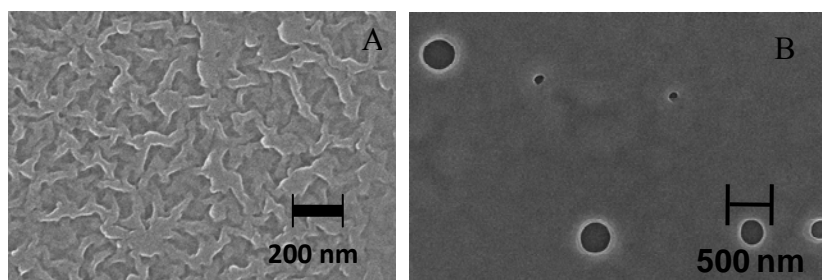
Figure 2.4 – SEM images of 5.5-bilayer (a) and 8.5-bilayer (b) PEM films.

2.5 ANALYSIS OF DATA

2.5.1 Blinking

Data collected by use of LabView[©] on the inverted confocal microscope setup, Figure 2.1, was saved as comma delimited values. Since much of the data analysis was performed repeatedly, several visual basic macros were devised to work with the data. Initial data analysis to determine survival lifetime and generate plots of emission intensity and polarization transients was accomplished using macros developed by colleagues in Dr. Yip's research group.[13]

Several new macros were useful due to the blinking properties and changing intensities characteristic of R6G and PyY, as well as the R6G/CB7 and PyY/CB7 complexes. Macros were specifically designed to determine the number and duration of blinks, calculate the average intensity of individual molecules without averaging in values below the "off" threshold, and count the repetitions of intensities detected within binned ranges for individual molecules.

Blinking was determined by using two threshold values for each molecule, an on threshold and an off threshold. Both the number of blinks and the duration of each blink were determined. Visual Basic was used to determine the amount of time each molecule was on before it blinked off and off before it blinked back on. Only blinks that passed both thresholds were counted.
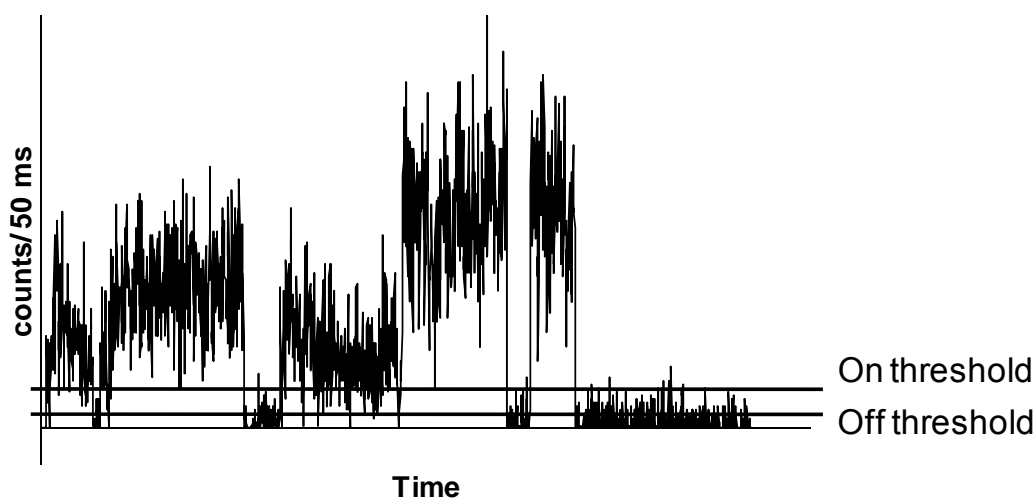
Figure 2.5 – Blinking Threshold Schematic

Blinking was used in chapter 6 with the Pyronin Y study to look at different environments. However, it was also an underlying requirement to determine the average intensity of R6G and R6G/CB7 emission in chapters 4 and 5. The low emission blinking values were not included in the calculation of average intensity to correct for any bias toward low values.

The intensity of each individual molecule was usually determined by summing the intensity recorded by each detector over the 50 ms intervals. However, some measurements were taken without polarization resolution, using only one detector. Since the intensity of the two detector measurements was added together, the two methods gave similar results.

2.5.2 Non-linear fittings

Fitting curves to the data allows a quantitative comparison between the samples in a way that disregards the number of results plotted. This is useful when

comparing data sets with different numbers of molecules, or a different number of

measurements of the samples. The relationships in the data determine the

appropriate curve to fit to the data sets, however, since much of the work presented

in this thesis is related to measurements taken during photobleaching experiments,

many relationships coincide to either single exponential or biexponential decay

functions.

The survival lifetime was a property of R6G and PyY that was found for each

material, whether thin film or monolith, with and without CB7-complexation,

chapters 4-7. In chapter 7 this lifetime was seen as decay in intensity. As

exponential decay curves were fit to histograms of survival lifetimes, some samples

decayed at a single rate, therefore only a single exponential function, Equation 2.3,

was used.

$$f(t) = A_1 e^{-\frac{\tau_1}{t}} \hspace{3cm} \text{(E2.3)}$$

In Equation 2.3, A is the pre-exponential factor, related to the height of the curve and

in the case of survival lifetimes related to the number of occurrences of the most

common survival lifetime; τ is the decay constant of the curve, which is the variable

best compared between samples; and t is time.

Samples that had multiple photophysical behaviors, especially the survival

lifetimes of dye molecules complexed by CB7, were commonly fit best by bi-

exponential curves, Equation 2.4. The biexponential function is an extension of the

single exponential.

$$f(t) = A_1 e^{-\frac{\tau_1}{t}} + A_2 e^{-\frac{\tau_2}{t}} \qquad \text{(E2.4)}$$

Chapter 7 also exhibited exponential growth of the emission intensity to a peak intensity. Equation 2.5 was used to fit a curve to this period of growth. The addition of a maximum y value allowed the curve to come to a maximum value without continuing to increase.

$$f(t) = y_{max} - A e^{-kt} \qquad \text{(E2.5)}$$

The gaussian function (Equation 2.6) was fit to the emission intensity data of chapters 4 and 6. The presentation of this data as a histogram of all molecules in the sample clearly shows a peak that tapers to the sides. The gaussian function allows other features to be calculated from the data, such as the most likely value, ω_0, as well as a measure of the heterogeneity of the system, found from the full width at half maximum height (FWHM, Equation 2.7).

$$f(x) = A e^{-\frac{(x-\omega_0)^2}{2\sigma^2}}, \qquad \text{(E2.6)}$$

$$\text{where } \sigma = \frac{FWHM}{2\sqrt{2 ln2}} \qquad \text{(E2.7)}$$

In the current application, f(x) represents the occurrence frequency of a particular average intensity.

To gain an idea of whether the functions fit the data well, the error value, R^2, was calculated by using Equation 2.8:[14]

$$R^2 = 1 - \frac{\Sigma(F_{pre}-F_i)^2}{\Sigma(F_{av}-F_i)^2} \qquad \text{(E2.8)}$$

where F_{pre} is the predicted value of the function at point i; F_{av} is the average of the raw data; and F_i is the value of the individual raw data point. This R-squared calculation was used for all non-linear fittings including the exponential decays, exponential growth, and gaussian curves.

Since ORG is a pH sensitive dye molecule, the ratio of deprotonated ORG molecules to protonated ORG molecules can be established using the Henderson-Hasselbach equation, Equation 2.9.

$$pH = pK_a + log\left(\frac{[base]}{[acid]}\right) \qquad \text{(E2.9)}$$

The full derivation of this relationship as it applies to the emission spectra intensities has been published previously for use with ORG.[13] Summarily, the protonated and deprotonated ORG molecules emit at different wavelengths. Therefore, the intensity of the emission peak at the wavelengths corresponding to the protonated and deprotonated ORG molecules can be used as the concentration of the basic and acid forms of the molecule. The adapted Henderson-Hasselbach then becomes Equation 2.10:

$$I_{total} = \frac{1}{x+1}(xI_{HA} + I_{A^-}) \qquad \text{(E2.10)}$$

where I_{total} is the intensity due to both the protonated and deprotonated states of ORG, I_{HA} is the intensity due the protonated state of ORG and I_{A^-} is the intensity due to the deprotonated state of ORG, x has been designated as the ratio of the concentration of the protonated state to the concentration of the deprotonated state.

2.6 CONCLUSIONS

Using a variety of samples, solutions, thin films and monoliths allowed a unique perspective on the abilities of solgel materials to encapsulate guest molecules. The explanations of methods presented in this chapter are meant to complement the detailed explanations in the following chapters of how the experiments were carried out by giving part of the reasoning for the choice of experiment and context to understand how the experiments complement each other. Since similar fluorescence measurements were performed on all of the samples, regardless of solgel formation, curve fitting of the data uses similar functional forms, which were presented here as a reference.

2.7 REFERENCES

1.	Raman, N. K.; Anderson, M. T.; Brinker, C. J., Template-Based Approaches to the Preparation of Amorphous, Nanoporous Silicas. *Chem. Mater.* **1996**, 8, (8), 1682-1701.

2.	Gilliland, J. W.; Yokoyama, K.; Yip, W. T., Effect of Coulombic Interactions on Rotational Mobility of Guests in Sol-Gel Silicate Thin Films. *Chem. Mater.* **2004**, 16, (20), 3949-3954.

3.	Gilliland, J. W.; Yokoyama, K.; Yip, W. T., Comparative Study of Guest Charge-Charge Interactions within Silica Sol-Gel. *J. Phys. Chem. B* **2005**, 109, (11), 4816-4823.

4.	Zhou, Y.; Yip, W. T., Balance between Coulombic Interactions and Physical Confinement in Silica Hydrogel Encapsulation. *J. Phys. Chem. B* **2009**, 113, (17), 5720-5727.

5.	Niu, Y.-H.; Ma, H.; Xu, Q.; Jen, A. K. Y., High-efficiency light-emitting diodes using neutral surfactants and aluminum cathode. *Appl. Phys. Lett.* **2005**, 86, (8), 083504/1-083504/3.

6.	He, Y.; Gong, S.; Hattori, R.; Kanicki, J., High performance organic polymer light-emitting heterostructure devices. *Appl. Phys. Lett.* **1999**, 74, (16), 2265-2267.

7.	Shoji, E.; Miyatake, K.; Hlil, A. R.; Hay, A. S.; Maindron, T.; Jousseaume, V.; Dodelet, J. P.; Tao, Y.; D'Iorio, M., Immiscible polymers in double spin-coated electroluminescent devices containing phenyl-substituted tris(8-hydroxyquinoline)aluminum derivatives soluble in a host polymer. *J. Polym. Sci., Part A: Polym. Chem.* **2003**, 41, (19), 3006-3016.

8.	Uznanski, P.; Pecherz, J., Surface plasmon resonance of azobenzene-incorporated polyelectrolyte thin films as an H+ indicator. *J. Appl. Polym. Sci.* **2002**, 86, (6), 1459-1464.

9.   Lefebvre, J.; Gray, D. G., AFM of adsorbed polyelectrolytes on cellulose I surfaces spin-coated on silicon wafers. *Cellulose (Dordrecht, Netherlands)* **2005**, 12, (2), 127-134.

10.   Lee, S.-S.; Lee, K.-B.; Hong, J.-D., Evidence for Spin Coating Electrostatic Self-Assembly of Polyelectrolytes. *Langmuir* **2003**, 19, (18), 7592-7596.

11.   Gorman, B. P.; Anderson, H. U., Processing of composite thin film solid oxide fuel cell structures. *J. Am. Ceram. Soc.* **2005**, 88, (7), 1747-1753.

12.   Decher, G., Fuzzy nanoassemblies: Toward layered polymeric multicomposites. *Science* **1997**, 277, (5330), 1232.

13.   Gilliland, J. Single-Molecule Spectroscopic Investigation of the Influence that Charge-Charge Interactions, Solvation, and Confinement have on Guest Molecule Rotational Mobility and Photostability within Silica Sol-Gel Host Matrices. University of Oklahoma, Norman, 2006.

14.   Dewey, B. R., *Introduction to Engineering Computing*. McGraw-Hill Primus: 1994.

Chapter III

Polyelectrolyte Thin Films as Scaffolds for Silica Solgel Thin Films

3.1 CHAPTER ABSTRACT

Silica solgel, commonly used as a host for sensor molecules, has been absorbed into PEM films. The PEM scaffold provides a novel way to produce thin solgel films, while stabilizing the solgel from cracking. Within the PEM scaffold, the solgel structure forms a porous network as it does when spincoated. Single molecule measurements of the composite films doped with rhodamine 6G (R6G) revealed that R6G exhibits a similar mobility as in silica solgel thin films. Guest molecules in the composite film are responsive to external stimuli, as seen by response to external pH buffers by the pH-sensitive dye, Oregon Green 514 (OG). Emission spectra of OG in the composite film also showed reabsorption behavior of OG. OG as an absorbed guest molecule within the silica solgel interacts with the polyelectrolyte scaffold as well as the solgel network.

3.2 INTRODUCTION

Polyelectrolyte multilayer (PEM) thin films are stable in ambient conditions and have thicknesses that are easily adjustable on the nanometer length scale. Porous PEM films are being used to control thickness and add mechanical stability to otherwise fragile materials. Polyelectrolyte multilayer (PEM) thin films have been deposited with molecular level thickness control by two main techniques, either by dip coating[1, 2] or spin coating,[3] both use a layer-by-layer (LBL) assembly. Either deposition technique can be used to build a film to the desired molecular thickness.

Both dipcoating and spincoating can use adsorption of the polyelectrolytes through electrostatic attraction between the oppositely charged electrolytes for film growth.[3,4] Dipcoating PEM films is a gentle method of depositing films that are compatible with biomolecules. Work has been done with PEM films to trap sensor proteins, such as glucose oxidase.[5, 6]

The tunable features of PEM thin films allow them to be used with many applications. As the Rubner group has shown, the thickness of PEM thin films is highly dependent on the pH of the polyelectrolytes during deposition.[7] PEM thin films can also respond to pH change after film formation by exceeding the pK_as or pK_bs of the polyelectrolytes.[8] PEM films form a highly porous structure that is stable for long durations.[9] However, it is widely known that changing the humidity, pH and other environmental factors will affect the structures of the PEM films.[10, 11] Porosity within PEM films is recognized as being diverse, though consistently networked throughout the films. Rubner and others have shown a network of webbed features or circular pores on the surface of PEM films.[12, 13] As with the thickness, the porosity of the PEM films also responds to pH changes.[10] Maintaining the porosity of the films is essential for development of these films as sensors to external aqueous stimuli.

Molecular level control of thickness has also been shown for silica alcogel materials. Most work with alcogels has been done by spincoating or dipcoating the samples. Spincoating causes the thickness of the sample to depend on spincoating speed and aging of solgel solution and requires the sample to be stable under the

conditions of the spinning. Dipcoating has been shown to have reproducible thicknesses,[14] but has not been developed to the extent of spincoating. Recent advances in thickness control have utilized high temperature and added reactants to the solgel mixture.[15, 16] In these works, the thickness of ZrO_2 films is adjusted based on the concentration of salt added.

Recent work combining solgels with polymer films has focused mainly on mechanical and electrolytic properties of the resulting composite film.[17-20] These works combine the polymer and solgel in solution together before solidifying, forming hybrid films.[17, 19, 20] One work put the solgel components into a polymer film with CO_2, then the solgel hydrolysis and condensation reactions were completed inside the polymer film.[18] Soaking a solgel solution into a formed polymer film is a novel approach to combining solgel and polymer films.

Silica solgel materials have seen such wide applicability in the area of sensor technology.[21, 22] By soaking the silica alcogels into PEM films molecular-level thickness control is extended to the absorbed solgel in a way that is biocompatible and could be extended to biocompatible hydrogels. Similar to silica solgel films, PEM thin films can be used for months after being deposited. However, the ability to reliably hold guest molecules with minimal leaching is much greater in silica solgels than PEM films. PEM thin films have remarkable stability and thickness control, but are likely to release guest molecules with addition of buffers.[23] This makes the addition of the solgel network to the PEM film advantageous for applications which require contact with solutions.

In this chapter, we report progress on absorbing silica solgel solutions into polyelectrolyte multilayer thin films. The solgel solution has been found to intercalate evenly into the PEM film, as seen by ellipsometric data, adopting the thickness of the PEM film while maintaining the porosity necessary for sensor applications. Using rhodamine 6G (R6G) as a probe molecule, the resulting dye mobility in the solgel-impregnated PEM film is compared to R6G mobility studies that had previously been conducted in spincoated silica solgel samples.[24] If the dye molecules have a different environment within the solgel matrix, due to increased hydrophobicity, or charge on the molecule,[24] the mobility of the individual dye molecules will be affected.

Previous work with 200 nm thick spincoated solgel samples reported long buffer equilibration times.[25] Developing a new control mechanism for the thickness of the solgel samples could allow rapid response to an external stimulus by the probe molecules. As an illustration, we report the pH response of a pH-sensitive dye molecule, Oregon Green 514 (OG), which demonstrates the maintained porosity in the current silica solgel-impregnated PEM film. The composite film of a PEM film with silica alcogel soaked into it combines the thickness control and mechanical stability of the PEM thin films with the small pores of the alcogel minimizing leaching of guest molecules. The combination of these two thin film materials allows the composite film to be more durable and useful for a greater range of applications.

3.3 MATERIALS AND METHODS

3.3.1 Materials

Polyacrylic acid, sodium salt (PAA MW: 20,000,), and polyallylamine hydrochloride (PAH MW: 60,000) were obtained from Polysciences. 99.9+% tetraethyl orthosilicate (TEOS), spectrophotometric grade 95% ethanol, and 85 wt % phosphoric acid were purchased from Sigma-Aldrich. Oregon Green 514 carboxylic acid (OG) and rhodamine 6G (R6G) were purchased from Molecular Probes. Sodium citrate, enzyme grade and Citric acid, anhydrous, enzyme grade were obtained from Fisher Scientific. All chemicals were used without further purification. Deionized water was obtained by purification through a Millipore system to at least 18Ω before use.

Fisherfinest* Premium Cover Glasses (Fisher Scientific, 12-548-5P) were cleaned with 4 consecutive sonications, 30 minutes each in 10% NaOH, distilled water, acetone, and deionized water. Silicon wafers (Si 1-0-0) were obtained from Ultrasil Corporation and used without any cleaning.

3.3.2 Polyelectrolyte Film Deposition

Polyelectrolytes, PAA and PAH, were diluted with Millipore water to 0.02 M by monomer concentration and adjusted to pH 3.5 and 7.5, respectively, using NaOH and HCl, prior to deposition. For each monolayer, the substrate, either coverglass or silicon wafer, was set into the polyelectrolyte solution, PAA or PAH, for 15 minutes, placed in deionized water for three separate rinses of 2 min., 1 min. and 1 min., respectively, as initially detailed by Decher[1] and blown dry with nitrogen. One

bilayer consists of one layer each of PAA and PAH. The initial priming monolayer of PAH gives the extra half bilayer for each film. Films were stored as formed, at constant humidity and characterized within 3 months of deposition, though longer storage should not have harmed the films.

Ellipsometric measurements were made using a Gaertner L117C Ellipsometer with a 1 mW HeNe laser (Gaertner Scientific Corporation) at an incident angle of 70º. Samples for ellipsometric thickness measurement were PEM films deposited on silicon wafers with or without solgel absorbed within the film. To prepare a composite film of PEM with solgel, a solgel solution, aged less than 5 days and usually 24 hours old to ensure a lower viscosity solution, was absorbed into the PEM thin films by placing one end of the PEM thin films in the solgel solution approximately 0.5 cm.

SEM images were obtained for 5.5- and 8.5-bilayer PAA/PAH films on coverglasses using a JEOL JSM-880 scanning microscope, at 15kV.

3.3.3 Single Molecule Dye Sample Preparation

R6G was diluted to 4.2×10^{-7} M in 95% ethanol and added to a solgel solution of TEOS, H_2O, and ethanol at a volume ratio of 3.5:2:7 (1.411 mL, 800 μL, and 2.817 mL) with catalytic phosphoric acid (15.6 μL of 0.148 M) to a final R6G concentration of 1.7×10^{-9} M and a total volume of 5 mL. One edge of the substrate with a 5.5-bilayer PAA/PAH film was submerged approximately 0.5 cm in fresh R6G/solgel solution for 20 minutes. The solgel-impregnated PEM composite film was characterized by single molecule fluorescence spectroscopy using a homebuilt

confocal microscope detailed previously.[24]   Mobilities of the R6G molecules in the

composite film were determined from the emission polarization of each molecule

and compared to the mobility distribution of R6G molecules in a spincoated solgel

thin film, using the characterization scheme of fixed, tumbling and intermediate

molecules.

3.3.4 OG Thin Film pH Sensor Preparation

OG (8 μL) was added to a solgel solution of TEOS, water and ethanol (1.411

mL, 800 μL and 2.817 mL, respectively) at a volume ratio of 3.5:2:7 with catalytic

phosphoric acid (15.6 μL of 0.148 M) to a final OG concentration of 34 nM for the

spincoated solgel samples and 13 μM for the solgel-impregnated PEM composite

films. This solgel solution was either spincoated at 6100 rpm for 70 s or absorbed

into 5.5-bilayer PAA/PAH PEM films, as described above with R6G, before being

equilibrated with various citrate buffer solutions to conduct the pH response work.

Citrate buffers were prepared in appropriate ratios of citric acid and sodium citrate to

obtain pH values between pH 2.1 and pH 7.5. In order to apply buffer solutions to

the films, an open-ended glass tube, 2 cm in diameter, was affixed to the sample with

epoxy. Films were equilibrated with buffer solutions for at least 5 minutes before

spectra were collected.

A 13 μM solution of OG was also absorbed directly into 5.5-bilayer PEM

films to measure the emission spectrum of OG in the PEM film. Emission spectra of

OG for the thin film samples were acquired using a spectrophotometer (Spectra Pro

150, Acton Research) and CCD camera (LN400, Roper Scientific), using 488 nm

excitation and an integration time of 120 s. Three consecutive spectra were obtained

after the equilibration period to ensure the equilibration time was sufficient. Since

this work focused on characterizing the response and not optimizing the response

time, the equilibration time was not minimized. During fluorescent imaging as well

as gathering emission spectra, the sample was moved with nanometer precision by a

nanostage (17ANC001/MD, Melles Griot) and raster scanned.

Excitation spectra were collected for 13.75 µM OG in 0.02 M solutions of

PAA or PAH in plastic cuvettes using a Shimadzu RF-5301 PC

Spectrofluorophotometer.

3.4 RESULTS AND DISCUSSION

3.4.1 Polyelectrolyte Multilayer Films as a Scaffold

The porous structure of PEM thin films has been well-established. Both of

the structures in Figures 3.1a and 3.1b are known to network throughout the films

and seem to be characteristic of different thickness films. A concentrated R6G

solution was used to test the capability of the PEM films to absorb solutions and

contain the absorbed solution. When one edge of a PEM film is placed in

approximately 0.5 cm of a 10^{-5} M solution of R6G the capillary effect pulls the dye
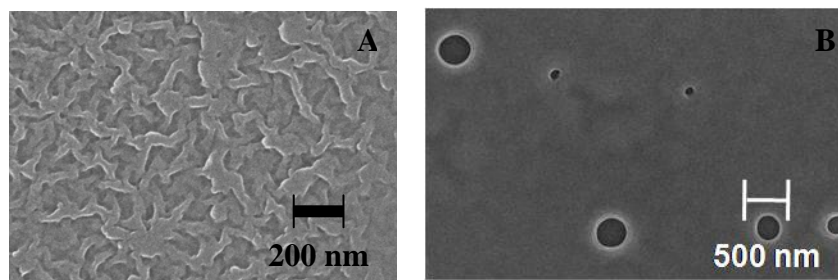
Figure 3.1 – SEM images of 5.5-bilayer (A) and 8.5 bilayer (B) PEM films.

solution into the PEM thin film. After 20 minutes, R6G had traveled approximately

2 cm up the 5.5-bilayer PEM film and a clear front was imaged, Figure 3.2. Though

the bright red solution was not visible to the naked eye, a simple fluorescent image
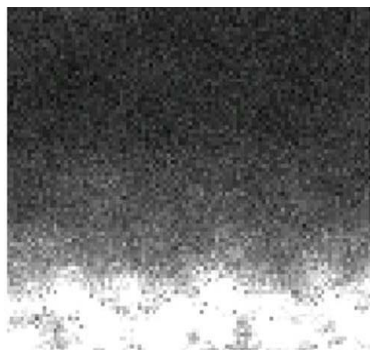
detected the absorbed dye solution. In a preliminary test when the film was allowed to absorb an R6G solution for 40 minutes, the R6G solution had been absorbed throughout the entirety of the 6 cm long PEM film.

Figure 3.2 – Fluorescent image of R6G soaked directly into 5.5-bilayer PEM film

Integral to the application of PEM films as scaffolds is their ability to hold their form upon integrating the sensor molecules. The PAA/PAH

polyelectrolyte films have controllable thicknesses and can be built-up, Figure 3.3,

by controlling the pH of the solutions during deposition and continuing the

deposition procedure. The layer-by-layer deposition process of these PEM films

provides the unique ability to form a thin film to specific thicknesses.
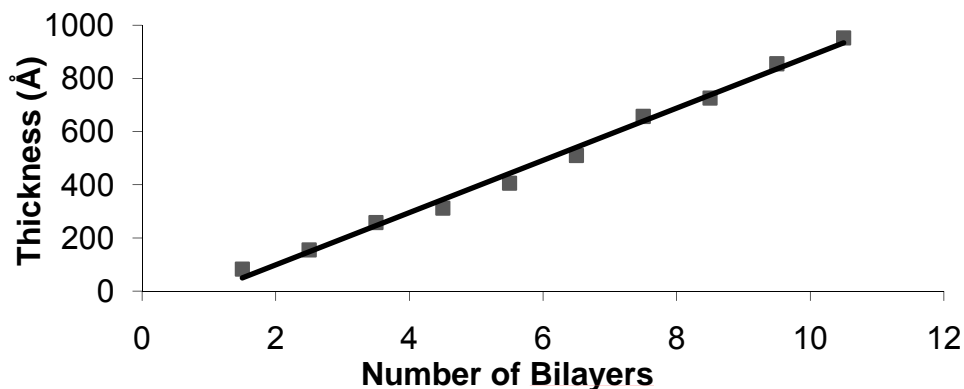
Figure 3.3 – Layer-by-layer thickness control of PEM film; PAA/PAH 3.5/7.5.

PEM thin films have characteristic thicknesses depending on the polyelectrolytes used as well as the pH of deposition. As Rubner's group has shown, PAA at pH 3.5 with PAH at pH 7.5 gives a high thickness for the PAA/PAH PEM films.[7] The thickness of the film can be altered with molecular-level thickness control during deposition by adding layers, or post-deposition by soaking the film in a buffer solution that exceeds the pK_a of the polyelectrolytes. Soaking 5.5-bilayer PAA/PAH films in pH 2.5 solution for 60 s caused the films to almost double in thickness, from 860 Å to 1470 Å. These features are not common to other types of thin films.

The pH range available to the composite film is limited by the inability of the polyelectrolytes to adhere to the substrate below pH 2 and the dissolution of silicates at pH values above 8. Within this pH range, the polyelectrolytes employed should not change interactions, and likewise thickness of the film, significantly.

In order to apply the thickness control of PEM films to solgel films, a solgel solution was absorbed into the PEM films. A 5.5-bilayer PEM film deposited on Si-100 wafers has a thickness of 750 ± 20 Å. After absorbing the solgel solution for 20 minutes and drying with nitrogen gas, the thickness of the 5.5-bilayer PAA/PAH films increased slightly to 820 ± 10 Å. The end of the PEM films that was below the surface of the solgel solution had an oily sheen; however, above that line the PEM film did not change appearance. The oily sheen was a product of the silicate solution adsorbing to the exterior of the film. The lack of the oily sheen above the level of the solgel solution indicates that the solgel solution was in fact absorbed into the

interior of the PEM film. The thickness of the PEM film increased only 10% when the solgel solution was absorbed. A profile of the film was measured by ellipsometry, which determined the thickness of the solgel-impregnated PEM film was consistent and independent of distance from the solution, see Figure 3.4. This is because the PEM film is determining the thickness of the composite film; the presence of the solgel absorbed in the PEM film does not affect the PEM film thickness.
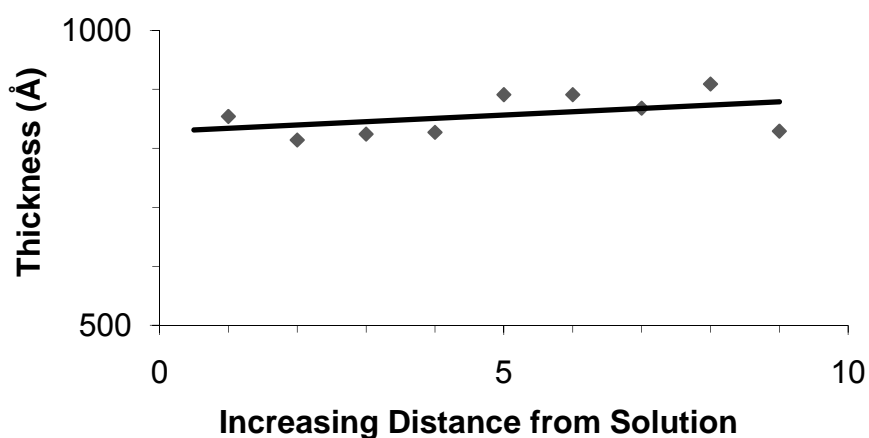
Figure 3.4. Ellipsometry measurements of the composite film. Measurements were taken approximately every 0.5 cm beginning near the solution discoloration line.

3.4.2 R6G Mobility in Composite Film

A composite film of solgel absorbed into a PEM thin film was formed by using the capillary effect, pulling a solgel solution within the PEM thin film. A solgel solution containing R6G was chosen for its clear comparison to our earlier work with R6G in silica alcogels.[24, 25] Absorbing a solgel solution containing R6G into the PEM thin film scaffold allowed the characterization of the composite film internal structure, where the dye molecules are residing. The rotational mobility of

the R6G dye molecules was analyzed to determine if absorbing the solgel solution

into the PEM thin film scaffold would alter the silica solgel structure. The mobility

of the probe dye molecules was determined using a fixed, tumbling or intermediate

classification scheme, dependent on the polarization of light emitted by the

molecules as detailed in previous work.[24] According to this classification scheme,

the 98 R6G molecules analyzed from the solgel-impregnated PEM films had the

following distribution: 32 % fixed, 1 % tumbling, 67 % intermediate, Table 1.

Table 3.1 – Comparison of R6G Mobility

Sample	Fixed	Tumbling	Intermediate
R6G in solgel[25]	23 ± 3 %	2 ± 1 %	75 ± 3 %
R6G in composite film	32 ± 5 %	1 ± 1 %	67 ± 5 %

The mobility of R6G in the composite films, solgel-impregnated PEM films,

is compared to the mobility of R6G in spincoated solgel films, also in Table 3.1. The

difference in mobility of R6G in the two thin films is minor. This indicates that the

size of the pores as well as the charge density of the pore environment in the

composite film is highly similar to the spincoated solgel film. Similar R6G mobility

distributions in the composite film and spincoated thin films demonstrate that the

PEM scaffold did not significantly perturb the structure formation of the solgel film.

3.4.3 pH Sensor Capabilities of OG in Composite Film

Important to sensor applications of the composite solgel-impregnated PEM film is the ability of analytes to access the interior of the film. Using OG, a pH-sensitive dye, the response of the films to external stimuli was tested. The changing emission spectra of OG in solution as a response to pH, Figure 3.5, were used for comparison to the thin films. Fitting the total peak area (Figure 3.5 inset) to the Henderson-Hasselbach equation gives an estimated pK_a value of 4.1 (mistakenly reported previously as 3.69).[26]
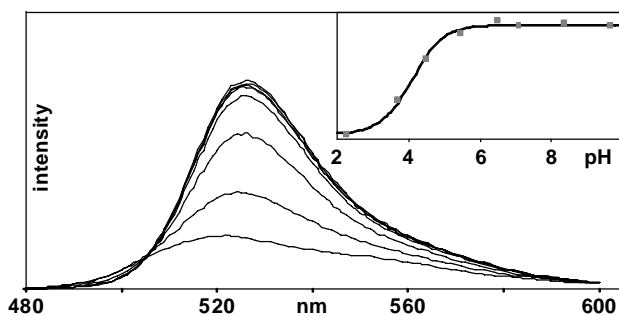
Figure 3.5– Fluorescence spectra of OG in bulk solution excited at 457 nm and monitored by a fluorometer. As the pH increases the peak sharpens, the peak maximum red shifts, and spectrum intensity reaches a plateau, indicating full deprotonation of the phenolic group. In the insert, the titration curve resulting from a consideration of total area under the peak is presented.[26]

Spincoated solgel thin films provided a comparison for the composite film. Cyclically adding and removing the same buffer solution to test reproducibility shows that at a single pH value, the overall intensity of OG emission decreases with time, Figure 3.6. Therefore, total peak area was not a consistent measure. This is due to the photobleaching and leaching of dye molecules. Therefore, the thin film

response to pH cannot be analyzed as dependent on overall intensity of the emission

peak.
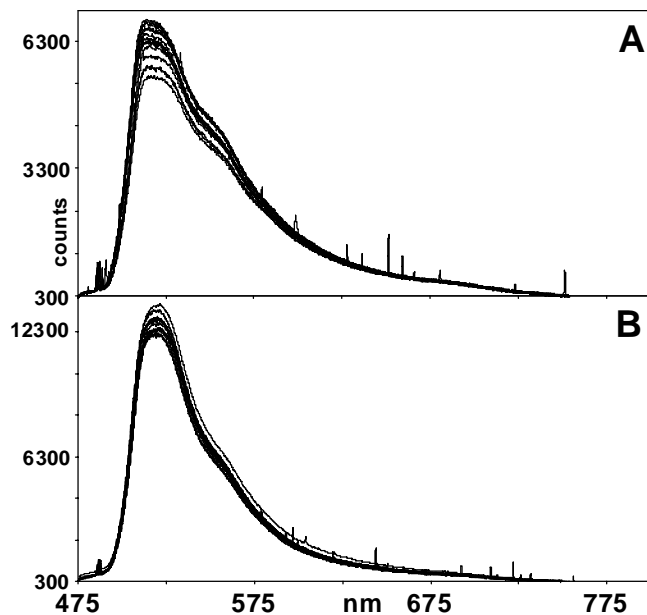
Figure 3.6 – The thin film intensity was found to be an unreliable indicator of the pH due to the OG intensity decrease over the course of testing. Presented are the spectra collected over 7 buffer cycles for the pH 3.6 (A) and pH 6.6 (B) data points. The pH 3.6 intensity maximum varies by $\approx$20% of the signal, and the pH 6.6 by $\approx$10%.[26]

The spincoated solgel films with a nanomolar OG concentration had pH-dependent peaks at 524 nm and 554 nm, corresponding to the protonated and deprotonated species of OG. In order to test OG response to pH change, buffers were cycled incrementally between pH 2 and pH 7.5 and allowed to equilibrate before each measurement. Figure 3.7 shows a reproducible and consistent pH-dependent response by OG with 20 minute equilibration. Plotting the ratio of the intensity of the peak at 524 nm to the peak at 554 nm and fitting to a Henderson-Hasselbach curve, OG in spincoated solgel has a pK_a of 4.3. Over 36 hours of

cycling the buffers, from pH 7 to pH 2 and back, there was little hysteresis of the signal, demonstrating the ability of OG to respond reproducibly to external stimuli. A pK$_a$ value of 4.3 is between the pK$_a$ value of OG in solution reported above, 4.1, and the published value of 4.7[27] It seems the solgel film does not hinder the response of OG to pH change as compared to solution.
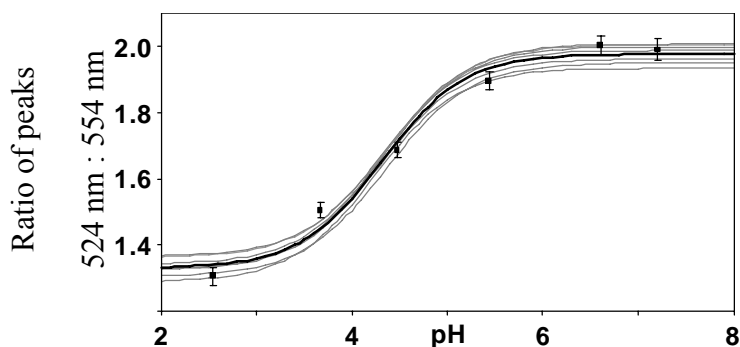
Figure 3.7 – pH Response of OG in spincoated solgel thin film as determined by the ratio of peaks at 524 nm and 554 nm (y-axis).[26] Average (black) and individual (grey) Henderson-Hasselbalch fits to seven buffer cycles over a 36 hour period. The black data points indicate the average value and standard deviation, which represents 2% RSD over the 36 hour period. The solid line indicates the Henderson-Hasselbalch fit to the solution response with a pKa of 4.3.

As opposed to the mobility of R6G, where it seems the dye is sensing a similar environment in the solgel thin film and the composite film, the pH-sensitive dye, OG, is able to detect a change in the local environments between the spincoated solgel film and the composite film. In addition to the peak ratio indicating the protonation of OG, the peak shape of OG emission in the spincoated silica thin film also indicates that self-absorption of OG would not be expected from this sample as the peak shoulder has a much lower intensity than the peak.[28] The presence of the

PEM film adds a new dimension of complexity in the emission spectrum. In Figure 3.8, the emission spectrum of OG in a PEM film has the two pH-dependent peaks of OG at 533 nm and 545 nm, and a signal due to scattered light from the PEM film between 560 nm and 625 nm that interferes with a clean, two-peak spectrum of OG. Though the pH-dependent peaks are still dominant, there are also smaller peaks at 650 nm, 732 nm and 770 nm. The pH-dependent peaks are shifted somewhat from OG in spincoated solgel, but still appear to be a peak and its shoulder. OG absorbed directly into the PEM scaffold demonstrates that the many extra features in the emission spectra are due to interactions between the dye and the polyelectrolyte scaffold. These features persist in the composite film with OG.
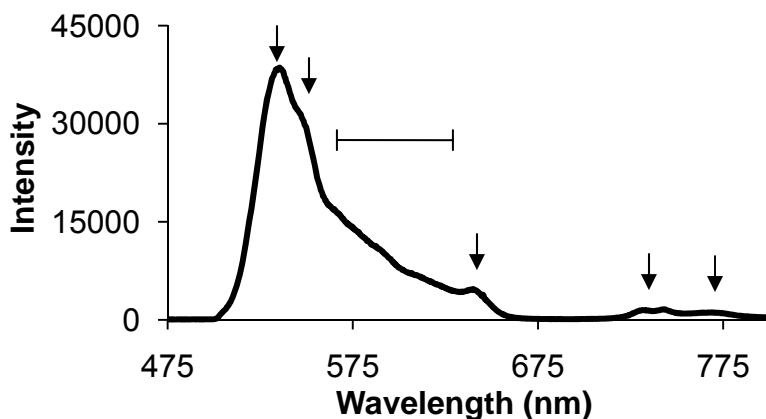
Figure 3.8 – Emission of OG absorbed into 5.5-bilayer PEM film. Compared to the emission spectra of OG in solution or OG in a solgel film, OG in a PEM film has a much broader spectrum, including peaks at 533 nm, 545 nm, 635 nm, 732 nm, and 770 nm.

In the emission spectra of OG in the composite solgel-impregnated PEM film, Figure 3.9, the two characteristic OG peaks have the same peak position as OG in the PEM scaffold. However, the OG emission intensity is dramatically reduced, even though the OG concentration was the same for both the composite film and the PEM film. This reduction in emission intensity causes the signal to noise ratio to be reduced as well, and the scattered light signal becomes more predominate. Figure 3.9 shows the emission spectra of OG in the composite film at 5 different pH values.
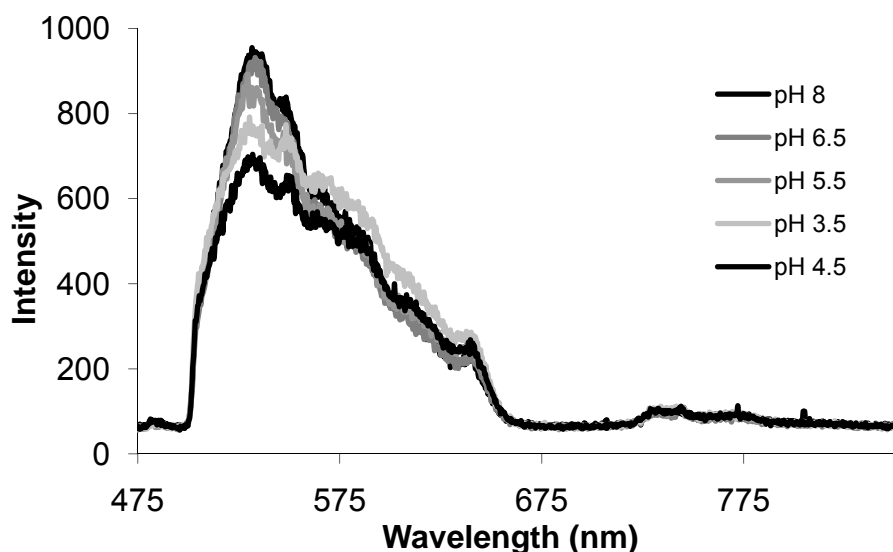
Figure 3.9 – Emission spectra of OG in composite film at each pH the film was equilibrated. In the composite film, OG emission peaks at 533 nm and 545 nm are pH dependent. The scattered light signal is independent of pH though it seems high, similar to OG in the PEM film.

The peaks at 533 nm and 545 nm indicate the level of protonation of the dye molecules.[29] The peak at 533 nm corresponds to the protonated OG population, while the peak at 545 nm corresponds to the deprotonated OG population. The protonated OG species is most likely the neutral species of the molecule, while the

deprotonated OG is the monoanionic species, having lost the carboxylic acid proton.[29] Fitting the ratio of the two pH-dependent peaks with a Henderson-Hasselbach curve, Figure 3.10, gives a pK$_a$ value of 4.6 for OG in the composite film. OG in the composite material responds to pH change much as OG in solution, pK$_a$ 4.7, as published by Lakowicz.[27]
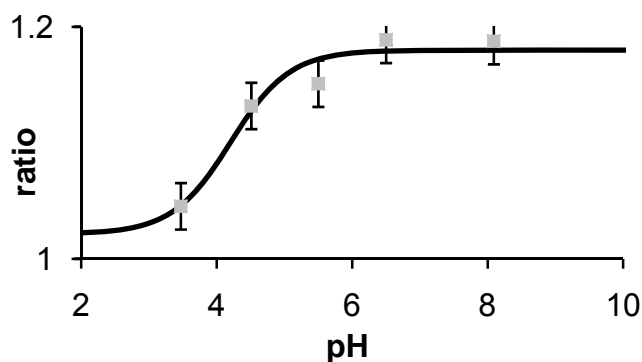
Figure 3.10 – Henderson-Hasselbach fit to the pH response of OG in the composite film. This fit gives a pKa of 4.6 using the ratio of the peak at 533 nm to the peak at 545 nm.

Since the single-molecule images do not show a drop in intensity between R6G in the solgel thin film sample and R6G in the composite film, Figure 3.11, the cause of the intensity drop in the composite film is unknown, however, there are a few possibilities to consider. First, when a fresh solgel solution with OG was absorbed into the PEM film, the intensity of OG emission was high as expected, Figure 3.12. Therefore, the PEM film is not impairing diffusion of the dye molecules into the film. The PEM scaffold is not interacting with the electronic structure of the dye molecules reducing fluorescence either. The intensity decrease with buffer exchange points to leaching of dye molecules, Figure 3.12. However, the

intensity drop during buffer exchange is comparable to the decrease in emission

intensity of OG in solgel during buffer exchange, Figure 3.6. Therefore, leaching
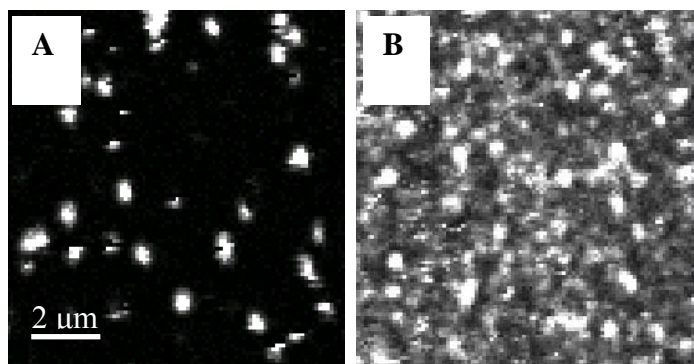
Figure 3.11 – Emission intensity comparison between the spincoated thin film, scaled to 100 counts (A) and the composite film, scaled to 250 counts (B). Dye molecules are nearly the same intensity, but background levels in the composite films are much higher.
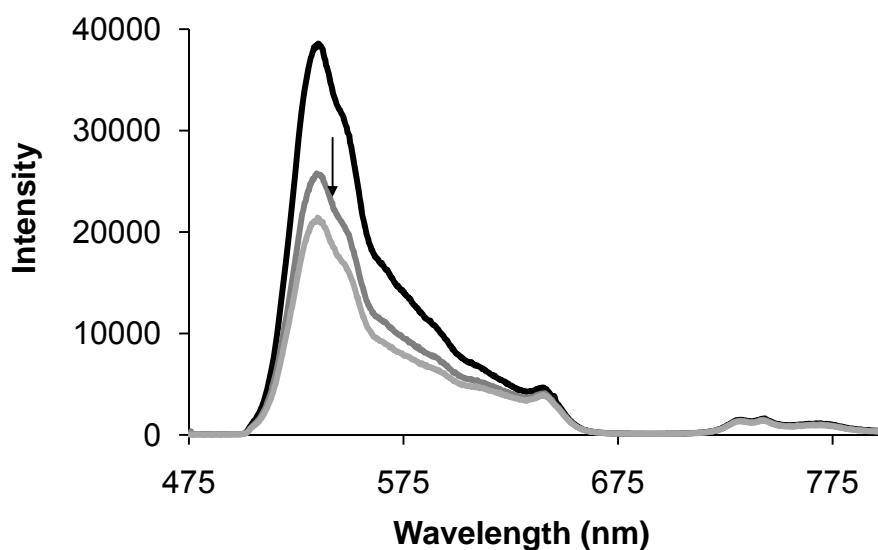
Figure 3.12 – Consecutive measurements of OG in PEM film with unbuffered water; intensity decreases by 66% as the buffer was cycled.

alone cannot explain the dramatic decrease in emission intensity. Second, there is a

difference in thickness between the spincoated film and the composite film, which

means fewer dye molecules are in the area being sampled. The spincoated solgel film is 200 nm thick whereas the PEM film is only 80 nm thick. The PEM film sample volume is then one-third the volume of the spincoated film. One-third the emission intensity could be expected if the smaller film volume being sampled held a comparable dye volume. However, the intensity difference attributable to a difference in thickness is only one-fourth of the total reduction in emission intensity. And the emission intensity of OG did not decrease in the PEM film alone, Figure 3.12, which counters the thickness explanation. It was only in the presence of both the solgel and PEM scaffold that OG emission intensity was dramatically reduced. The combination of solgel and the PEM film has reduced the detectable emission intensity of OG.

However, the OG emission spectra have more information than just intensity changes. The less intense peaks in the OG emission spectrum near 732 nm give more insight into the environment of the OG molecules in the PEM film and in the composite film as the peaks near 732 nm are only present when the PEM scaffold is part of the sample. It is possible OG may be interacting with either polyelectrolyte, PAA or PAH, of the PEM scaffold. The peaks near 732 nm seem to be pH-independent. The lack of pH-dependence helps to narrow down the possibilities of what OG interaction is producing the long wavelength peaks. Monitoring the emission of OG at 732 nm while collecting excitation spectra shows where OG absorbs when it emits at 732 nm. In an aqueous solution of PAH, OG emission at 732 nm seems to have excitation peaks near 520 nm and 635 nm, and neither of the

excitation peaks appears to change significantly with pH, Figure 3.13. In a solution of PAA, OG emission at 732 nm seems to be pH-independent with excitation between 600 nm and 700 nm, Figure 3.14. However, in less acidic conditions, those with pH values significantly above the pKa of PAA, there is another excitation peak near 520 nm that has a pH-dependent intensity. Because the emission peaks near 732 nm are pH-independent through the pH range tested, it is likely the emission at 732 nm is due to excitation between 600 and 700 nm where OG was excited in both solutions. Since the peaks at 732 nm are pH-independent, emission at 732 nm cannot be linked singularly to the interaction between OG and PAH or OG and PAA; both interactions can yield OG emission at 732 nm that is pH-independent. However, the thin films were excited with 488 nm laser light. This leads to the possibility that the small emission peaks near 732 nm in the PEM film and in the solgel-impregnated PEM film may be due to absorbing light emitted by other OG molecules in the sample. The possibility of self-absorption is likely as the high shoulder seen for OG emission in the composite film is characteristic of self-absorption. This has been noted for zeolite systems,[28] which are comparable to the composite film in their ability to hold dye molecules at a fixed distance from each other.
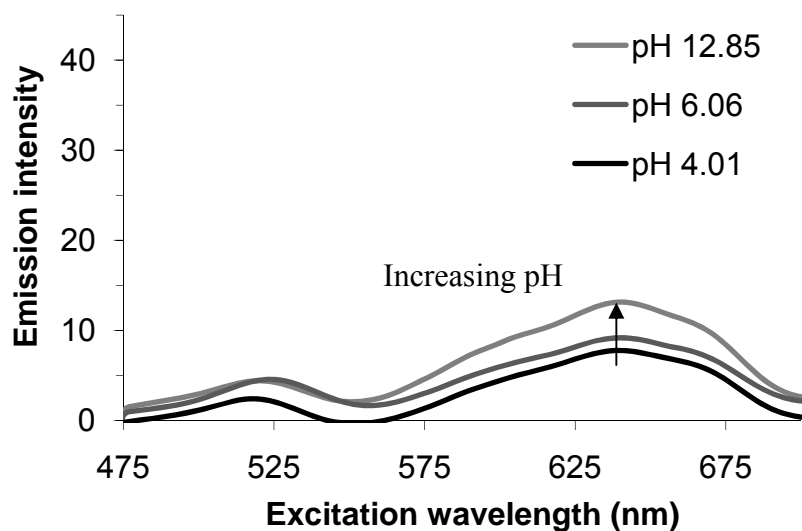
Figure 3.13 – OG in PAH pH-independent excitation spectra; emission monitored at 732 nm.
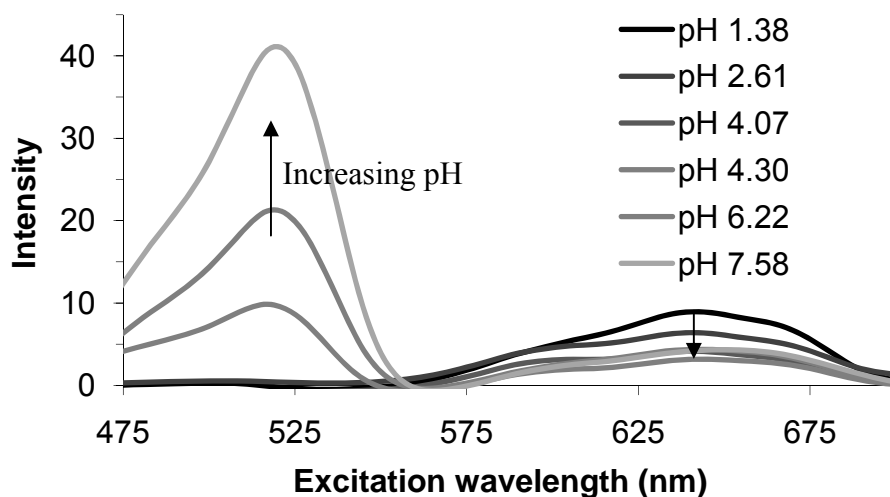
Figure 3.14 – OG in PAA pH-dependent excitation spectra; emission monitored at 732 nm. The peak at 520 nm is clearly pH-dependent with pH values above 4, while the peak near 635 nm is not highly pH-dependent.

Either excitation at 635 nm or 520 nm could explain OG emission at 732 nm in PAA and PAH. However, absorption at 520 nm is more pH-dependent than

absorption at 635 nm in PAA. Though absorption at 520 nm due to an alternate wavelength available from the Ar^+ laser seems more likely, due to the intensity of light available, emission at 732 nm due to absorption at 520 nm should be more pH-dependent, because it was highly pH-dependent in the PAA solution. Therefore, the pH-independent OG emission at 732 nm is likely a result of self-absorption or reabsorption of the emission at 635 nm.

Since OG emission spectra in separate PAA or PAH solutions do not show the peak at 635 nm that seems to cause the OG emission at 732 nm (spectra not included), it seems that OG in the PEM film is interacting with both the PAA and PAH to emit at 635 nm. The emission at 635 nm then excites other OG molecules which emit at 732 nm, though with much less intensity and independent of pH. A comparison of the excitation spectra and emission spectrum for OG is given in Figure 3.15, showing the presence of an emission peak near 635 in the PEM film which could be the source of excitation for the longer wavelength emission peaks. Since these long wavelength peaks are present in both the PEM film as well as the composite film, this is evidence that OG in the solgel-impregnated PEM film also interacts with the PAA and PAH of the PEM film and is not surrounded exclusively by the solgel network.
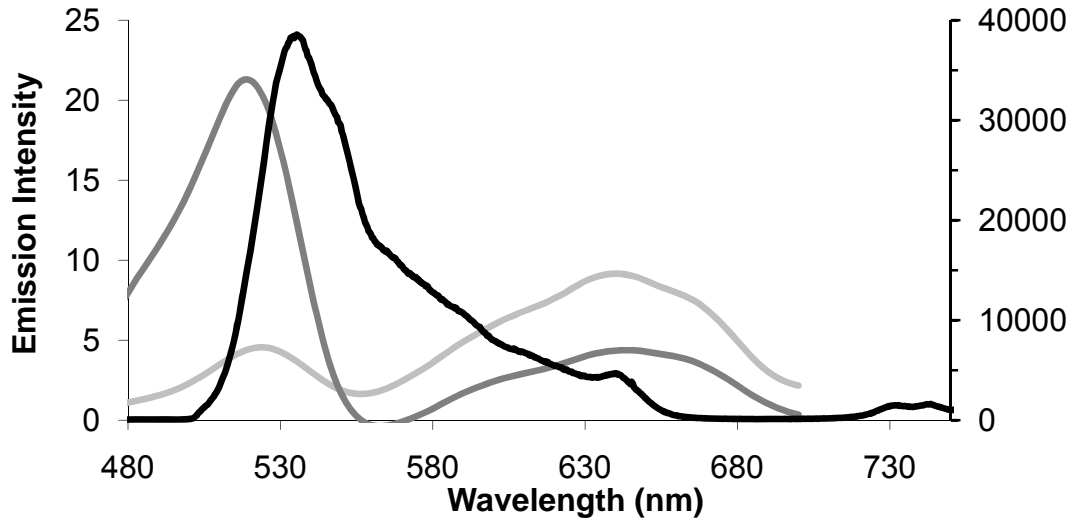
Figure 3.15 – Comparison of OG emission spectrum in the composite film (black; excited at 488 nm) and excitation spectra in each of the polyelectrolyte solutions (OG in PAA, dark gray; OG in PAH, light gray). Emission was monitored at 732 nm for each of the excitation spectra.

3.5 CONCLUSION

The thickness control of polyelectrolyte thin films has been granted to a silica solgel film by absorbing the solgel solution into a 5.5-bilayer PEM thin film. Characterization of the solgel-impregnated PEM composite films by single molecule spectroscopy and bulk fluorescence spectroscopy indicates that the porosities of the silica solgel network and the polyelectrolyte thin film have been maintained. When the PEM thin films and solgel material are combined, the mobility of R6G molecules and pH response of OG molecules in the solgel-impregnated PEM composite films are consistent with the spincoated solgel films. Furthermore, the combination of the solgel matrix and the PEM film seems to be a truly composite film as the emission spectra of OG have new features when in the PEM film as compared to the solgel

film. The dye does not reside in the solgel alone but also interacts with the polyelectrolyte matrix. This work demonstrates the ability of PEM thin films to act as a scaffold system to host other materials of interest without compromising the structure of the PEM film.

3.6 REFERENCES

1.   Decher, G., Fuzzy nanoassemblies: Toward layered polymeric multicomposites. *Science* **1997**, 277, (5330), 1232.

2.   Yoo, D.; Shiratori, S. S.; Rubner, M. F., Controlling Bilayer Composition and Surface Wettability of Sequentially Adsorbed Multilayers of Weak Polyelectrolytes. *Macromolecules* **1998**, 31, (13), 4309-4318.

3.   Lee, S.-S.; Lee, K.-B.; Hong, J.-D., Evidence for Spin Coating Electrostatic Self-Assembly of Polyelectrolytes. *Langmuir* **2003**, 19, (18), 7592-7596.

4.   Chiarelli, P. A.; Johal, M. S.; Holmes, D. J.; Casson, J. L.; Robinson, J. M.; Wang, H.-L., Polyelectrolyte Spin-Assembly. *Langmuir* **2002**, 18, (1), 168-173.

5.   Burchardt, M.; Wittstock, G., Kinetic studies of glucose oxidase in polyelectrolyte multilayer films by means of scanning electrochemical microscopy (SECM). *Bioelectrochemistry* **2008**, 72, (1), 66-76.

6.   Zhang, S.; Yang, W.; Niu, Y.; Li, Y.; Zhang, M., Construction of glucose biosensor based on sorption of glucose oxidase onto multilayers of polyelectrolyte/nanoparticles. *Anal. Bioanal. Chem.* **2006**, 384, 736-741.

7.   Shiratori, S. S.; Rubner, M. F., pH-Dependent Thickness Behavior of Sequentially Adsorbed Layers of Weak Polyelectrolytes. *Macromolecules* **2000**, 33, (11), 4213-4219.

8.   Hiller, J. A.; Rubner, M. F., Reversible Molecular Memory and pH-Switchable Swelling Transitions in Polyelectrolyte Multilayers. *Macromolecules* **2003**, 36, (11), 4078-4083.

9.   Yang, S. Y.; Mendelsohn, J. D.; Rubner, M. F., New Class of Ultrathin, Highly Cell-Adhesion-Resistant Polyelectrolyte Multilayers with Micropatterning Capabilities. *Biomacromolecules* **2003**, 4, (4), 987-994.

10.   Zhai, L.; Nolte, A. J.; Cohen, R. E.; Rubner, M. F., pH-Gated Porosity Transitions of Polyelectrolyte Multilayers in Confined Geometries and Their Application as Tunable Bragg Reflectors. *Macromolecules* **2004**, 37, (16), 6113-6123.

11.   Tan, H. L.; McMurdo, M. J.; Pan, G.; Van Patten, P. G., Temperature Dependence of Polyelectrolyte Multilayer Assembly. *Langmuir* **2003**, 19, (22), 9311-9314.

12.   Zhai, L.; Cebeci, F. C.; Cohen, R. E.; Rubner, M. F., Stable Superhydrophobic Coatings from Polyelectrolyte Multilayers. *Nano Lett.* **2004**, 4, (7), 1349-1353.

13.   Mendelsohn, J. D.; Barrett, C. J.; Chan, V. V.; Pal, A. J.; Mayes, A. M.; Rubner, M. F., Fabrication of Microporous Thin Films from Polyelectrolyte Multilayers. *Langmuir* **2000**, 16, (11), 5017-5023.

14.   Huang, M. H.; Dunn, B. S.; Zink, J. I., In Situ Luminescence Probing of the Chemical and Structural Changes during Formation of Dip-Coated Lamellar Phase Sodium Dodecyl Sulfate Sol-Gel Thin Films. *J. Am. Chem. Soc.* **2000**, 122, (15), 3739-3745.

15.   Chang, S.-m.; Doong, R.-a., ZrO_2 thin films with controllable morphology and thickness by spin-coated sol-gel method. *Thin Solid Films* **2005**, 489, (1-2), 17-22.

16.   Diaz-Parralejo, A.; Guiberteau, F.; Caruso, R., Influence of heat treatment on thickness and porosity of ZrO_2 thin films obtained by sol-gel route. *Bol. Soc. Esp. de Ceram. Vid.* **2004**, 43, (2), 477-479.

17.   Doherty, W. J., III; Armstrong, N. R.; Saavedra, S. S., Conducting polymer growth in porous sol-gel thin films: formation of nanoelectrode arrays and mediated

electron transfer to sequestered macromolecules. *Chem. Mater.* **2005**, 17, (14), 3652-3660.

18.   Sun, D.; Zhang, R.; Liu, Z.; Huang, Y.; Wang, Y.; He, J.; Han, B.; Yang, G., Polypropylene/silica nanocomposites prepared by in-situ sol-gel reaction with the aid of CO_2. *Macromolecules* **2005**, 38, (13), 5617-5624.

19.   Hsiao, C. N.; Huang, K. S., Synthesis, characterization, and applications of polyvinylpyrrolidone/SiO_2 hybrid materials. *J. Appl. Polym. Sci.* **2005**, 96, (5), 1936-1942.

20.   Chen, G.; Zhou, S.; Gu, G.; Wu, L., Acrylic-based polyurethane/silica hybrids prepared by acid-catalyzed sol-gel process: Structure and mechanical properties. *Macromol. Chem. Phys.* **2005**, 206, (8), 885-892.

21.   Shi, Y.; Seliskar, C. J., Optically Transparent Polyelectrolyte-Silica Composite Materials: Preparation, Characterization, and Application in Optical Chemical Sensing. *Chem. Mater.* **1997**, 9, (3), 821-829.

22.   Kim, H.-J.; Ahn, J.-E.; Haam, S.; Shul, Y.-G.; Song, S.-Y.; Tatsumi, T., Synthesis and characterization of mesoporous Fe/SiO_2 for magnetic drug targeting. *J. Mater. Chem.* **2006**, 16, (17), 1617-1621.

23.   Chung, A. J.; Rubner, M. F., Methods of Loading and Releasing Low Molecular Weight Cationic Molecules in Weak Polyelectrolyte Multilayer Films. *Langmuir* **2002**, 18, (4), 1176-1183.

24.   Gilliland, J. W.; Yokoyama, K.; Yip, W. T., Effect of Coulombic Interactions on Rotational Mobility of Guests in Sol-Gel Silicate Thin Films. *Chem. Mater.* **2004**, 16, (20), 3949-3954.

25.   Gilliland, J. W.; Yokoyama, K.; Yip, W. T., Comparative Study of Guest Charge-Charge Interactions within Silica Sol-Gel. *J. Phys. Chem. B* **2005**, 109, (11), 4816-4823.

26.   Gilliland, J. Single-Molecule Spectroscopic Investigation of the Influence that Charge-Charge Interactions, Solvation, and Confinement have on Guest Molecule Rotational Mobility and Photostability within Silica Sol-Gel Host Matrices. University of Oklahoma, Norman, 2006.

27.   Lin, H.-J.; Szmacinski, H.; Lakowicz, J. R., Lifetime-Based pH Sensors: Indicators for Acidic Environments. *Anal. Biochem.* **1999**, 269, (1), 162-167.

28.   Yatskou, M. M.; Meyer, M.; Huber, S.; Pfenniger, M.; Calzaferri, G., Electronic Excitation Energy Migration in a Photonic Dye - Zeolite Antenna. *ChemPhysChem* **2003**, 4, (6), 567-587.

29.   Orte, A.; Crovetto, L.; Talavera, E. M.; Boens, N.; Alvarez-Pez, J. M., Absorption and Emission Study of 2',7'-Difluorofluorescein and Its Excited-State Buffer-Mediated Proton Exchange Reactions. *J. Phys. Chem. A* **2005**, 109, (5), 734-747.

Chapter IV

Single Molecule Spectroscopic Analysis of the Complexation of

Cationic Rhodamine 6G by Cucurbit[7]uril

4.1 CHAPTER ABSTRACT

Cucurbit[7]uril (CB7)-complexation of rhodamine 6G (R6G) enhances R6G fluorescence properties in bulk solutions. This chapter extends the understanding of the dynamic complexation relationship between CB7 and R6G. Through single-molecule fluorescence measurements of CB7-complexed R6G, multiple sets of interactions are indicated between CB7 and R6G. Since the complexation is a non-covalent interaction, the orientation of R6G about CB7 is open to many conformations. The positioning of R6G is directed by the electronegative portal to the CB7 cavity which attracts the cationic portion of the R6G molecule. Of particular interest is whether R6G is complexed in a static conformation, or as part of a dynamic relationship with CB7. The interaction between CB7 and R6G seems to be continuous, though with changing extent of contact as R6G experiences greater or lesser complexation effects. The motion of R6G could include a straight translation in and out of the CB7 cavity, a rolling out of the CB7 cavity or a combination of motions. Movement of R6G in the CB7 cavity and possibly out of the CB7 cavity is suggested to cause fluctuations in the emission intensity enhancement provided by CB7-complexation. This leads to an understanding of a dynamic interaction on a single-molecule basis, not merely a collection of static interactions. Polarization

changes that seem to correspond to the change in intensity enhancement give further support to a dynamic complexation.

CB7-complexation also seems to extend the survival lifetime of R6G. Possible causes of photobleaching impacted by complexation include interactions between dye molecules or bombardment of R6G by solvent molecules. A complexation of R6G that provides partial encapsulation of the molecule would reduce the possibility of collisions that would lead to photobleaching, thus leading to a longer survival lifetime.

4.2 INTRODUCTION

The probing of photophysical properties of dyes on the single-molecule level is limited by the ability to study one molecule for an extended time, whether because of movement, low emission intensity, or low photostability of the molecules. In order to immobilize dye molecules, techniques such as encapsulation in organic macromolecules,[1, 2] inorganic matrices, such as solgel silicates[3] or zeolites,[4] or micelle-type structures, such as liposomes[5] have been utilized. Immobilizing the dye molecules with organic macromolecules commonly utilizes non-covalent interactions to form a macromolecular complex.[6] Cyclodextrins, calixarenes and cucurbiturils are common cage-like molecules capable of complexing molecules of different shapes, sizes and charges. Each group of macromolecules has characteristics that host certain guests more strongly. CB7, Figure 4.1, has similar dimensions as β-cyclodextrin[7] and has been shown to complex similar molecules,[8, 9] but is able to selectively bind to cationic molecules[10] due to its ring of highly electronegative

oxygen atoms that forms a crown at the two symmetric openings to its internal cavity.[7, 11] Rhodamine 6G (R6G), Figure 4.1, is expected to complex with CB7 by having a portion of the R6G molecule within the cavity of CB7. The electronegative portal of CB7 attracts the cationic portions of R6G which would add stability to the complex. With association constants near 10^5 M^{-1},[12] simply combining aqueous solutions of CB7 and R6G allows 1:1 complexation[13] to occur with millimolar CB7 and micromolar R6G concentrations.
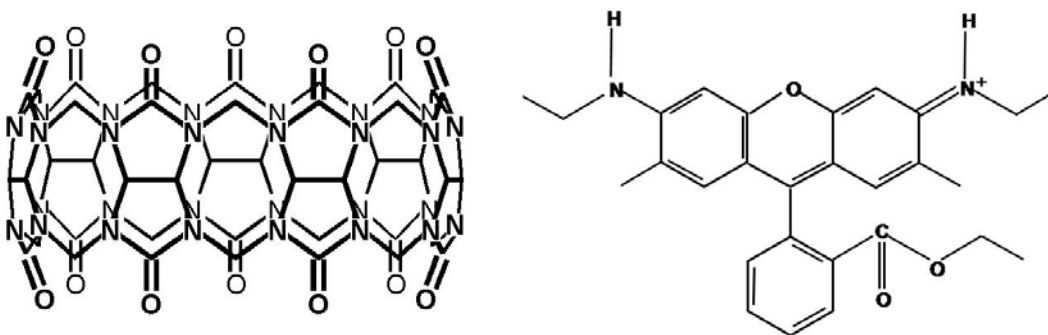
Figure 4.1 – Molecular structures of cucurbit[7]uril (left) and rhodamine 6G (right)

For fluorescence spectroscopy applications, using CB7 as an encapsulation method is an excellent choice. CB7 maintains an extremely low background, since it is not inherently fluorescent. CB7 also increases the signal to noise ratio by increasing the fluorescence emission intensity of the dye molecule.[14] While most of the matrices utilized to immobilize dye molecules interact with the electronic structure of the dye in a way that influences the fluorescence emission of the molecules, CB7 has the added advantage of allowing measurements of guest molecule properties in a near solvent-free environment due to the hydrophobic nature of the cavity.[15]

R6G is mobile on glass due to the water layer that accumulates in ambient conditions.[16] The interactions between a naturally negative glass surface and the cationic dye are not sufficient to immobilize the R6G molecules. Since CB7 is mostly hydrophobic, it is less likely to experience the same solubility by a thin layer of water and is capable of remaining stationary on the glass surface. The charge on R6G is complexed by CB7, masking the charged portion and causing the complex to seem more hydrophobic, while the combined size of an R6G/CB7 complex slows mobility. Together, size and hydrophobicity are expected to reduce R6G mobility when it is complexed.

Measuring the photostability, or survival lifetime, of dye molecules is a means to understand how the surroundings affect the fluorescence of the dye molecules. To improve the survival lifetime of individual molecules requires reducing the occurrences of photobleaching. The most common reasons for dyes to photobleach include: photo-oxidation,[17] intermolecular collisions and intramolecular motions that lead to conformations that favor photodegradation.[18] All of these processes can be affected by the complexation of a dye with a host. Intermolecular collisions and oxidations are reduced by surrounding or partially enclosing the dye molecule with a macromolecular host, limiting access to the dye molecule. Intramolecular motions are hindered as the host macromolecule commonly binds to a preferred conformation[19] or restricts the available space around the guest dye molecule.

Using R6G as a model dye molecule, complexation by the organic macromolecule, CB7, is sufficient to immobilize the cationic dye molecule, while enhancing the emission intensity and photostability of R6G on a single molecule basis. R6G is also a well-known dye molecule in terms of absorbance and emission spectra, which allows comparisons to other systems. With the goal of making highly concentrated, long-lasting, and bright optical materials, it is of fundamental importance to understand how CB7-complexation enhances fluorescence and reduces photobleaching. Exploring the nature of interaction between R6G and CB7 should lead to a better understanding of the fluorescence enhancement of CB7-complexed R6G.

4.3 MATERIALS AND METHODS

R6G/CB7 Deposition

One method to obtain the R6G/CB7 samples was by preparing a CB7 laminate film and dipping the film into an R6G solution. The laminate was prepared by pipetting 50 µL of 0.1 mM CB7 in distilled water onto a clean coverglass. The coverglasses were then placed onto a glass petri dish and heated on a hotplate at 50 °C to evaporate the excess water. The CB7 laminates were dipped into 100 nm R6G solutions and rinsed three times in distilled water to remove excess R6G and CB7. Though this procedure was adequate, the evaporation step of the CB7 laminate procedure required an extended preparation time and produced only a few immobilized R6G/CB7 complexes per sample area.

To reduce preparation time and improve the number density of complexes per 10 μm x 10 μm sample area, the majority of the R6G/CB7 complexes were spincoated onto a clean coverglass. 60 μL of an R6G and CB7 mixture (0.05 μM R6G and 50 μM CB7, originally formed with 1 mL 0.1 μM R6G and 1 mL 100 μM CB7) in 18 Ω Millipore water was spincoated onto a clean coverglass for 70 s at 6100 rpm. This preparation did not require additional rinse steps.

R6G in PEM/silica composite film

The polyelectrolyte (PEM)/silica composite film was used as a possible way to immobilize R6G molecules. First the 5.5-bilayer PEM film was deposited, as adopted from literature.[20-22] A coverglass was first primed with a layer of poly(allylamine hydrochloride) (PAH) by dipping the coverglass substrate into a 0.02 M PAH monomer solution for 15 min and then rinsed three consecutive times with Millipore water for 2 min, 1 min and 1 min, respectively. The PAH-primed coverglass was then subjected to alternate depositions of poly(acrylic acid) (PAA) at pH 3.5, and poly(allylamine hydrochloride) (PAH) at pH 7.5, to form 5-bilayers of PAA/PAH. For each deposition, the coverglass was immersed into a 0.02 M monomer solution of the appropriate polyelectrolyte for 15 min, then rinsed three times with Millipore water for 2 min, 1 min and 1 min, and blown dry with nitrogen before deposition of the next monolayer.

Separately, R6G was diluted to 1.8×10^{-5} M in 95% ethanol and added to a solgel precursor solution of tetraethyl orthosilicate (TEOS), H_2O, and ethanol at a ratio of 3.5:2:7 by volume (2.82 mL, 1.60 mL, and 5.63 mL) with catalytic

phosphoric acid (31.2 μL of 0.148 M H_3PO_4) to obtain a final R6G concentration of

140 nM. Then, one edge of the 5.5-bilayer PEM thin film was submerged

approximately 0.5 cm in 5 mL of the fresh R6G/silica solgel precursor solution for

20 min to absorb the R6G/silica solgel mixture. The composite film was blown dry

with nitrogen and stored in a closed dish in a dark, room-temperature cabinet before

it was examined by a confocal microscope.

Fluorescent images of all samples were obtained by raster scanning 10 μm x

10 μm areas at 100 nm x 100 nm resolution. Using the setup described earlier

(Section 2.4.1), individual molecules were photobleached and dye emission data

were collected via two APD detectors. From the emission data, the average emission

intensity, the time-resolved intensity, and the survival lifetime of the individual

molecules and complexes were extracted. Use of two detectors allowed analysis of

time-resolved polarization change during R6G and R6G/CB7 fluorescence emission.

4.4 RESULTS AND DISCUSSION

4.4.1 Immobilizing R6G

Cationic dyes are highly mobile on glass surfaces,[16, 23] limiting the types of

single-molecule measurements that can be performed with them. The first

achievement of CB7-complexation of R6G was to immobilize R6G on a clean

coverglass. Most measurements of stationary single molecules include the effects of

an immobilizing matrix, so the ability to acquire information about immobilized

single molecules without using a matrix is significant. As can be seen from the

fluorescent image in Figure 4.2A, cationic R6G is highly mobile when spincoated

onto a coverglass by itself. Though the glass was cleaned and dried before R6G was added to the surface, clean glass is known to attract a layer of water.[16] The single line streaks of fluorescence show the molecule had moved before the scan returned to that portion of the sample. Stationary molecules would appear as round, white spots because the molecule is still emitting from the same position each time the scan returns to that portion of the sample. Though R6G is mobile on glass, complexing R6G with CB7 yields stable, immobilized fluorescent signals from the dye molecules, Figures 4.2B and 4.2C.
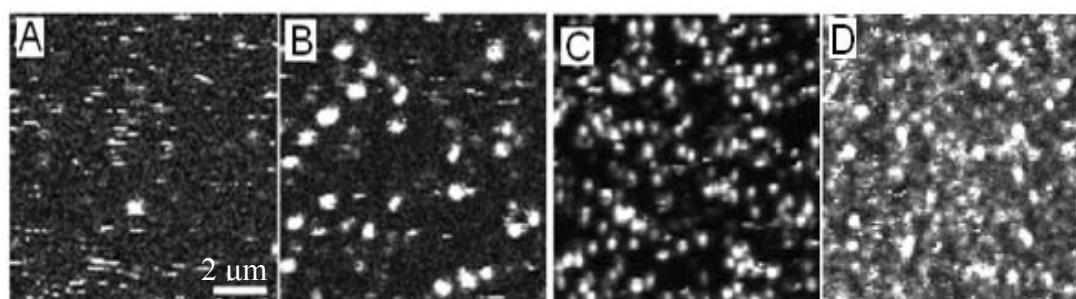
Figure 4.2 – The ability of CB7 to immobilize R6G on a coverglass is shown by the presence of round stationary fluorescent signals: A) R6G pipetted onto a coverglass and dried with nitrogen remains mobile, B) A CB7 laminate on a coverglass dipped into an R6G solution, rinsed with water, and dried with nitrogen yields several immobilized complexes, C) R6G/CB7 spin-coated onto clean coverglasses yields a high number of immobile complexes, D) R6G immobilized by a PEM/silica composite film. Image C demonstrates that R6G/CB7complexes were effectively immobilized on glass whereas image A indicates that under the same conditions, uncomplexed R6G appears to diffuse quite freely on the wet glass surface, creating numerous fluorescence streaks.

CB7-complexation has multiple effects on the interactions between R6G and the glass surface. R6G mobility relies on the water layer that adsorbs to the glass surface. Since the R6G/CB7 complex has a larger molecular weight than R6G alone, the complex will have a slower diffusion rate. Secondly, CB7 is mostly hydrophobic and will be more likely to adsorb to the glass, even in high humidity situations. Immobilization of R6G has been achieved by forming a film of CB7 on a coverglass prior to adding R6G in solution to the CB7 film, Figure 4.2B, as explained in section 4.3,[23] as well as by spincoating the R6G/CB7 mixture, Figure 4.2C. In order to immobilize R6G without CB7, a PEM/silica composite film was used as an immobilizing matrix. The background from the composite film is slightly higher, Figure 4.2D, but the molecules are still clearly distinct from background fluorescence levels.

4.4.2 CB7 Enhances R6G Fluorescence Emission Intensity

Since immobilization of the R6G/CB7 complexes has simplified single-molecule fluorescence measurements of the complexed-R6G by immobilizing R6G without interaction with an external matrix, the effects of CB7-complexation are more accessible. Ensemble measurements have shown CB7-complexation to increase fluorescence emission intensity of cationic dyes.[14, 24] However, there has been some evidence of the enhancement in solutions coming from reduction of non-specific adsorption,[12] not necessarily as an effect of complexation. On the single-molecule scale we have found that CB7-complexation does seem to enhance the emission intensity of R6G molecules.

The enhancement of R6G emission intensity upon complexation by CB7 is evident when the emission intensity is averaged for each R6G molecule or R6G/CB7 complex. Since R6G is known to go to 'dark states,' or times when it does not fluoresce under continuous excitation, a threshold was set and intensities below the threshold were not included in the average for the molecule. The threshold eliminates intensity values where R6G was not fluorescing for most of the time interval related to that data point. With a fluorescent lifetime of 4 ns[12] R6G could emit millions of photons during the 50 ms of each measurement interval and commonly emits more than 50 that are detected by the instrument. The threshold was set at two photons emitted during 50 ms, much less than would be expected for fluorescing R6G. Below the threshold R6G is not fluorescing during most of the 50 ms time interval of a data point.

A histogram of the average emission intensity for R6G shows most R6G molecules emit at less than 3000 Hz, Figure 4.3. Fitting the histogram with a Gaussian function, $f(x) = Ae^{\frac{-(x-\omega_0)^2}{2\sigma^2}}$, where σ is related to the full width at half of the maximum intensity (FWHM), shows there is a single preferred intensity for R6G molecules in the PEM/silica composite matrix, (950 Hz; σ = 950 Hz) Table 4.1. The corresponding histogram of R6G/CB7 complexes is both shifted to higher count rates and bimodal. Most R6G/CB7 complexes emit near 2,100 Hz (σ = 2400 Hz), however, a smaller population emits near 10,000 Hz (σ = 3,000 Hz). This indicates the complexation of R6G by CB7 has increased R6G fluorescent emission intensity on a single molecule level as well as in bulk solution.
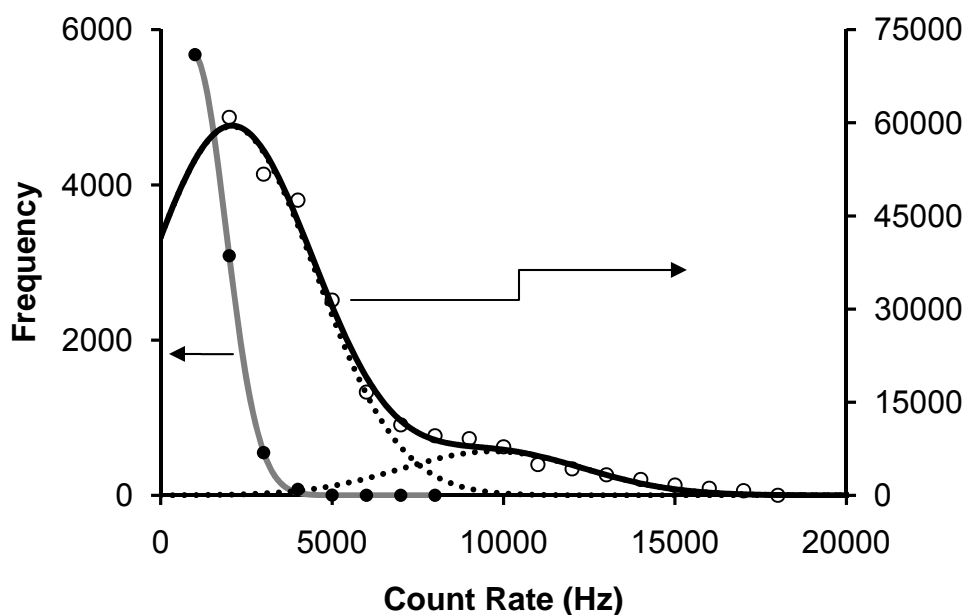
Figure 4.3 – Emission rate histogram of 103 R6G molecules (●), left axis, and 219 R6G/CB7 complexes (○), right axis. Dashed lines are Gaussian fittings to the emission-rate distributions; $R^2 = 0.9999$ and 0.9934 for R6G and R6G/CB7, respectively.

Table 4.1 – Gaussian Functions Fitting Parameters for Intensity Histogram

	Peak Max Frequency	Count rate center, ω_0 (Hz)	σ (Hz)	Ratio FWHM:$\omega_0^{1/2}$
R6G	5690 ± 20	950 ± 20	950 ± 20	72.6
R6G/CB7$_1$	59000 ± 2000	2100 ± 300	2400 ± 400	123
R6G/CB7$_2$	7000 ± 1000	10000 ± 1000	3000 ± 1000	70.6

The overlap of R6G emission intensities and the lesser intense of the

R6G/CB7 emission intensities implies the low intensity R6G/CB7 complexes may be

behaving as if CB7 is not in close enough proximity to enhance the fluorescence of

R6G. This is an acceptable result considering the non-covalent nature of CB7-

complexation, as well as the value of the equilibrium constant of association for the complex, which, though high, does not indicate uninterrupted complexation.

4.4.3 Variety of Emission Intensities Points to Dynamic Motion

The inclusion of R6G by CB7 increased the average emission intensity of the R6G molecules, but not uniformly. As shown by the presence of two peaks in the gaussian fitting of the R6G/CB7 emission intensity histogram and the increased width of the peaks, R6G/CB7 complexes have 2 main average emission intensities with the average among the complexes varying more than for R6G molecules (R6G FWHM 2,240 Hz, R6G/CB7$_1$ FWHM 5,700 Hz, and R6G/CB7$_2$ FWHM 7,000 Hz). This bimodal histogram indicates either dynamic complexation of R6G by CB7, or multiple static conformations.

The larger peak width of intensities due to R6G/CB7 complexes as compared to R6G molecules, Figure 4.2, demonstrates the greater variety of average emission intensities measured for R6G/CB7 complexes as opposed to the narrow peak and almost singular average emission intensity of R6G when not complexed. A wider peak indicates greater heterogeneity between R6G/CB7 complexes. The peak widths are statistically large considering Poisson statistics, where a stronger signal has an expected larger quantity of noise. Qualitatively, the fittings indicate the R6G peak should have the smallest full width at half maximum intensity (FWHM), as it has the lowest peak frequency. However, the R6G sample is 72.6 times wider than expected due to random shot noise. The R6G/CB7$_1$, low count rate peak, is 123 times wider than expected with Poisson statistics and the R6G/CB7$_2$, high count rate peak, is

wider than statistically expected by a factor of 70.6. In all cases, the width of the peak is much greater than the shot noise allowance. This means R6G in the PEM/silica composite film still possesses heterogeneity in this composite matrix, as would be expected from a solgel silicate. However, the increase in heterogeneity in the R6G/CB7 complexes is greater, as there are two peaks with similar quantities of excess peak width as R6G (FWHM:$\omega_o^{1/2}$).

Considering R6G is a T-shaped molecule and only one portion of R6G can fit within the CB7 cavity at a time, an incomplete complexation is expected. The distribution width of R6G/CB7 intensities suggests that not all R6G/CB7 complexes are experiencing equal fluorescence enhancement when R6G is complexed. This may be due to varied complexation conformations as complexes are compared to each other, or a dynamic complexation conformation for each molecule.

Figure 4.4 – Molecular modeling of a possible R6G/CB7 inclusion complex

A collection of static complexations could produce a variety of average intensities, though each molecule would be expected to emit at one count rate. However, a dynamic relationship between R6G and CB7 would be expected to have a much wider variety of average intensities as a whole and each individual complex

could also emit at multiple emission intensities. The main differences between static complexation and dynamic complexation would be the peak width of the average intensity histogram and the ability of individual complexes to emit at substantially different intensities.

4.4.4 Dynamic R6G/CB7 Conformations

A set of multiple static conformations would mean each molecule emits at a single intensity. If the relationship between R6G and CB7 is composed of dynamic motions and this in turn changes the amount CB7 is able to enhance the fluorescence of R6G, the emission intensity of a single molecule should be dynamic as well, increasing as the extent of complexation increases and decreasing as the extent of complexation decreases. Further analysis of the fluorescent emission of individual R6G/CB7 complexes substantiates a changing influence of CB7 on the emission intensity of R6G. Individual R6G/CB7 complexes emit at different rates during different portions of their fluorescence. A histogram was constructed of the count rates for each 50 ms time interval for an individual R6G/CB7 complex. Figure 4.5 shows histograms for four different R6G/CB7 complexes.
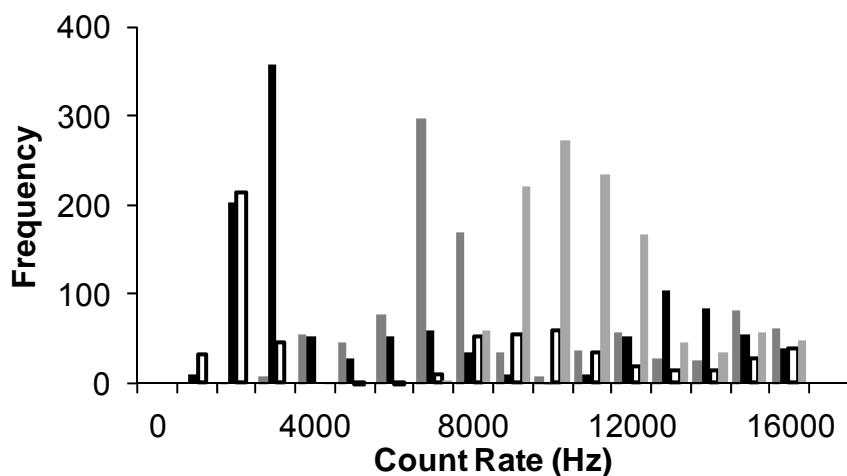
Figure 4.5 – Histogram of count rates of individual R6G/CB7 complexes. The emission count rate for each 50 ms time interval has been plotted.

Two features of the complexes have become evident. Individual R6G/CB7 complexes do not emit at the same rate throughout their fluorescence. Each molecule represented in Figure 4.5 had at least two preferred count rates and a variety of less-likely emission count rates. For example, the molecule represented by the black bars emitted most frequently near 3,000 Hz and 13,000 Hz. This indicates a changing influence on R6G by CB7, which is likely due to motion affecting the amount of R6G that is included within the CB7 cavity.

The other significant feature of R6G/CB7 complexes shown by Figure 4.5 is that individual complexes do not necessarily prefer the same emission count rates. The molecule represented by light gray has a preference for 10,000 Hz and 15,000 Hz, whereas the dark gray represents a molecule which emits with greatest frequency at 7,000 Hz and 15,000 Hz. The four molecules represented do not sum to yield the shape of the histogram of Figure 4.3, because some molecules do emit at a single

count rate until they are photobleached and there is a majority of R6G/CB7 complexes that emit most frequently near 2,100 Hz. For the four molecules represented in Figure 4.5, the average intensities are: 7796 Hz, 8283 Hz, 9552 Hz, and 12,526 Hz, therefore, they most likely contribute to the higher count rate peak, R6G/CB7$_2$, as well as the large FWHM of this peak.

The four complexes depicted are a representative sample of high count rate R6G/CB7 complexes. The variety of emission rates of each R6G/CB7 complex indicates a dynamic relationship between R6G and CB7. This supports the understanding of multiple emission rates available to R6G/CB7 complexes. The peak width seen in Figure 4.3 is not due to a multitude of static conformations, but each complex can have a dynamic emission rate. In order to have a dynamic emission rate, R6G is likely moving in relation to CB7.

The possible interactions between R6G and CB7 that could explain the multiple emission intensities include: an exclusion complex, with R6G on the exterior of CB7; an inclusion complex that allows R6G to move straight out of the CB7 cavity; and an inclusion complex that maintains contact between R6G and CB7 along the CB7 cavity portal, causing R6G to roll out of the cavity as it moves. If R6G complexes with CB7 in an exclusion complex, it is possible that different portions of the exterior of CB7 would cause more or less enhancement of the emission, such as along the CB7 equator, at the cavity portal and when the R6G is not in contact with CB7. However, this method of complexation seems to be the least likely to maintain contact between R6G and CB7 for extended times as R6G

would only be contacting CB7 in an electrostatic manner, which would not limit the mobility of R6G significantly. If R6G complexes with CB7 forming an inclusion complex, multiple emission intensities would be possible as R6G moves directly in and out of the cavity portal. In the scenario that allows linear motion of R6G as it leaves the CB7 cavity, the lowest emission intensity is again expected to correlate to R6G without contact with CB7. It would be expected that once the low emission intensity is reached, R6G would not emit at higher intensities commonly, as that would indicate re-complexation. With the limitation that R6G moves linearly out of the CB7 cavity, R6G would not change emission polarization until it was at a low emission intensity. Likewise, the R6G molecule may have to return to its original emission polarization before it could re-enter the CB7 cavity. If only a linear entrance and exit is possible, it seems probable that there would be some delay between the change in emission intensity and a change in polarization. The third complex to consider is an inclusion complex that maintains contact between R6G and the portal of CB7 while R6G is moving. Again, this allows for multiple emission intensities as R6G is capable of moving about the cavity portal. However, in contrast to the inclusion complex with linear motion, maintaining contact with the cavity portal would allow R6G to re-enter the CB7 cavity with less entropy change as the two molecules are already in electrostatic contact. This would allow the intensity to change more frequently between high and low emission intensities. When contact is maintained between R6G and the CB7 cavity portal, changes in

emission intensity are expected to be coincidental with changes in polarization as R6G is rolling in and out of the cavity.

4.4.5 Intensity Fluctuations Correlate to Change in Polarization

In attempting to differentiate between the two inclusion complex scenarios, linear motion of R6G or a rolling R6G, we look at the emission polarization of the complexes. A changing polarization would indicate turning of the emitting molecule. Figure 4.6, lower trace, shows one example of a molecule that changes emission intensity repeatedly, between higher and lower levels. The polarization resolved emission of the individual complex allows calculation of the emission polarization, Figure 4.6, upper trace. Comparison of the timings of intensity and polarization changes shows that the two occur concurrently. A likely explanation is that the motion of the R6G/CB7 complex, or part of the complex, affects the emission intensity. From the earlier discussion of how CB7-complexation enhances the emission intensity, the decrease in emission intensity is likely coinciding with R6G partially leaving the CB7 cavity.
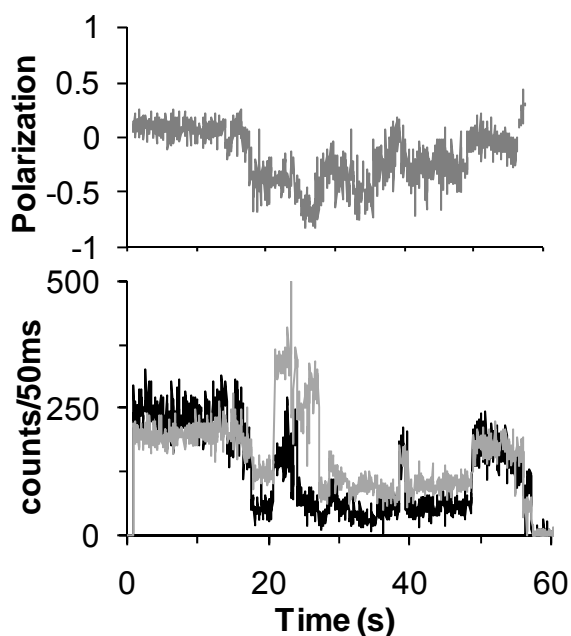
Figure 4.6 – Polarization resolved emission from a R6G/CB7 complex (lower trace) and the corresponding emission polarization (upper trace)

Since R6G is partially leaving the CB7 cavity (as seen by emission fluctuations) and turning (as seen by polarization change) concurrently, R6G seems to be rolling out of the CB7 cavity, not exiting in a linear direction. This rolling motion explains how R6G can maintain contact with CB7 and re-enter the cavity, experiencing the fluorescence enhancement repeatedly. The continued interactions between R6G and CB7 could also be possible through a linear motion of R6G that does not completely sever the interactions with the CB7 portal. A straight translation of R6G out of the CB7 cavity before turning beyond the cavity could explain the intensity and polarization observations. However, the number of possible rolling motions makes a rolling motion of R6G more probable. The translation of R6G out of the CB7 cavity is much smaller than the resolution of the fluorescent image,

therefore it would still seem to not undergo translational motion on the scale of the fluorescent image during the time the R6G/CB7 complex is being photobleached.

4.4.6 Increased Photostability on Single-Molecule Level

In addition to CB7 complexation enhancing emission intensity, an increased stability toward photobleaching is also indicated with ensemble measurements.[12] This thesis extends the understanding of ensemble photostability enhancement by CB7 complexation to include higher photostability on the single molecule level.

Histograms of the survival lifetimes for 103 R6G molecules and 219 R6G/CB7 complexes have been plotted in Figure 4.7. Fitting the data with exponential decays shows multiple behaviors, as was seen in the width of the average intensity plots, Figure 4.2. Though a more homogeneous environment was expected through CB7 complexation, the changing interactions between R6G and CB7 evident from intensity variations seem to also affect the survival lifetimes of the molecules.
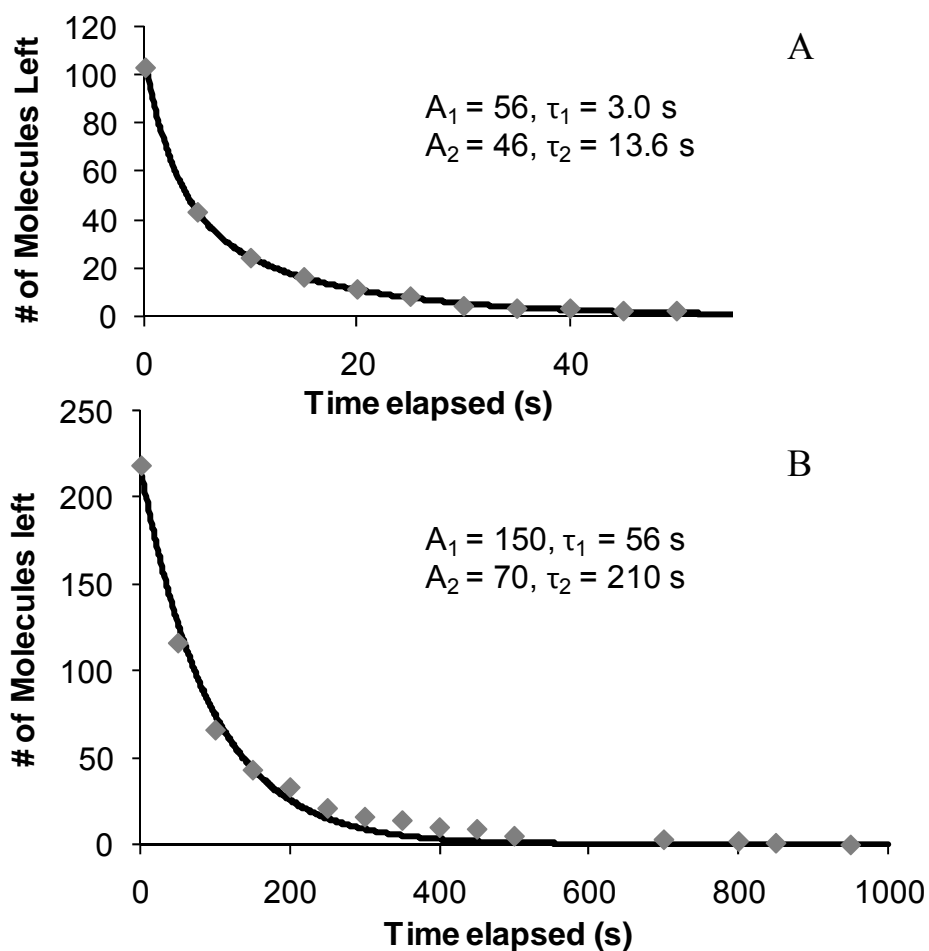
Figure 4.7 – Survival lifetime histograms of polyelectrolyte/silica composite film-embedded R6G (A) and R6G/CB7 complexes (B). Solid lines are biexponential decay curves fit to the histograms using: $y = A_1 e^{\frac{-t}{\tau_1}} + A_2 e^{\frac{-t}{\tau_2}}$.

The biexponential decay curves fit to the survival lifetime histograms, Figure 4.7, show both R6G molecules and the R6G/CB7 complexes display two distinct survival lifetimes, Table 4.2. R6G has one set of molecules that fluoresce for approximately 3.0 s, and another set of molecules that fluoresce for approximately 13.6 s. The values of the pre-exponential factors, 56 and 46, indicate these two sets include nearly equal numbers of molecules. Though there is a difference between

the survival lifetimes of the two sets of R6G molecules, the fluorescence of all R6G molecules are very short-lived when compared to the survival lifetimes of the R6G/CB7 complexes. The two sets of R6G/CB7 complexes have survival lifetimes of 56 s and 210 s. As opposed to the nearly equal distribution of survival lifetimes with R6G molecules, the R6G/CB7 complexes clearly favor the shorter survival lifetime by a factor of 2, as indicated by the pre-exponential factors, 150 and 70.

Table 4.2 – Exponential Survival Lifetime Fitting Parameters

	A_1	τ_1 (s)	A_2	τ_2 (s)	τ_{avg} (s)
R6G	56 ± 5	3.0 ± 0.3	46 ± 5	13.6 ± 0.9	7.8
R6G/CB7	150 ± 10	56 ± 4	70 ± 10	210 ± 20	104

As both sets of R6G molecules have survival lifetimes less than 15 s, and most R6G/CB7 complexes have survival lifetimes greater than 55s, the difference in survival lifetime can be attributed to complexation by CB7. Our current understanding of the CB7 inclusion of R6G leads to protection of the R6G molecule from collisions with surrounding molecules, including other R6G molecules that could cause photobleaching through singlet-singlet annihilation. Photobleaching caused by interactions between dye molecules or collisions between the fluorescing dye molecule and solvent molecules has also been reduced by reducing motion of the dye molecules or reducing the amount of solvent near the dye molecule.[25, 26] As an inclusion complex with CB7 would require displacement of the solvent molecules in the cavity of CB7,[15] there would be few solvent molecules left in the cavity to interact with the included portion of R6G. Since at least part of the non-included

portion of R6G is expected to be in electrostatic contact with CB7, less than half of the R6G surface is available to interact with solvent or other dye molecules. This is advantageous, since dye molecules in contact with solgel surfaces[27] or metal oxide surfaces[28] have shown increased rates of photodegradation. The dynamic motion of R6G in relation to CB7 changes the proportion of R6G that is included in the CB7 cavity, therefore changing the accessibility of R6G to other influences. However, by partially surrounding, or at least providing a boundary between an R6G molecule and other molecules, CB7 reduces the interactions R6G can have with anything else, thereby reducing the number of collisions that could lead to photobleaching.

Though both emission intensity and survival lifetime show multiple behaviors upon complexation with CB7, the link between complexation and survival lifetime does not seem to be the same relationship complexation has with emission intensity. Plotting the emission intensity against the survival lifetime of each R6G molecule or R6G/CB7 complex, Figure 4.8, does not show a correlation between increased count rate and longer survival lifetime.
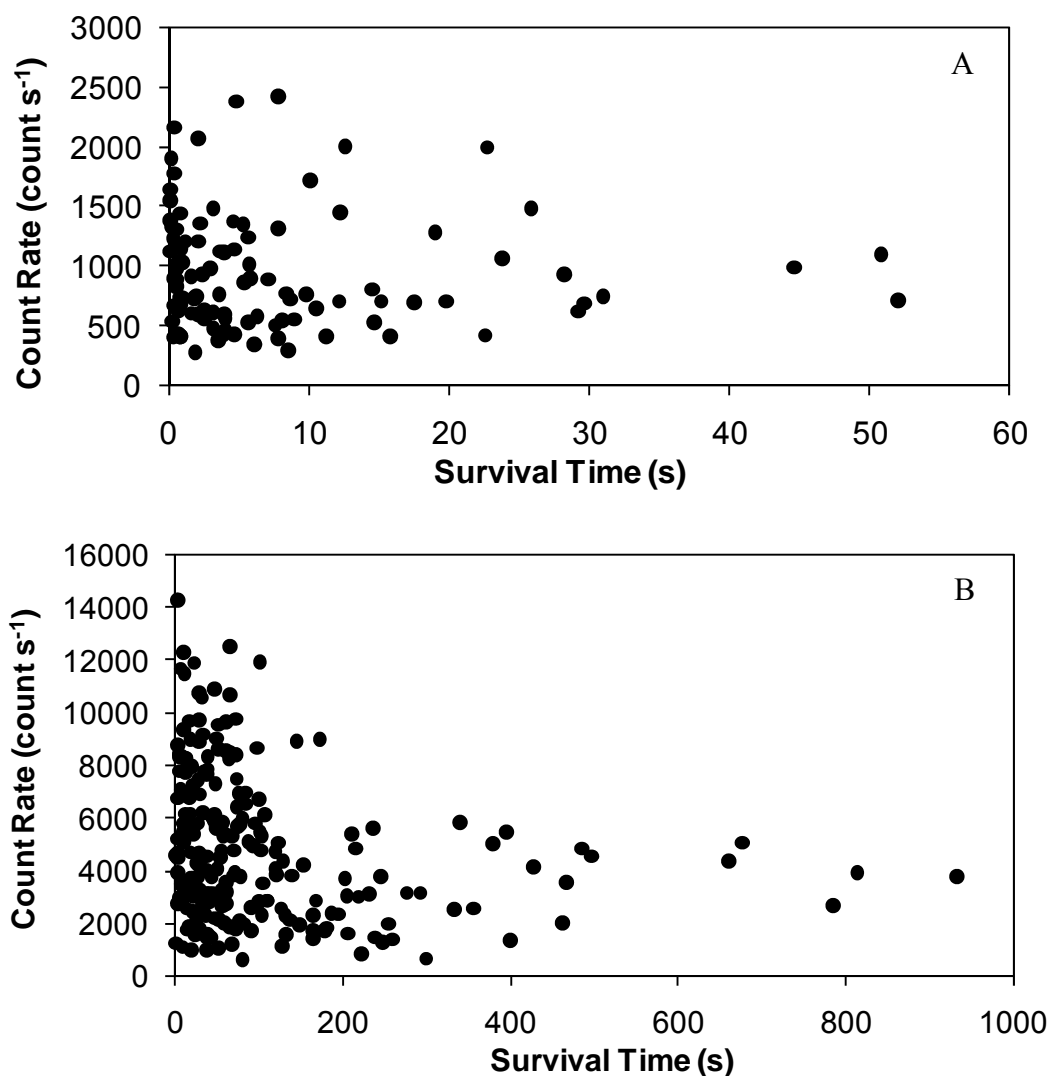
Figure 4.8 – Plots of average fluorescence intensity versus survival lifetime of 103 R6G molecules embedded in a 5-bilayer polyelectrolyte/silica composite film (A) and 219 CB7/R6G molecules on glass (B). The figures show that CB7 simultaneously enhances the fluorescence intensity and the survival lifetime (photostability) of R6G.

R6G molecules of all intensities seem to have the same likelihood of extended survival lifetime. Though there seem to be two sets of survival times from the fitting of the histogram, Figure 4.6a, the sets are not distinguished by emission

intensity. R6G/CB7 complexes show a similar variation of emission intensities as compared to R6G molecules for complexes that fluoresce less than 100 s. However, R6G/CB7 complexes that fluoresce longer than 200 s show a preference for emission between 2000 Hz and 6000 Hz. The correlation between longer survival lifetime and a preferred emission rate may be due to stabilizing a complexation conformation between R6G and CB7 that does not experience the full intensity enhancement of CB7 complexation.

If the greatest R6G emission intensity enhancement is gained upon including the most R6G as CB7 can, it may be a different conformation of R6G partially inside the CB7 cavity that provides better protection from photobleaching. Since R6G is a T-shaped molecule, the intensity enhancement may depend on which portion of the structure is included by CB7. Inclusion of parts of R6G most susceptible to photobleaching, or exclusion complexes with CB7,[29] may lead to enhanced photostability without increasing emission intensity as much as other conformations. Alternatively, a less common complexation of R6G by two CB7 molecules simultaneously could also provide a barrier from interactions with other molecules, but not have the desired emission intensity enhancement. The wide variety of interactions between R6G and CB7 make any singular description of R6G/CB7 complex conformation inadequate to describe the full collection of complexes. However, it is still clear that both characteristics, emission intensity and photostability, have been enhanced with CB7-complexation.

4.5 CONCLUSIONS

CB7-complexation of R6G presents contrasting situations. Though there are clearly dynamic interactions for some complexes, there are also molecules that seem to complex statically. Just as the dynamics of R6G/CB7 complexation are found through changing emission intensity and polarization, other R6G/CB7 complexes have consistent emission intensities and polarizations. However, it is the dynamic complexes and pursuit of control over how the dynamic properties of CB7-complexation affect fluorescent dye molecules that are of great interest.

The changing interactions between R6G and CB7 as they are complexed affect the dynamic emission intensity of the individual complexes as well as the average emission intensity for the complex. These dynamic intensity fluctuations correlate well with changes in polarization, which indicates a turning R6G molecule. The average intensity for each complex is not clearly correlated with an expected survival lifetime. Likewise, the longer-lived complexes do not have the highest emission rates. If the polarization data leads us to believe that CB7-included R6G gives a more intensely fluorescent molecule, perhaps those less-included into the CB7 cavity are longer-lived. This does not negate the fact that CB7-complexation clearly prolongs fluorescence emission by single R6G molecules. It seems CB7 can enhance the two characteristics independently through different complex conformations. This work also does not rule out the possible, though unlikely, situation that the entire complex is rotating on the glass surface. Rotation in the z-direction would affect the ability of the dye molecule to absorb the excitation light

by altering the overlap with the transition dipole of R6G. A rotating complex is

unlikely as CB7 has been immobilized on the glass.

4.6 REFERENCES

1.   Schäfer, C.; Decker, B.; Letzel, M.; Novara, F.; Eckel, R.; Ros, R.; Anselmetti, D.; Mattay, J., On the way to supramolecular photochemistry at the single-molecule level. *Pure Appl. Chem.* **2006**, (78), 12.

2.   Briquet, L.; Staelens, N.; Leherte, L.; Vercauteren, D. P., Structural, energetic, and dynamical properties of rotaxanes constituted of α-cyclodextrins and an azobenzene chain. *J. Mol. Graphics Model.* **2007**, 26, (1), 104-116.

3.   Larson, D. R.; Ow, H.; Vishwasrao, H. D.; Heikal, A. A.; Wiesner, U.; Webb, W. W., Silica Nanoparticle Architecture Determines Radiative Properties of Encapsulated Fluorophores. *Chem. Mater.* **2008**, 20, (8), 2677-2684.

4.   Calzaferri, G.; Huber, S.; Maas, H.; Minkowski, C., Host–Guest Antenna Materials. *Angew. Chem., Int. Ed. Engl.* **2003**, 42, 3732-3758.

5.   Chen, R. F.; Knutson, J. R., Mechanism of Fluorescence Concentration Quenching of Carboxyfluorescein in Liposomes: Energy Transfer to Nonfluorescent Dimers. *Anal. Biochem.* **1988**, 172, (1), 61-77.

6.   Rekharsky, M. V.; Mori, T.; Yang, C.; Ko, Y. H.; Selvapalam, N.; Kim, H.; Sobransingh, D.; Kaifer, A. E.; Liu, S.; Isaacs, L.; Chen, W.; Moghaddam, S.; Gilson, M. K.; Kim, K.; Inoue, Y., A synthetic host-guest system achieves avidin-biotin affinity by overcoming enthalpy– entropy compensation. *Proc. Natl. Acad. Sci. U.S.A.* **2007**, 104, (52), 20737-20742.

7.   Lee, J. W.; Samal, S.; Selvapalam, N.; Kim, H.-J.; Kim, K., Cucurbituril Homologues and Derivatives: New Opportunities in Supramolecular Chemistry. *Acc. Chem. Res.* **2003**, 36, 621-630.

8.   Shaikh, M.; Mohanty, J.; Singh, P. K.; Naub, W. M.; Pal, H., Complexation of acridine orange by cucurbit[7]uril and β-cyclodextrin: photophysical effects and pKa shifts. *Photochem. Photobiol. Sci.* 2008, 7, (4), 408-414.

9.   Leclercq, L.; Noujeim, N.; Sanon, S. H.; Schmitzer, A. R., Study of the Supramolecular Cooperativity in the Multirecognition Mechanism of Cyclodextrins/Cucurbituril/ Disubstituted Diimidazolium Bromides. *J. Phys. Chem. B* **2008**, 112, (45), 14176-14184.

10.   Marquez, C.; Hudgins, R. R.; Nau, W. M., Mechanism of Host−Guest Complexation by Cucurbituril. *J. Am. Chem. Soc.* **2004**, 126, (18), 5806-5816.

11.   Jeon, W. S.; Moon, K.; Park, S. H.; Chun, H.; Ko, Y. H.; Lee, J. Y.; Lee, E. S.; Samal, S.; Selvapalam, N.; Rekharsky, M. V.; Sindelar, V.; Sobransingh, D.; Inoue, Y.; Kaifer, A. E.; Kim, K., Complexation of Ferrocene Derivatives by the Cucurbit[7]uril Host: A Comparative Study of the Cucurbituril and Cyclodextrin Host Families. *J. Am. Chem. Soc.* **2005**, 127, (37), 12984-12989.

12.   Mohanty, J.; Nau, W. M., Ultrastable rhodamine with cucurbituril. *Angew. Chem., Int. Ed. Engl* **2005**, 44, (24), 3750-3754.

13.   Moore, J. L. Host-Guest Complexation of Cationic Xanthene Dyes with Cucurbit[7]uril. University of Oklahoma, Norman, 2008.

14.   Nau, W. M.; Mohanty, J., Taming fluorescent dyes with cucurbituril. *Int. J. Photoenergy* **2005**, 07, 133-141.

15.   Marquez, C.; Nau, W. M., Polarizabilities Inside Molecular Containers. *Angew. Chem., Int. Ed. Engl* **2001**, 40, (23), 4387-4390.

16.   Mitani, Y.; Shimada, A.; Koshihara, S.; Fukuhara, K.; Kobayashi, H.; Kotani, M., Role of adsorbed water in diffusion of rhodamine 6G on glass surface. *Chem. Phys. Lett.* **2006**, 431, (1-3), 164-168.

17.   Vogelsang, J.; Kasper, R.; Steinhauer, C.; Person, B.; Heilemann, M.; Sauer, M.; Tinnefeld, P., A Reducing and Oxidizing System Minimizes Photobleaching and Blinking of Fluorescent Dyes. *Angew. Chem., Int. Ed. Engl* **2008**, 47, (29), 5465-5469.

18.   Viteri, C. R.; Gilliland, J. W.; Yip, W. T., Probing the dynamic guest-host interactions in sol-gel films using single molecule spectroscopy. *J. Am. Chem. Soc.* **2003**, 125, (7), 1980-1987.

19.   Rekharsky, M. V.; Yamamura, H.; Inoue, C.; Kawai, M.; Osaka, I.; Arakawa, R.; Shiba, K.; Sato, A.; Ko, Y. H.; Selvapalam, N.; Kim, K.; Inoue, Y., Chiral Recognition in Cucurbituril Cavities. *J. Am. Chem. Soc.* **2006**, 128, (46), 14871-14880.

20.   Chung, A. J.; Rubner, M. F., Methods of Loading and Releasing Low Molecular Weight Cationic Molecules in Weak Polyelectrolyte Multilayer Films. *Langmuir* **2002**, 18, (4), 1176-1183.

21.   Hiller, J. A.; Rubner, M. F., Reversible Molecular Memory and pH-Switchable Swelling Transitions in Polyelectrolyte Multilayers. *Macromolecules* **2003**, 36, (11), 4078-4083.

22.   Choi, J.; Rubner, M. F., Influence of the Degree of Ionization on Weak Polyelectrolyte Multilayer Assembly. *Macromolecules* **2005**, 38, (1), 116-124.

23.   Martyn, T. A.; Moore, J. L.; Halterman, R. L.; Yip, W. T., Cucurbit[7]uril Induces Superior Probe Performance for Single-Molecule Detection. *J. Am. Chem. Soc.* **2007**, 129, (34), 10338-10339.

24.   Mohanty, J.; Bhasikuttan, A. C.; Nau, W. M.; Pal, H., Host-guest complexation of neutral red with macrocyclic host molecules: Contrasting pKa shifts and binding affinities for cucurbit[7]uril and b-cyclodextrin. *J. Phys. Chem. B* **2006**, 110, (10), 5132-5138.

25.   Avnir, D.; Levy, D.; Reisfeld, R., The Nature of the Silica Cage as Reflected by Spectral Changes and Enhances Photostability of Trapped Rhodamine 6G. *J. Phys. Chem.* **1984**, 88, (24), 5956-5959.

26.   Rahn, M. D.; King, T. A.; Gorman, A. A.; Hamblett, I., Photostability enhancement of Pyrromethene 567 and Perylene Orange in oxygen-free liquid and solid dye lasers. *Appl. Opt.* **1997**, 36, (24), 5862-5871.

27.   Quan, X.; Zhao, X.; Chen, S.; Zhao, H.; Chen, J.; Zhao, Y., Enhancement of p,p'-DDT photodegradation on soil surfaces using TiO_2 induced by UV-light. *Chemosphere* **2005**, 60, (2), 266-273.

28.   Vinodgopal, K.; Kamat, P. V., Photochemistry on Surfaces. Photodegradation of 1,3-Diphenyiisobenzofuran over Metal Oxide Particles. *J. Phys. Chem.* **1992**, 96, (12), 5053-5059.

29.   Wagner, B. D.; Stojanovic, N.; Day, A. I.; Blanch, R. J., Host Properties of Cucurbit[7]uril: Fluorescence Enhancement of Anilinonaphthalene Sulfonates. *J. Phys. Chem. B* **2003**, 107, (39), 10741-10746.

Chapter V

Single Molecule Spectroscopic Analysis of the Complexation of

Cationic Rhodamine 6G by Cucurbit[7]uril in Silica Solgel

5.1 CHAPTER ABSTRACT

The dynamic interactions of rhodamine 6G (R6G) as it is complexed with cucurbit[7]uril (CB7) are interrupted when the system is in a silica solgel matrix. Silica solgel competes with CB7 for the cationic R6G with similar electrostatic attractions. The effect of the competition is an inability of CB7 to enhance the emission intensity or the photostability of R6G as compared to CB7-complexed R6G without the silica solgel matrix. The R6G molecules do not seem to be adequately complexed by CB7 when a R6G/CB7 mixture is in a silica solgel matrix.

5.2 INTRODUCTION

Recent interest in macromolecular complexes includes incorporating them into heterogeneous, solid-state systems. The ability to incorporate cyclodextrins into clay structures has been explored for more than two decades for applications in chromatography and slow release materials.[1, 2] More recently, calixarenes and cyclodextrins have been co-polymerized with other monomers to incorporate the complexation ability of the macromolecules within the structure of the polymer for use as optical waveguides and to modify polymeric surfaces for biomaterials.[3-5] Some work is also being done to incorporate cyclodextrin in polymer systems outside of co-polymerization and found the cyclodextrin anchors to the polymer

surface.[6] As cucurbiturils are relatively new in the macromolecule world, the work

incorporating organic macromolecules into inorganic matrices seems to not yet

include cucurbituril systems.

As was mentioned previously, cucurbiturils host a different set of molecules

than are hosted by calixarenes and cyclodextrins.[7, 8] Therefore, the ability to utilize

them in solid-state systems would expand the possibilities for this type of organic-

inorganic system. Building on the emission intensity and survival lifetime

enhancement of R6G discussed in Chapter 4, a further investigation of the CB7-

complexation of R6G on the single-molecule level develops our understanding of the

stability of the R6G/CB7 complex in different environments and how these materials

could be developed as bright, photostable optical materials.

Host-guest complexation by organic macromolecules is non-covalent in

nature. It is expected that the guest molecules are complexed and uncomplexed at

different periods of time, as characterized by the association constant, K_a, which is

the ratio of time the guest molecule spends in the complex to the time the guest is

uncomplexed. This is especially true for solutions, which allow molecular motion

through the solvent without much interaction with the container. The common

discussion of competitive binding for molecules that fit the properties of the host is

usually within the context of solutions. However, as a matrix is introduced and

interactions with the matrix are as frequent as interactions with a macromolecular

host, the competition may now be between two hosts, not two different guests,

Reaction 5.1.

$$\text{dye/host} \leftrightarrow \text{dye (unbound)} \leftrightarrow \text{dye:matrix} \qquad \text{R5.1}$$

The interaction that holds R6G and CB7 together seems to be electrostatic in nature, which may be influenced if another electronegative moiety is in close proximity to R6G. To determine the best method of incorporating a CB7-complexed dye into solid state materials, it is important to understand whether the complexation, as well as the complexation effect, is maintained when the complex interacts with a heterogeneous matrix environment. The work presented here explores how the silica solgel material influences the ability of CB7 to complex with R6G by examining the fluorescence properties of R6G and R6G/CB7 complexes.

5.3 MATERIALS AND METHODS

99.9+% tetraethyl orthosilicate (TEOS), 95% ethanol (spectrophotometric grade), and 85 wt % phosphoric acid were purchased from Sigma-Aldrich. Rhodamine 6G (R6G) was purchased from Molecular Probes. All chemicals were used without further purification. Deionized water was obtained by purification through a Millipore system to at least 18 Ω before use. Cucurbit[7]uril (CB7) was obtained as a gift from Dr. Halterman at the University of Oklahoma.[9] Fisherfinest* Premium Cover Glasses (Fisher Scientific, 12-548-5P) were cleaned with 4 consecutive sonications, 30 minutes each in baths of 10% NaOH, distilled water, acetone, and deionized water, before being used to support a sample.

There are 3 sample types being compared in this work. The first will be referred to as R6G/CB7 on glass and was prepared according to the following

specifications. 60 µL of an R6G and CB7 mixture (0.05 µM R6G and 50 µM CB7) in 18 Ω Millipore water was spincoated onto a clean coverglass for 70 s at 6100 rpm.

The second sample type will be referred to as R6G in solgel. R6G was diluted to 4.2 x 10^{-7} M in 95% ethanol and 5 µL was added to a solgel solution of TEOS, H_2O, and ethanol at a volume ratio of 1.7:1:3.5 (176.35 µL, 100 µL and 352.1 µL) with 1.95 µL of 0.148 M phosphoric acid to obtain a final R6G concentration of 3.3 nM. 60 µL of 3.3 nM R6G in solgel solution was then spincoated onto a clean coverglass for 70 s at 6100 rpm.

The third sample type combined the two previous types and will be referred to as R6G/CB7 in solgel. 49.4 µL of the R6G/CB7 mixture, above, was added to the 630.4 µL TEOS solgel solution as above with the final concentrations of R6G and CB7 being 4.4 x 10^{-8} M and 4.9 x 10^{-5} M, respectively. 60 µL of R6G/CB7 in solgel solution was then spincoated onto a clean coverglass for 70 s at 6100 rpm. Samples were used immediately with measurements made under ambient conditions.

Fluorescent measurements were made using an inverted confocal microscope (Nikon Eclipse TE300). The fluorescence emission was passed through a dichroic mirror, wavelength dependent notch filter and long pass filter, then split by a polarization beam splitter before two avalanche photodiode detectors that acted as single photon counting devices, as seen in Figure 2.1.

During imaging the sample was moved by a nanostage (Queensgate) and raster scanned to collect fluorescent images (10 µm x 10 µm) of the sample. The stage and Labview software enable returning to a particular pixel (100 nm x 100 nm)

for photobleaching. Single molecule photobleaching was achieved by continuously

exciting the molecule at 514 nm with 1.10 mW light from an Ar^+ laser.

Instrumentation has been described more fully in previous publications and in

Chapter 2.[10]

Data analysis included finding the intensity variation, average intensity

(2.5.1), survival lifetime (2.4.1.2) and polarization (2.4.1.3) of each molecule, as

detailed in the noted sections of Chapter 2. Due to the common blinking events of

R6G, analysis of the data included averaging the intensity of each molecule when it

was fluorescing, not in a dark state. Averaging the fluorescent emission intensities

was accomplished by setting a threshold level for each molecule and averaging the

emission intensity when the intensity was above the threshold. A threshold level was

necessary, because the intensities are collected at 50 ms intervals. A molecule that is

emitting only one or two times in 50 ms has been in a nonradiative state for the

majority of that time, because the normal fluorescent lifetime for R6G molecules is

approximately 4 ns.[11] The average intensities have been binned during data

processing by 20 count increments, for ease of viewing the data.

Survival lifetime is determined by the difference in time between when the

molecule begins to fluoresce, which is when the laser light reaches the sample, and

when the molecule has photobleached, Figure 2.3. Photobleaching is said to have

occurred when the molecule has irreversibly gone to a dark state.

The polarization of light emitted by each dye molecule has been analyzed by

comparing the intensity of light detected by the 2 APD detectors. The two APDs

allow determination of how much light is emitted with either horizontally or vertically polarized light. Changing emission polarization is due to a change in the ratio of light emitted in the different directions, which indicates a turning dye molecule.

5.4 RESULTS AND DISCUSSION

As was discussed in Chapter 4, a spincoated sample of R6G/CB7 in solution fluoresces from translationally immobilized R6G/CB7 complexes. Here, a comparison of R6G/CB7 on coverglass is made to R6G and R6G/CB7 in an alcogel matrix, providing a clear comparison between the R6G/CB7 complex and R6G molecules in the same immobilization matrix.

5.4.1 Emission Count Rate Variations

During photobleaching experiments, the transient emission of each molecule was collected. Plotting the emission intensity of each molecule for the duration of the survival lifetime allowed a visual inspection of the emission behavior of the molecule. A simple single molecule transient would have only one emission intensity that is consistent until the molecule photobleaches to zero intensity, in one step. However, there are other behaviors that can be recognized from the transients. A drop to zero intensity that is short-lived, followed by the emission intensity returning to the previous intensity level is called a blink, Figure 5.1A. R6G is a molecule that commonly blinks, and the ability to blink down to zero intensity is one means to confirm there is only one molecule being photobleached. Especially when

the emission has been split by a polarization beam splitter, a blink that is registered

by both detectors is a clear indication of a single emitting molecule.
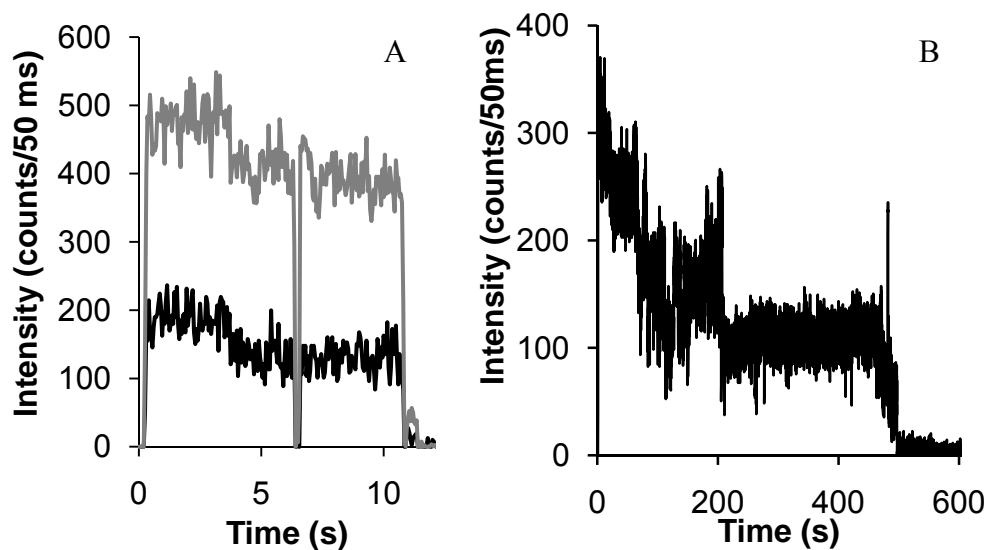
Figure 5.1 – Fluorescent transients of R6G molecules. A) A simple fluorescent transient with a single blink. B) The intensity fluctuation of a possible R6G aggregate in solgel. Features that indicate the possibility of multiple chromophores include the four intensity levels from a single fluorescent spot on the image, the sloping decay of intensity before photobleaching near 500 s, and the inability of the fluorescence to blink to zero intensity.

Another behavior that is obvious from the emission transients and seems to be characteristic of R6G molecules is emission at multiple intensities. If an aggregate is photobleached it is likely to photobleach in multiple steps, Figure 5.1B, showing the reduction in emission intensity due to photobleaching each individual molecule.[12] Several molecules may also photobleach in an extended slope-like manner where the reduction in intensity due to each molecule is blurred by other molecules bleaching nearly simultaneously. This looks more like a decay curve that

would be seen when a solution is photobleached. However, R6G molecules are able to emit at different intensities and return to the previous emission intensity, as well as blink at both the higher and lower emission intensities, Figure 5.2. The ability to emit at a lower emission intensity prior to a higher emission intensity implies a change in a single molecule that changes the rate of photons emission, whether due to turning of the molecular transition dipole in the z-direction, reducing absorption of excitation light, or a change in the fluorescent lifetime. It is also possible with 50 ms collection intervals that a lower intensity emission is caused by the molecule being in a dark state for part of each collection interval, but it is unlikely a molecule would do so repeatedly for extended periods. However, a change in fluorescent lifetime or turning of the molecule would change the number of photons emitted during the 50 ms interval.
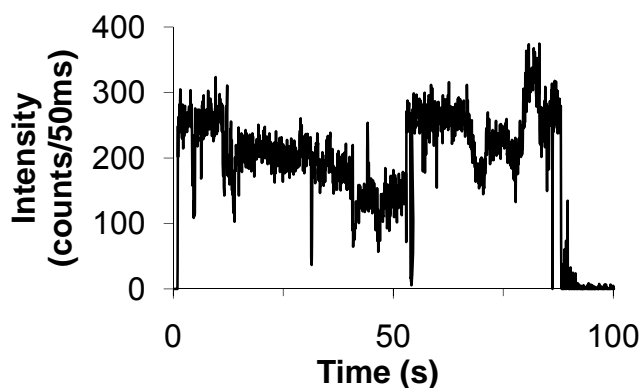
Figure 5.2 – The transient of a single R6G/CB7 complex on glass. The molecule is emitting at multiple intensities and capable of blinking at multiple intensities.

An analysis of R6G in a TEOS alcogel shows that each molecule does not necessarily emit at the same intensity as other R6G molecules, nor do multi-level emitting R6G molecules emit at the same two intensity levels, Figure 5.3, as would

be expected due to differences in transition dipole orientation of nearly immobilized molecules. However, it seems common for multi-level emitting molecules to emit at a higher level for a shorter duration and at a lower level for a much longer duration. When this occurs, the most common progression is for the molecule to emit at the higher count rate early during its fluorescence, and emit at a lower count rate for the extended latter part of its survival lifetime. This behavior leads to a much larger number of occurrences of count rates near 1000 Hz and fewer at the higher count rates, Figure 5.3.
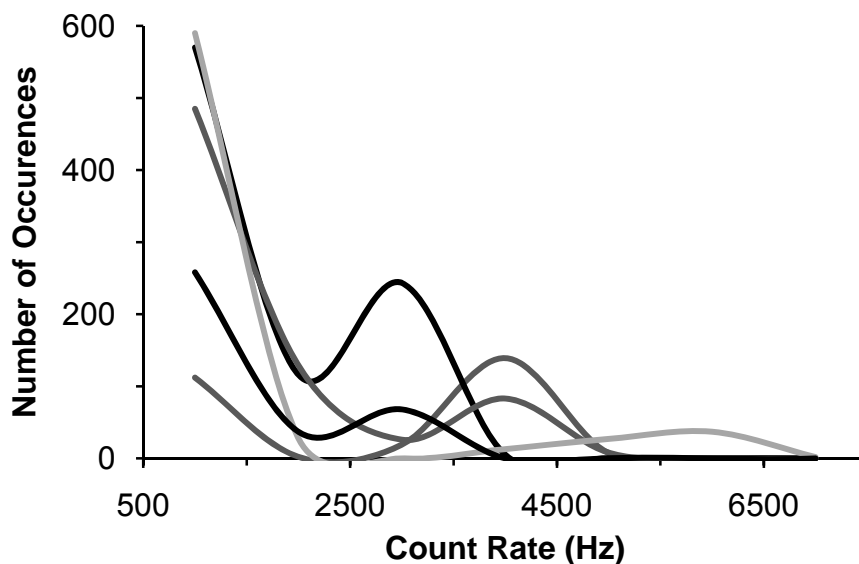
Figure 5.3 – Multilevel R6G emission intensities for a few molecules in solgel. Each line represents the emission of a single molecule over its survival lifetime. Intensities were collected at 50 ms intervals and for this representation in increments of 1000 Hz.

Comparing R6G in three environments, whether solely in solgel or complexed with CB7 on glass or in solgel, shows R6G emits at multiple levels in all three cases, Table 5.1. However, the likelihood of multiple levels is much higher

when R6G is complexed with CB7 in the absence of the solgel matrix. The two solgel samples, R6G molecules or R6G/CB7 complexes, show a great similarity as both sample types had a maximum of two emission intensity levels and single-digit percentages of molecules displaying two-level behavior. This calls into question the strength of interaction in the R6G/CB7 complex. Since R6G is a cationic dye and attracted to the electronegative crown of the CB7 cavity,[8] it is possible that the same electrostatic interactions cause R6G to be attracted to the deprotonated oxygens of unreacted silanol groups[13] in the solgel matrix. Likewise, the abundance of emission intensities available to the spincoated R6G/CB7 on glass sample also imply a richer dynamic interaction between the guest R6G and host CB7 molecules in the absence of the solgel matrix. As was discussed in Chapter 4 and is important to an understanding of the current data, higher R6G emission intensities may be a product of greater extent of complexation. The fact that R6G can return to previous enhanced emission intensities implies that there is some contact maintained with CB7. However, as it has been shown that the R6G molecule cannot fit completely within the CB7 cavity, it is possible that the external portion of R6G is interacting with the environment also, and in the case of the R6G/CB7 on glass sample, the external environment may be a thin water layer forming on the glass.[14] For molecules that emit at a higher count rate initially, then an extended lower count rate, it seems appropriate to suggest that the extended lower emission intensity may be the R6G emitting at its un-enhanced level, but maintaining some protection from bombardment and likewise photobleaching due to its proximity to CB7.

Table 5.1 – Summary of R6G and R6G/CB7 Emission Intensity Variations

Sample	Number of Molecules	2 Levels	3 Levels	4 Levels
R6G/CB7 on glass	219	92 (42 ± 7%)	17 (8 ± 4%)	2 (1 ± 1%)
R6G in solgel	98	9 (9 ± 3%)		
R6G/CB7 in solgel	200	11 (5 ± 3%)		

5.4.2 CB7 Enhances Average Count Rate in Absence of Solgel

An average of the emission intensity of each molecule is also useful for comparing R6G in different systems. Averaging the emission intensity for each R6G molecule over its survival lifetime allows a comparison of how bright each molecule is compared to others within the sample set, or between samples of different types, without getting distracted by count rate fluctuations.

Since R6G commonly blinks, the average intensity was found for the fluorescing times, not including the times a R6G molecule or R6G/CB7 complex is in a dark state. A histogram of the average count rates of R6G and R6G/CB7 in all three sample types, Figure 5.4, shows a clear difference between the samples. Both solgel samples have a preference for low average emission values. The R6G/CB7 in solgel peaks at a slightly higher intensity than R6G in solgel without CB7, but does not have the few extremely high average count rates of R6G in solgel. The histogram also shows that R6G/CB7 on glass allows many different average intensities with nearly equal likelihood, therefore making it harder to predict the intensity of an individual CB7-complexed R6G. What is lost in the average is whether the R6G in solgel emits at a higher count rate for a while and has a long-tailing lower count rate, as was discussed previously. Such an emission behavior

would cause the average count rate to remain only slightly elevated compared to a consistently low count rate.
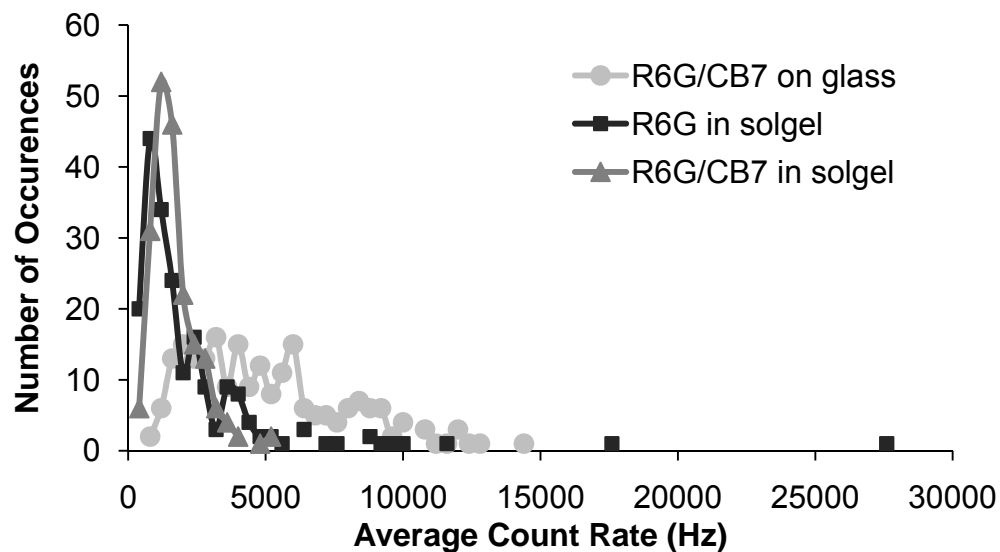
Figure 5.4 – Histogram of average intensities of R6G or CB7-complexed R6G. Intensities were collected at 50 ms intervals, and for this representation in increments of 400 Hz.

R6G/CB7 on glass has a much higher average intensity than either of the solgel samples. This is apparent from the histogram, Figure 5.4, as well as Table 5.2, which quantifies the differences between the samples. Table 5.2 summarizes the average counts per 50 ms collection interval without post-collection binning, which shows a difference between the solgel samples that initially seems opposite of the data in the histogram. R6G/CB7 in solgel has a lower average count rate than R6G in solgel. The large standard deviation for R6G in solgel accounts for the difference as compared to the histogram where it seems R6G/CB7 in solgel has a higher count rate. The large standard deviation can be attributed to the few extremely high count rate R6G molecules in solgel. These few high intensity R6G molecules increase the

average above the R6G/CB7 in solgel average. Again, the solgel seems to counteract the effect of CB7 complexation, since R6G/CB7 on glass has a much higher average count rate than either solgel sample and does not display a strong preference for any average count rate. Similar interference by silica gels has been seen before with quantum dots protected by a silica shell.[15]

Table 5.2 Summary of R6G Characteristics in all Samples

Sample	Average Intensity (counts per 50 ms)	Number of Molecules
R6G/ CB7 in alcogel	70 ± 40	200
R6G in alcogel	100 ± 100	200
R6G/ CB7 on glass	200 ± 100	219
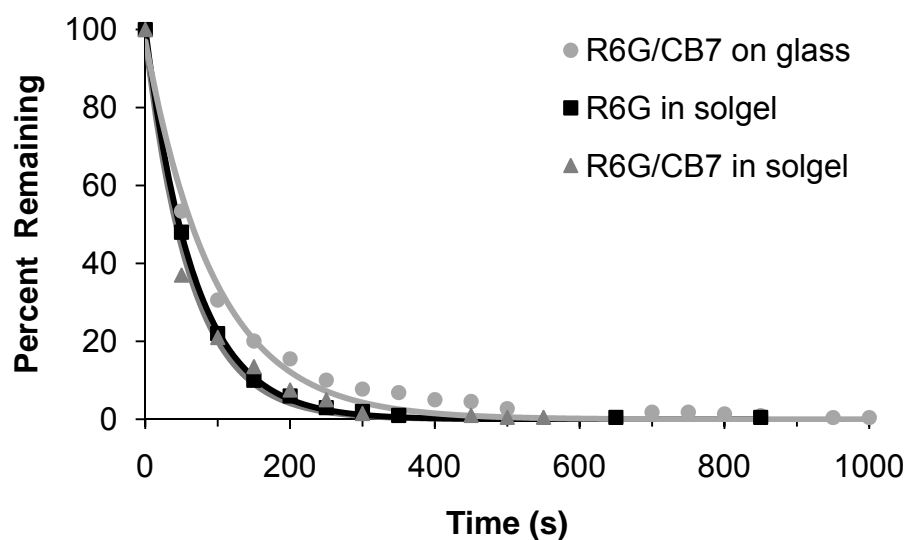
Figure 5.5 – Survival lifetimes of R6G or CB7-complexed R6G in solgel or spincoated. Percent remaining has been plotted due to slightly different numbers of molecules measured for each sample type.

5.4.3 Photostability of R6G and R6G/CB7

The survival lifetime of each molecule is a measure of the photostability of the molecule, or how long the molecule fluoresces before photobleaching while being continuously excited. The percent of molecules still fluorescing at each time period has been plotted in Figure 5.5, as opposed to the number of molecules remaining at each time, due to slightly different numbers of molecules tested for each type of sample, showing a clear difference between the solgel samples and R6G/CB7 on glass. R6G/CB7 on glass has the longest survival lifetime, seen as the slowest decay, signifying that on average this sample is more likely to yield longer-lived fluorescence of each R6G/CB7 complex than the other two samples. The two solgel samples are nearly identical in their decay curves, with the exception that the R6G in solgel had a single molecule that significantly outlived the R6G/CB7 in solgel. The lengthened survival lifetime of R6G/CB7 complexes on glass demonstrates the ability of CB7 to protect R6G from photobleaching when a matrix does not interfere with the interactions between CB7 and R6G. The suggestion earlier that the complexation between R6G and CB7 in incomplete and may allow R6G to experience elongated durations of unenhanced fluorescence emission does not exclude the possibility of CB7-interaction improving photostability by reducing interactions with surrounding molecules.

Table 5.3 clarifies the difference between R6G survival lifetimes in the three sample types. R6G/CB7 on glass has the longest survival lifetime, with the smallest exponential decay constant, $k = 0.0104$ s^{-1}. The two solgel samples have nearly

identical photostability, as seen from the decay constant of their survival lifetimes, $k = 0.0149$ s^{-1} for R6G in solgel and $k = 0.0159$ s^{-1} for R6G/CB7 in solgel. Therefore, both in intensity and photostability measurements, it seems solgel encapsulation reduces or negates the ability of CB7 to complex with R6G.

Table 5.3 – Exponential Decay Fitting Parameters of R6G and R6G/CB7

Sample	A	$k(s^{-1})$	R^2
R6G/ CB7 in alcogel	97.98	0.01585	0.9826
R6G in alcogel	100.32	0.01489	0.9993
R6G/ CB7 on glass	97.17	0.01039	0.9862

Since R6G cannot fit within the CB7 cavity, much of the R6G molecule is outside CB7 and accessible to interactions with the silica solgel. As was mentioned earlier, the electrostatic interactions between the cationic R6G and the electronegative cavity portal of CB7 may not be strong enough to maintain complexation of R6G by CB7 when an unprotonated oxygen with a full negative charge is near the cationic R6G. This seems a likely explanation for the lack of enhancement by CB7 in silica solgel. The R6G may not be complexed by CB7, or CB7 and the solgel matrix are competing for the R6G molecules.

5.5 CONCLUSIONS

The affect of CB7 complexation on the fluorescence emission is more significant in the absence of the alcogel matrix. CB7 complexation enhances the emission intensity and photostability of R6G on glass, while neither the emission intensity nor the photostability of R6G in solgel is significantly affected by the presence of CB7. It seems that the multiple conformations available to an R6G/CB7

complex noted previously, allow a competition between CB7 complexation and binding by the solgel pore surface that reduces the ability of CB7 to affect fluorescence properties of R6G. This is a significant consideration when trying to incorporate CB7-complexed dye molecules into materials.

5.6 REFERENCES

1.   Kijima, T., Complexation of sodium-, calcium-, and copper-montmorillonites with some parent and methylated cyclodextrins. *J. Incl. Phenom.* **1986**, 4, (4), 333-338.

2.   Villaverde, J.; Sopena, F., Use of clay/β-cyclodextrin formulations to obtain a slow release of a hydrophobic herbicide. *Fresenius Environ. Bull.* **2008**, 17, (12b), 2250-2254.

3.   Al'tshuler, G. N.;Malyshenko, N. V.;Shkurenko, G. Y.; Al'tshuler, O. G., The kinetics of cation exchange in network calixarene-containing polymers: the nanoreactor effect. *Russ. J. Phys. Chem. A (Engl. Transl.)* **2008**, 82, (13), 2202-2206.

4.   Kim, T.; Komatsu, K.; Sugihara, O.; Kaino, T.; Kudo, H.; Nishikubo, T., Optical properties of calixarene polymers. *Proc. SPIE-Int. Soc. Opt. Eng.* **2008**, 6891, (1), 68910D/1-68910D/10.

5.   Sun, P.; Chen, J.; Liu, Z.-W.; Liu, Z.-T., Poly(vinyl alcohol) Functionalized β-Cyclodextrin as an Inclusion Complex. *J. Macromol. Sci., Pure Appl. Chem.* **2009**, 46, (5), 533-540.

6.   Zhao, X.; Courtney, J.M., Novel "anchor modification" of polymeric biomaterial surfaces by the utilization of cyclodextrin inclusion complex supramolecules. *J. Biomed. Mater. Res., Part A* **2009**, 90A, (1), 282-291.

7.   Liu, Y.; Li, C.-J.; Guo, D.-S.; Pan, Z.-H.; Li, Z., A Comparative Study of Complexation of β-Cyclodextrin, Calix[4]arenesulfonate and Cucurbit[7]uril with Dye Guests: Fluorescence Behavior and Binding Affinity. *Supramol. Chem.* **2007**, 19, (7), 517-523.

8.   Mohanty, J.; Bhasikuttan, A. C.; Nau, W. M.; Pal, H., Host-guest complexation of neutral red with macrocyclic host molecules: Contrasting pKa shifts and binding affinities for cucurbit[7]uril and β-cyclodextrin. *J. Phys. Chem. B* **2006**, 110, (10), 5132-5138.

9.   Day, A.; Arnold, A. P.; Blanch, R. J.; Snushall, B., Controlling Factors in the Synthesis of Cucurbit[7]uril and Its Homologues. *J. Org. Chem.* **2001**, 66, (24), 8094-8100.

10.   Li, Y.; Yip, W. T., Coulombic Interactions on the Deposition and Rotational Mobility Distributions of Dyes in Polyelectrolyte Multilayer Thin Films. *Langmuir* **2004**, 20, (25), 11039-11045.

11.   Martinez, V. M.; Arbeloa, F. L.; Prieto, J. B.; Arbeloa, I. L., Characterization of Rhodamine 6G Aggregates Intercalated in Solid Thin Films of Laponite Clay. 2 Fluorescence Spectroscopy. *J. Phys. Chem. B* **2005**, 109, (15), 7443-7450.

12.   Das, S. K.; Darshi, M.; Cheley, S.; Wallace, M. I.; Bayley, H., Membrane Protein Stoichiometry Determined from the Step-Wise Photobleaching of Dye-Labelled Subunits. *ChemBioChem* **2007**, 8, (9), 994-999.

13.   Gilliland, J. W.; Yokoyama, K.; Yip, W. T., Effect of Coulombic Interactions on Rotational Mobility of Guests in Sol-Gel Silicate Thin Films. *Chem. Mater.* **2004**, 16, (20), 3949-3954.

14.   Sherratt, M. J.; Bax, D. V.; Chaudhry, S. S.; Hodson, N.; Lu, J. R.; Saravanapavan, P.; Kielty, C. M., Substrate chemistry influences the morphology and biological function of adsorbed extracellular matrix assemblies. *Biomaterials* **2005**, 26, (34), 7192-7206.

15.   Correa-Duarte, M. A.; Kobayashi, Y.; Caruso, R. A.; Liz-Marzan, L. M., Photodegradation of SiO_2-coated CdS nanoparticles within silica gels. *J. Nanosci. Nanotechnol.* **2001**, 1, (1), 95-99.

Chapter VI

Photophysical Behavior of Cucurbit[7]Uril Complexed Pyronin Y

6.1 CHAPTER ABSTRACT

Strong complexation of the cationic dye Pyronin Y (PyY) by cucurbit[7]uril (CB7) enables a better understanding of complexation effects on single dye molecule photophysical behavior. Upon complexation with CB7, PyY photophysical properties of emission intensity and blinking rates do not change much. However, the prolonged survival lifetime yielded by protecting PyY from photodegradation allows more reliable statistical analysis of blinking kinetics by individual molecules.

CB7 is well-known to complex cationic dyes effectively and has previously been studied with other dyes. PyY was identified as an interesting dye companion due to its size compatibility with CB7, allowing more complete insertion into the CB7 cavity. Stronger complexation by CB7 affords better protection to the dye molecules. The PyY should remain inside the CB7 cavity once complexed; thereby eliminating the additional dynamic situations associated with larger dyes like R6G, which have been shown to migrate in and out of the cavity occasionally.

In this work PyY/CB7 complexes maintain the immobilization on a glass surface and long survival lifetime characteristics of CB7 complexation found previously with R6G. In addition to these advantages, PyY has the additional benefit of displaying more blinking events, allowing statistical analysis of individual molecules, which allows the local heterogeneity of the sample to be analyzed. PyY/CB7 complexes do not experience the dramatic fluorescence intensity

enhancement found in R6G/CB7 complexes, demonstrating the lack of connection between strength of complexation and ability to enhance fluorescent properties of the guest dye molecules.

Analysis of the blinking kinetics of PyY molecules and PyY/CB7 complexes yields a range of times related to the duration of the dark state. Two non-fluorescent states of PyY have been suggested to explain the diversity of relaxation kinetics, a possible triplet state and a charge transfer state.

6.2 INTRODUCTION

Strong binding of R6G by CB7 leads to enhanced fluorescence emission intensity and photostability of R6G. Since binding of PyY by CB7 is slightly stronger than R6G is bound by CB7, Table 6.1, CB7 is expected to enhance fluorescence emission intensity and extend the survival lifetime of PyY, at least as much as R6G was enhanced. However, the effects of complexation on organic dye molecules have had varied results. Some dye molecules have experienced enhanced fluorescence properties, such as R6G. Others only have shifted absorption and emission spectra.
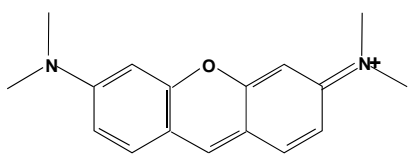
Figure 6.1 – Pyronin Y

Pyronin Y, Figure 6.1, when complexed by β-cyclodextrin (β-CD) has a lower absorbance and lower emission intensity than PyY without cyclodextrin.[1] In the case of PyY and β-CD, complexation stabilizes the non-fluorescent charge transfer state of PyY, which is susceptible to photodegradation.[1] Therefore, fluorescence emission may not always increase by complexing dye molecules. However, PyY is complexed much

more strongly by CB7 ($K_a \sim 10^6$ M^{-1}) than by β-CD ($K_a \sim 10^3$ M^{-1}). CB7

preferentially complexes PyY in a 1:1 ratio[2] as opposed to β-CD, which complexes

PyY either in 1:1 ratio or in a 1:2 ratio (PyY(β-CD)$_2$).[3] A 10^4 enhancement in K_a

value for PyY/CB7 complexes over PyY/β-CD complexes is indicative of the

stronger electrostatic interactions between PyY and the CB7 cavity. Still,

complexation by β-CD or CB7 is known to change properties of dye molecules in

different ways, as demonstrated by fluorescent lifetimes in Table 6.1. The

fluorescent lifetime of PyY decreases when PyY is complexed by β-CD, but

increases when PyY is complexed by CB7. R6G/β-CD and R6G/CB7 complexes

have nearly identical fluorescent lifetimes, indicating less sensitivity to

environmental changes due to complexation than PyY. Upon strong complexation,

PyY may also have greater changes in other photophysical characteristics, such as

intensity and photostability enhancements. Exploring the photophysical changes for

PyY/CB7 complexes enables a discussion of whether stronger association (greater

K_a) between dye and host coincides with fluorescence enhancement.

Table 6.1 – Complexation Effects on R6G and PyY

Molecule/ Complex	Association Constant (M^{-1})	τ_f (ns)
R6G	N/A	4.08,[4] 4.2[5]
R6G/ β-CD	330 ± 30[6]	4.6[5]
R6G/CB7	>5 x 10^5 [7]	4.76[4]
PyY	N/A	1.69,[4] 1.7[1]
PyY/ β-CD	0.4 x 10^3 [1]	~1[1]
PyY/CB7	4.56 ± 0.1 x 10^6 [2]	3.44[4]

CB7-complexation of R6G (chapters 4 and 5) showed extended survival

lifetimes as well as enhanced emission intensity. Though not all complexed dye

molecules experience enhanced emission intensity, greater photostability of a complexed dye is expected as collisions are limited with the included dye molecule. Enhanced photostability of blinking dye molecules can improve the reliability of blinking kinetics analyses, which depend on the total number of blinking events available from fluorescence transients. Longer-lived molecules are expected to give more blinking data for more reliable statistical analysis, which has been difficult to obtain for single small organic dye molecules. Some blinking studies of long-lived molecules have been accomplished using the fluorescence of single polymer molecules,[8] a dye bound to gold nanoparticles,[9] redox systems to accelerate the recovery of molecules from the triplet state,[10] and inert atmospheres.[11] In these studies, the blinking activity was related to the local environment, including the size of the bound nanoparticle. The ability to blink has also been found to be controllable and limited in photostable polymer nanoparticles.[12] Information from dye molecule blinking can be related to radiative and non-radiative decay processes. Gaining a better understanding of what enhances radiative decay while minimizing non-radiative decay processes can help to maximize the quantum yield ($\varphi = k_{rad}/ k_{rad} +k_{non-rad}$ = photons$_{emitted}$/photons$_{absorbed}$) for a fluorescent dye. Higher quantum yield dye molecules are of interest to maximize the output of solid-state dye lasers.

From what was learned with CB7-complexation of R6G, the solgel matrix interrupted complexation of R6G by CB7 (chapter 5). Two factors seemed to contribute to the interruption of CB7-complexation: (1) the mismatch in size for R6G to fit completely within the cavity of CB7, and (2) the similar attractive forces

between R6G and CB7 or R6G and the solgel matrix. Both of these factors are being addressed in this work. First, PyY has been chosen as a cationic dye molecule of similar xanthene structure to R6G, but lacking the large side group which limited R6G to only partial complexation. Second, a weak polymer electrolyte layer has been used to immobilize the mobile cationic PyY instead of an encapsulating silica solgel. The polymer layer should be an electrically neutral surface that is not expected to interact substantially with the cationic PyY. As opposed to the silicate matrix, which had negative charges on pore surfaces, the weakly positive charges on the selected polyelectrolyte layer (PAH) should not compete with CB7 for the cationic PyY guest molecules. On the other hand, the polymer layer can exist as a lumpy surface to reduce translational motion of dye molecules,[13] providing a way to immobilize PyY that will allow an independent assessment of the effect of attraction toward the silica solgel matrix. As different macromolecular hosts affect guest dye molecules to different extents as well as in opposing manners, a study of a strongly-complexed PyY/CB7 system will help to gain information about the ability to predict characteristics of other xanthene/CB7 complexes.

6.3 MATERIALS/METHODS

There are 3 sample types being compared in this work. The first will be referred to as PyY/CB7 on glass and was prepared according to the following specifications. 60 μL of a PyY/CB7 mixture (100 μL of 1 μM PyY and 100 μL of 0.1 mM CB7) in 18Ω Millipore water with final concentrations of 0.5 μM PyY and 50 μM CB7 was spincoated onto a clean coverglass for 70 s at 6100 rpm.

Deposition of the PyY/CB7 mixture was followed by one water rinse, dipping the sample in deionized water for 30 s, and blown dry with N_2 gas.

The second sample type will be referred to as PyY on PAH. Two consecutive treatments were added to a clean coverglass by spincoating for 70 s at 6100 rpm. The first treatment was 60 μL of 0.02 M aqueous solution of pH 7 polyallylamine hydrochloride (PAH); the second was 30 μL of 1 μM PyY in 18Ω Millipore water. The sample was allowed to age for 1 min., rinsed 3 times in deionized water and blown dry with N_2 gas.

The third sample type combined the two previous types and will be referred to as PyY/CB7 on PAH. A layer of PAH was spincoated on a coverglass, followed by a layer of PyY/CB7. First, 60 μL of 0.02 M aqueous solution of pH 7 PAH was spincoated at 6100 rpm for 70 s on a clean coverglass. Then, 60 μL of 0.5 μM PyY/ 50 μM CB7 mixture (from 100 μL of 1 μM PyY and 100 μL of 0.1 mM CB7 mixture) was spincoated onto the PAH layer. This sample was not rinsed.

Samples were used immediately, though no efforts were made to maintain dry conditions during the measurements. Individual PyY molecules and PyY/CB7 complexes were photobleached and dye emission was measured, usually via two APD detectors as in the laser setup detailed in section 2.4.1. From the emission data, analysis included determining the survival lifetime, the average intensity, and the number of blinks for each molecule. The blinking kinetics were also determined for several molecules that possessed a high number of blinking events. The collection of survival lifetime and average intensity has been described fully in chapter 2 as

indicators of photostability and fluorescence enhancement, respectively (Sections 2.4.1.2 and 2.5.1). The number of blinking events was determined by first determining two threshold levels for each molecule, a number of photons that qualified the molecule as fluorescing ('on') or not fluorescing ('off') during the 50 ms collection intervals, Figure 6.2.
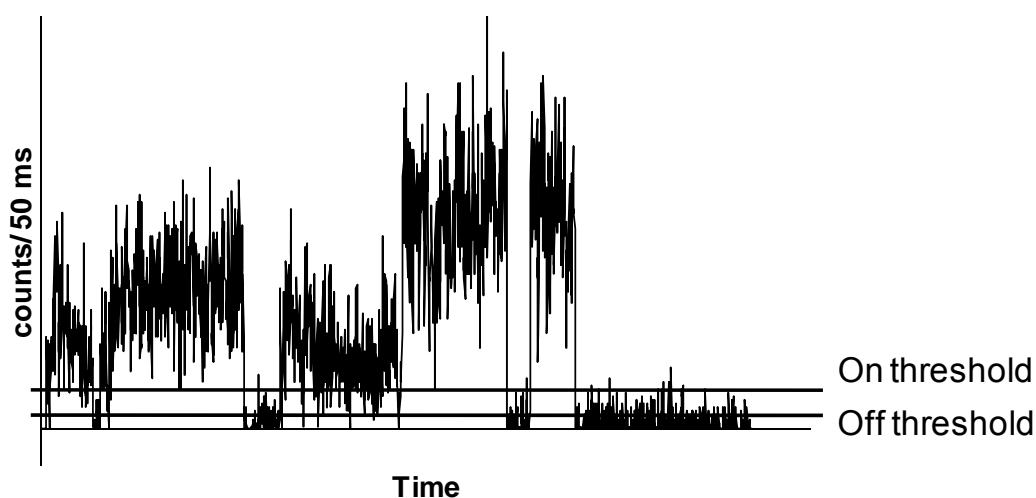
Figure 6.2 – Blinking threshold schematic

The duration of each on time and off time was then determined and a histogram of the on times and off times was made to obtain a statistical analysis of the blinking kinetics for each molecule.

6.4 RESULTS/DISCUSSION

6.4.1 Immobilization

In order to detect the emission for a single PyY molecule for extended durations, it was useful to immobilize the molecules. PyY is a cationic dye that is mobile on glass, Figure 6.3A. Adding PyY on top of a layer of PAH immobilizes the dye molecules allowing round fluorescent images of individual molecules, Figure

6.3B. The PAH is not intended to be a thick layer, but is likely able to produce a rough surface upon which it would be more difficult for the dye molecules to freely diffuse. Complexation of PyY by CB7 is also able to immobilize the dye molecules, Figure 6.3C. In the case of complexation, CB7 sticks to the glass and has enveloped the charge of PyY, reducing the mobility of PyY in the adsorbed water layer common to clean glass surfaces.[14] The hydrophobic CB7 prefers adsorbing to the glass surface and is not easily solvated by the thin water layer that adsorbs to clean glass under normal humidity levels. As was the case with R6G/CB7 and PyY/β-CD complexes, the increased molecular weight of the PyY/CB7 complex also slows diffusion.[15] Figure 6.3D shows the resulting fluorescence from an alternate method of preparing a PyY/CB7 sample using a CB7 laminate film, as described in chapter 4. To ascertain if PAH affects PyY/CB7 complexation, the PyY/CB7 complex has also been added to a layer of PAH, Figure 6.3 E. Intensity and photostability of the PyY/CB7 complexes on PAH were compared to PyY/CB7 complexes on glass and PyY molecules on PAH.
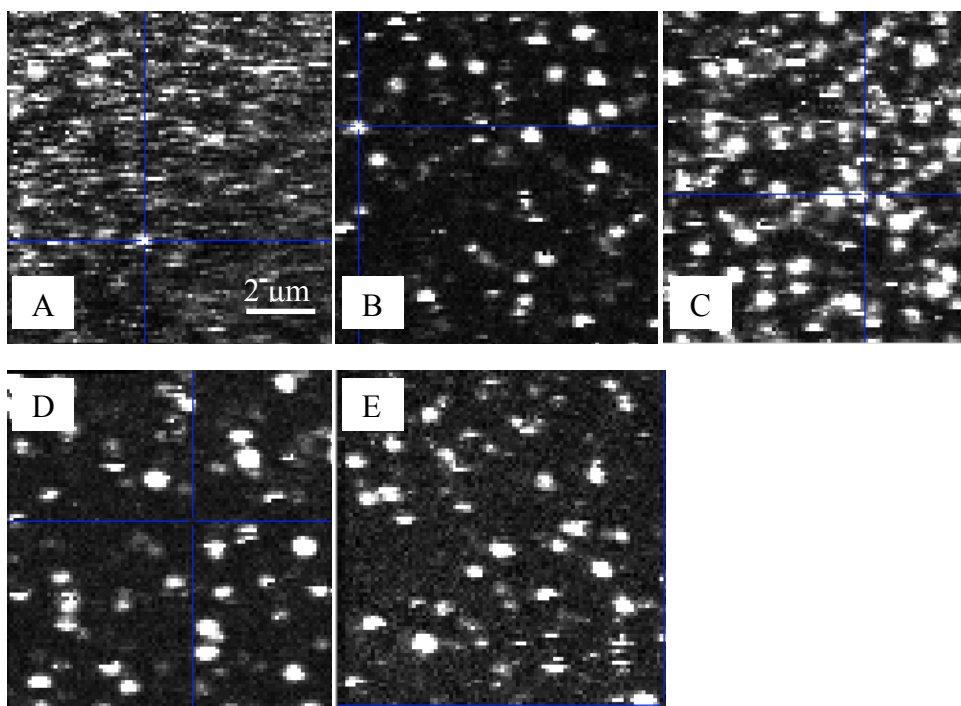
Figure 6.3 – Immobilization of PyY by PAH monolayer or CB7; A) PyY spincoated on a clean coverglass is mobile. This sample was also rinsed and dried with nitrogen. B) PyY pipetted onto a spincoated PAH monolayer is stationary. C) Spincoating a PyY/CB7 mixture, rinsing with water, and drying with nitrogen yields several immobilized complexes on glass. D) PyY pipetted onto a CB7 laminate and rinsed three times with water gave good separation between stationary PyY/CB7 complexes. E) A PyY/CB7 mixture pipetted onto a spincoated PAH monolayer, rinsed three times and dried with nitrogen expectedly yielded stationary PyY/CB7 fluorescent signals.

6.4.2 – Fluorescence Enhancement through CB7 Complexation

Emission Intensity

The emission intensity of each PyY molecule and PyY/CB7 complex is presented in histograms of count rates recorded during 50 ms intervals, Figures 6.4 (PyY on PAH), 6.5 (PyY/CB7 on PAH) and 6.6 (PyY/CB7 on glass). Gaussian

peaks ($f(x) = Ae^{\frac{-(x-\omega_0)^2}{2\sigma^2}}$, where $\sigma = \frac{FWHM}{2\sqrt{2ln2}}$) were fit to each of the histograms,

indicating the most common count rates, ω_0, and a measure of the variation of count

rates as full width at half maximum, FWHM. Two gaussian peaks (parameters in

Table 6.2) were necessary to fit both the strong preference for a single count rate and

the large variation of count rates for each sample type.
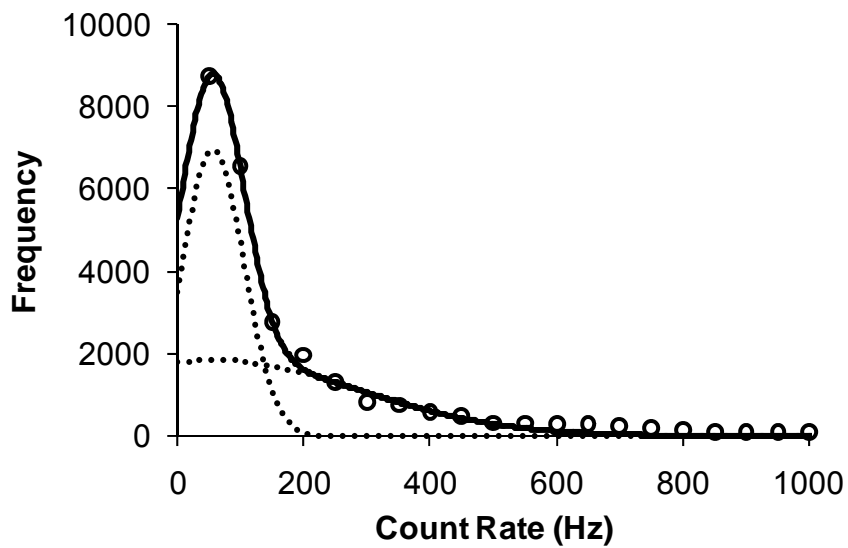
Figure 6.4 – PyY on PAH intensity histogram, fit with 2 gaussian peaks, R^2 = 0.9964.
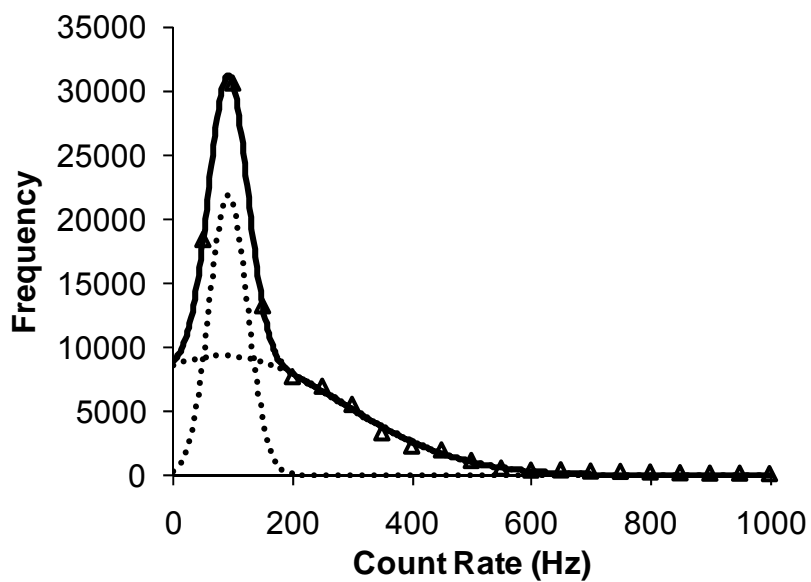
Figure 6.5 – PyY/CB7 on PAH intensity histogram, fit with 2 gaussian peaks, $R^2 =$ 0.9991.
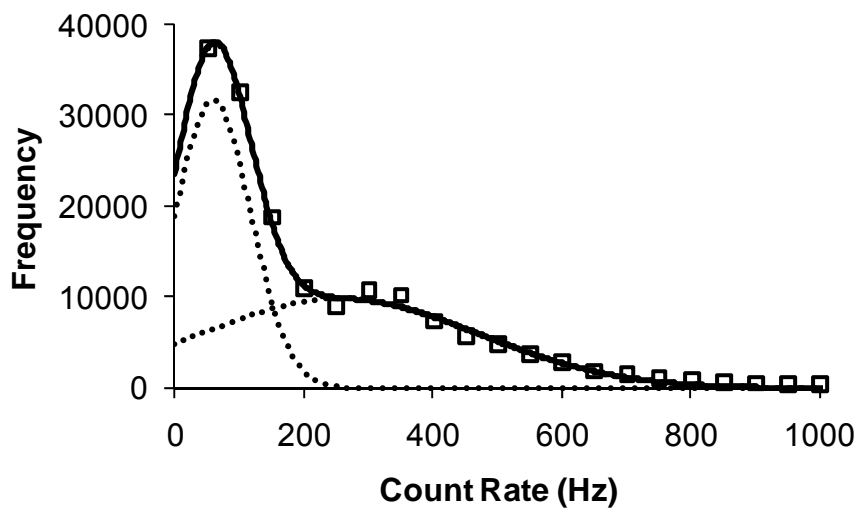
Figure 6.6 – PyY/CB7 on glass intensity histogram, fit with 2 gaussian peaks, $R^2 =$ 0.9972.

Table 6.2 – Pyronin Y Emission Intensity Fitting Parameters

	Peak Max Frequency	Count rate, ω_0 (Hz)	FWHM (Hz)	Ratio FWHM:$\omega_0^{1/2}$
PyY on PAH$_1$	7000 ± 200	56.88	49 ± 2	6.5
PyY on PAH$_2$	1900 ± 200	56.88*	230 ± 20	31
PyY/CB7 on PAH$_1$	22000 ± 2000	92 ± 2	32 ± 2	3.3
PyY/CB7 on PAH$_2$	9000 ± 2000	80 ± 70	200 ± 30	22
PyY/CB7$_1$	32000± 2000	60 ± 4	59 ± 5	7.6
PyY/CB7$_2$	9900 ± 600	260 ± 40	210 ± 30	13

*Fitting constraint added to keep peak position greater than or equal to the other peak.

While PyY on PAH and PyY/CB7 on PAH show the two gaussian peaks at nearly the same count rate, Table 6.2, PyY/CB7 shows a shift to higher count rates in the lower frequency peak, PyY/CB7$_2$, as compared to the high frequency peak, PyY/CB7$_1$. When comparing the two PyY/CB7 samples, the difference in count rate for the PyY/CB7 on glass peaks shows that in the absence of PAH CB7-complexation enhances the emission intensity of only some PyY/CB7 complexes. Whereas almost all PyY/CB7 complexes on PAH are enhanced almost the same amount as compared to PyY on PAH. It may be that without PAH interacting with PyY, the PyY/CB7 complex is more stable, allowing PyY/CB7 to maintain the conformations it adopts without competition from the PAH. Based on the peak count rates of PyY on PAH and PyY/CB7 on PAH, ω_0 in Table 6.2, CB7-complexation seems to increase the emission count rate of PyY 1.5-fold, not as significantly as initially indicated by solution measurements of fluorescence intensity, which indicated a 37-fold enhancement.[16] The single molecule results are

more consistent with the ensemble work of Moore, which found a modest 1.3 fold increase in fluorescent intensity.[17]

Also indicated by the gaussian peaks fit to the intensity data are large FWHM values. The values for FWHM are much larger than expected from shot noise alone according to Poisson statistics, as discussed in Chapter 4. The ratio of FWHM to the square root of ω_0, Table 6.2, gives an indication of the excess width of the curve. The FWHM:$\omega_0^{1/2}$ ratio for the three samples is largest for uncomplexed PyY on PAH, indicating the greatest heterogeneity in count rates. The smallest ratio is given for PyY/CB7 complexes on glass, indicating the least heterogeneity. This leaves PyY/CB7 complexes on PAH as the intermediate sample, having emission intensity heterogeneity between PyY on PAH and PyY/CB7 on glass. The additional heterogeneity for PyY/CB7 on PAH as compared to PyY/CB7 on glass may come from the morphology of the PAH surface or the random charge distribution of PAH. At a pH near 7, PAH has portions with a positive charge, since the pK_a of PAH is between 9 and 10.[18] The charge on PyY may localize on different parts of the molecule depending on whether it is immobilized near a protonated amine of PAH, or the chloride counter ion. When the charge is localized on the central portion of the xanthene forming the charge transfer state, Figure 6.7, complexation with CB7 may place PyY only halfway in the CB7 cavity. When the charge is localized on the amines, PyY is expected to be fully included in the CB7 cavity. A fully-included PyY would be more protected from environmental differences, as seen in the FWHM values for PyY/CB7 complexes as compared to PyY molecules.
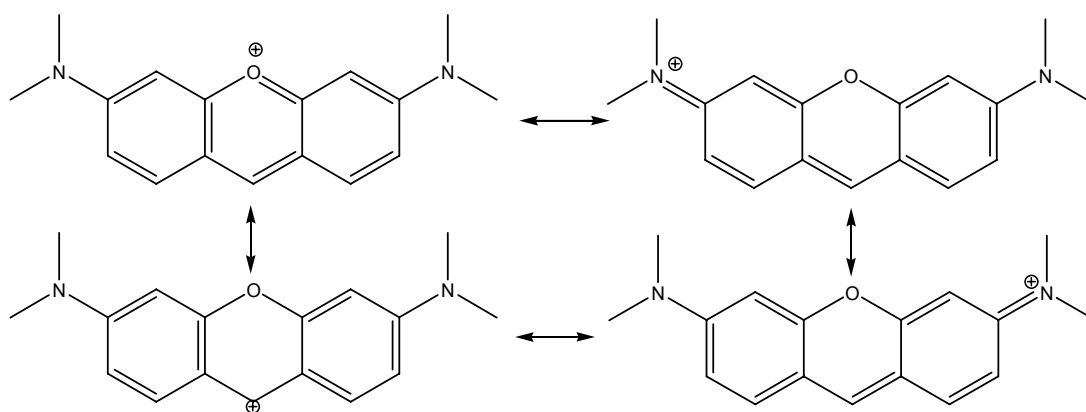
Figure 6.7 – Localization of charge on PyY, charge transfer state (left structures)

Between the two PAH samples, the PyY/CB7 on PAH has a small increase in average count rate and a reduction in FWHM over the PyY on PAH. The trends continue for PyY/CB7 on glass, with a higher average count rate, Table 6.3, and lower FWHM. It seems CB7-complexation confers emission intensity enhancement, indicated by the larger ω_0 for PyY/CB7 complexes as compared to PyY molecules alone. A smaller ratio of

Table 6.3 – Average Intensity of PyY and PyY/CB7

Sample	Average Count Rate (Hz)
PyY on PAH	56.88
PyY/CB7 on PAH	89.31
PyY/CB7 on glass	107.5

FWHM: $\omega_0^{1/2}$ with CB7-complexation on glass also indicates a more homogeneous environment of PyY/CB7 complexes without PAH present. The combination of enhanced intensity and homogeneity for PyY/CB7 on glass relative to PyY/CB7 on PAH could indicate that CB7-complexation of PyY is partially interrupted in the presence of PAH, causing PyY to only experience part of the complexation benefits on PAH. The PyY and PyY/CB7 emission count rates mirror what is expected of the

sample environments. The PAH surface is expected to be lumpy and heterogeneous, while the CB7 cavity should be more homogeneous.

The data supports what was expected, that PyY count rates should be more homogeneous in the CB7 cavity, as opposed to the uncomplexed environment. PyY/CB7 on PAH has an average count rate between the other two samples, indicating the binding between PyY and CB7 may not be as strong as previously thought. With a K_a value only 10x greater than complexation between R6G and CB7, there may still be some competition between the surrounding environment and CB7. However, instead of the strong electrostatic charge of unprotonated silanol groups in solgel, PAH competes for PyY with only its counter ion, as the main polymer structure is positively charged and should not attract the cationic PyY.

Stronger binding of PyY by CB7 is expected to show only a single intensity peak as a result of a more homogeneous environment. However, all PyY samples required two gaussian peaks to fit the intensity histogram data. Two intensity peaks indicate multiple conformations for the PyY/CB7 complexes. The different conformations may arise from movement of PyY relative to the CB7 cavity or multiple static PyY/CB7 conformations.

Enhanced Photostability

The emission intensity of PyY is moderately enhanced by CB7-complexation. However, CB7-complexation extends the survival lifetime much more significantly. Both on the PAH layer and directly on the coverglass, PyY/CB7 complexes have a higher photostability than uncomplexed PyY. This can be seen in

Figure 6.8 where the survival lifetimes of PyY molecules and PyY/CB7 complexes are plotted. Biexponential decay curves (fitting parameters in Table 6.4) have been fit to the survival lifetime histograms of PyY and PyY/CB7 in all three samples. The average survival lifetime for PyY and PyY/CB7 is included in Table 6.4 as well. PyY on PAH has the shortest survival lifetime and PyY/CB7 on glass the longest (4-fold enhancement over PyY on PAH), with the survival lifetime of PyY/CB7 on PAH between the other two samples (2-fold enhancement over PyY on PAH).
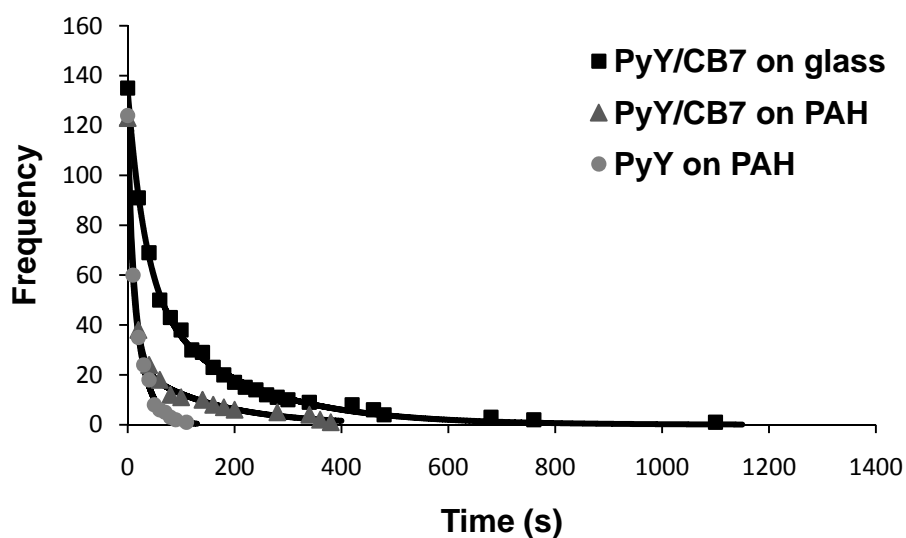
Figure 6.8 – Survival lifetimes of PyY and PyY/CB7

Table 6.4 – Fitting Parameters for PyY and PyY/CB7 Survival Lifetimes

$$f(x) = A_1 e^{-\frac{t}{\tau_1}} + A_2 e^{-\frac{t}{\tau_2}}$$

Sample	τ_1 (s)	A_1	τ_2 (s)	A_2	R^2	τ_{avg} (s)
PyY on PAH	24 ± 2	80 ± 10	5 ± 2	40 ± 10	0.999	17.6
PyY/CB7 on PAH	140 ± 20	25 ± 2	11.5 ± 0.8	98 ± 3	0.999	38.4
PyY/CB7	180 ± 10	56 ± 5	32 ± 3	79 ± 5	0.999	93.4

The large difference between the average survival lifetime for the two

PyY/CB7 samples indicates either interactions between PyY/CB7 with the PAH

monolayer or incomplete complexation of PyY by CB7 in the presence of PAH.

Incomplete complexation of PyY, either as PyY is in the charge transfer state or

complexation where much of PyY is extending beyond CB7, could reduce the

photostability of PyY/CB7 complexes by reducing the protection given by CB7. It

seems in PyY/CB7 on PAH, PyY is still able to interact with the environment outside

of the CB7 cavity, even though it is expected to be fully-included by CB7 in a 1:1

complex. Some environmental interactions with the ends of PyY could be expected

even with a fully-included PyY, since PyY has a planar structure, unlikely to bend,

that is a few angstroms longer than the CB7 cavity. However, it seems the PAH

layer has almost negated any photostability enhancement of CB7-complexation.

Therefore, it is possible that PyY/CB7 does not maintain a fully-included

conformation on a PAH layer.

Correlation between Photostability and Emission Intensity

Unlike R6G and R6G/CB7, which did not relate survival lifetime to emission

intensity, there is an inverse relationship between extended survival lifetime and

increased emission intensity for PyY and PyY/CB7. As was just discussed, CB7-

complexed PyY has a longer survival lifetime than uncomplexed PyY, whether the

PyY/CB7 complexes are on glass or a layer of PAH. It is also true that CB7-

complexed PyY has a higher average intensity than uncomplexed PyY. In addition,

knowing the survival lifetime or emission intensity of PyY or PyY/CB7 will allow

prediction of the other quantity. PyY molecules and PyY/CB7 complexes have a higher count rate when the fluorescence of the molecule is short-lived and have a low average count rate when the molecule fluoresces for a long time, Figures 6.9, 6.10 and 6.11.
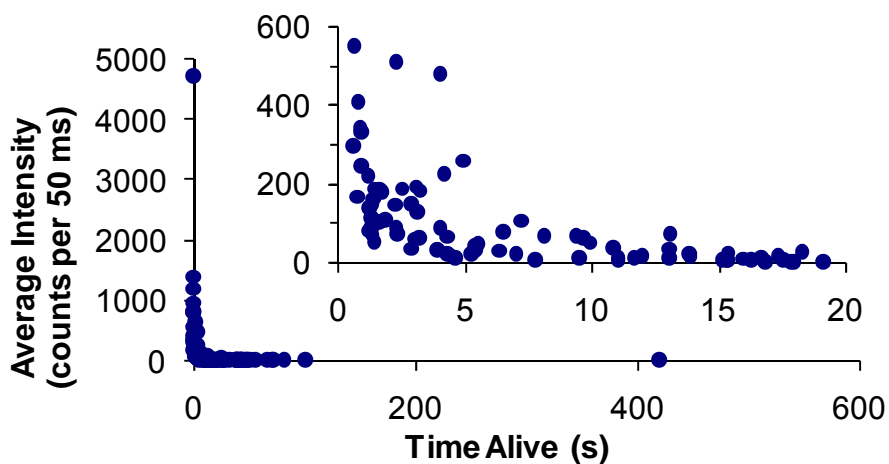
Figure 6.9 – PyY on PAH, comparison between average intensity and time alive; Variety allowed within low intensity and short survival lifetimes, inset.
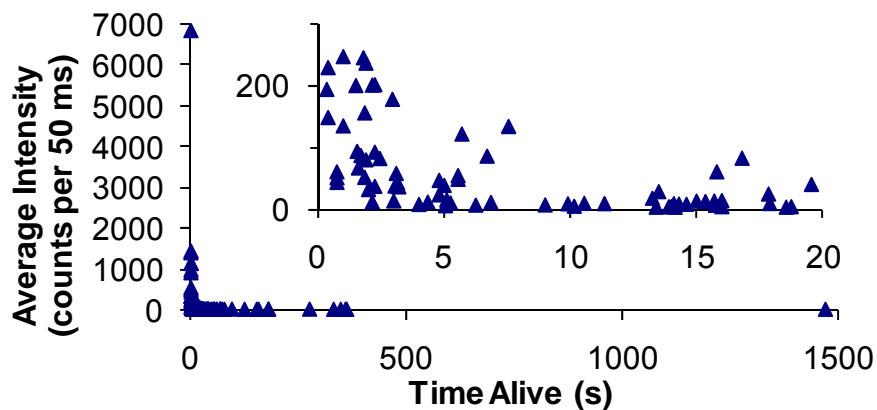
Figure 6.10 – PyY/CB7 on PAH, comparison between average intensity and time alive; Variety allowed within low intensity and short survival lifetimes, inset.
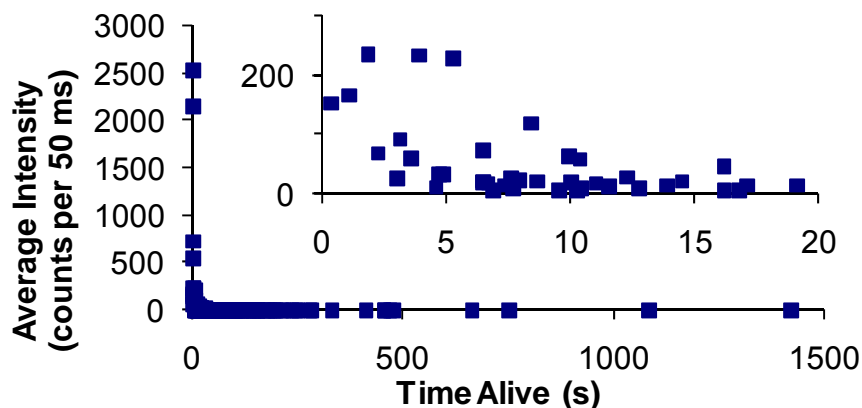
Figure 6.11 – PyY/CB7 on glass, comparison between average intensity and time alive; Variety allowed within low intensity and short survival lifetimes, inset.

The connection between emission intensity and survival lifetime is mostly a characteristic of PyY, but may be partially an environmental effect, as CB7 complexation does have some effect on the extent of correlation. The presence of CB7 seems to enhance the correlation between lower emission intensity and longer survival lifetime. PyY on PAH has a larger intensity range allowed for PyY molecules that last up to 5 s, Figure 6.9. Whereas, PyY/CB7 on PAH and PyY/CB7 on glass both have molecules that emit up to 250 counts per 50 ms, PyY on PAH emits up to 500 counts per 50 ms for molecules emitting for up to 5 s. The complexation between CB7 and PyY both increases emission intensity and protects PyY from interacting with other molecules that would lead to photodegradation extending the survival lifetime. However, CB7-complexation does not explain why uncomplexed PyY exhibits the same non-linear correlation between longer survival lifetime and lower emission intensity. Therefore, PyY must also have a characteristic correlation between longer survival lifetime and lower emission

intensity that remains intact when the molecules are kept at a distance from each other. The correlation between lower emission intensity and better photostability is uninterrupted by CB7-complexation, only enhanced, which demonstrates that CB7 does not affect the photophysics of PyY much, despite having a strong binding constant.

6.4.3 PyY Blinking Affected by Environment

It is not surprising that longer-lived molecules, those complexed by CB7, are likely to have more blinking events. This is what was expected and one of the reasons CB7-complexation is crucial to being able to more fully understand fluorescent dyes. However, from an analysis of the number of blinks per second for each of the samples, CB7 seems to remove any correlation between the rate of blinking and extended survival lifetime. Only the uncomplexed PyY on PAH seems to correlate the rate of blinking with survival lifetime, Figure 6.12. The one long-lived PyY molecule had a blink rate of 1.8 blinks per second, not included in Figure 6.12. In contrast, PyY/CB7 complexes on PAH and PyY/CB7 complexes on glass do not show any correlation between the rate of blinking and the survival lifetime, Figures 6.13 and 6.14. The only molecule not included in Figure 6.13 was an extremely long-lived molecule with a blink rate of 1.2 blinks per second. In PyY/CB7 complexes, it seems CB7 removes the correlation between survival lifetime and blinking rate of PyY.
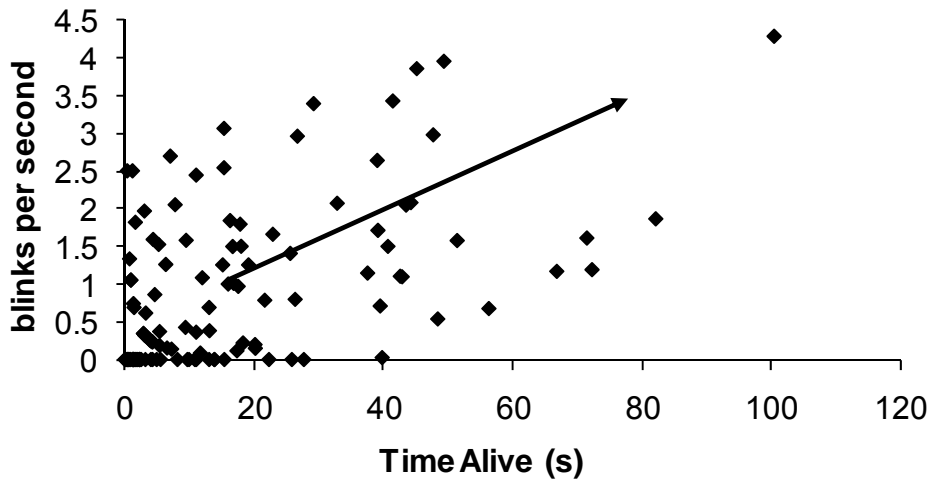
Figure 6.12 – Blinking rate of PyY on PAH as a function of survival lifetime; arrow indicates correlation between blinking rate and survival lifetime.
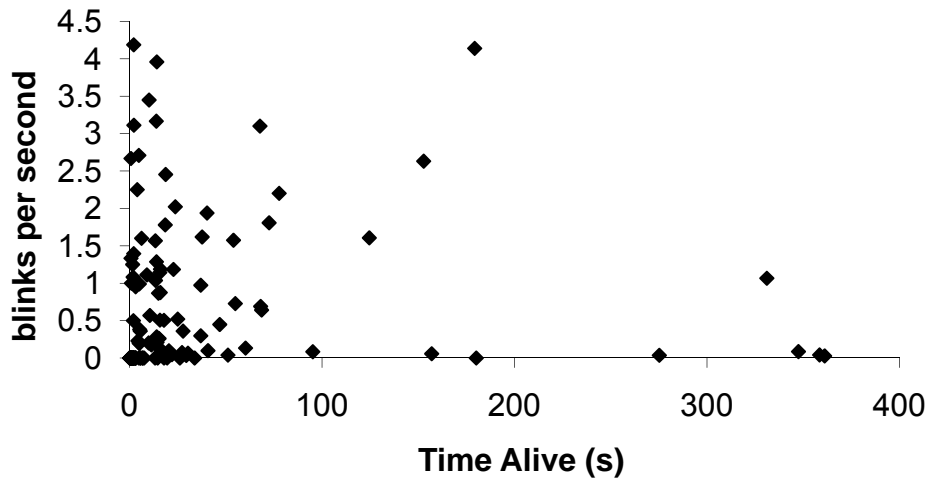
Figure 6.13 – Blinking rate of PyY/CB7 on PAH as a function of survival lifetime

134
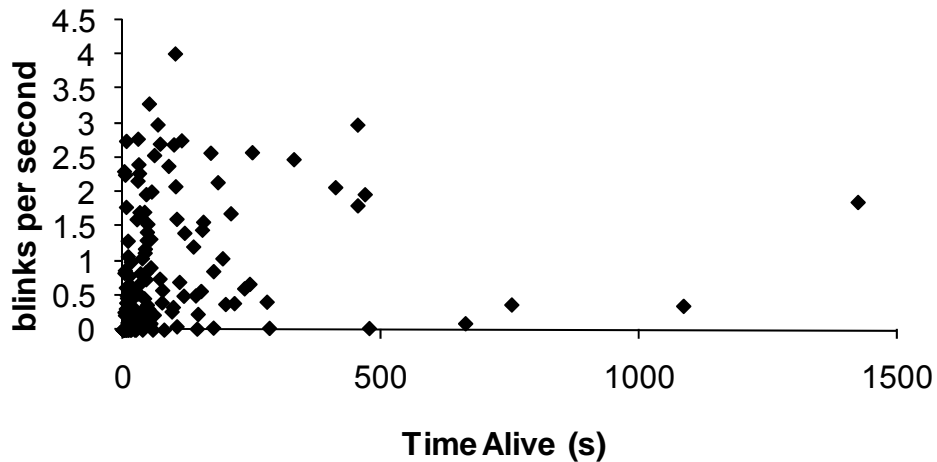
Figure 6.14 – Blinking rate of PyY/CB7 on glass as a function of survival lifetime

More importantly, the lengthened survival lifetime has enabled a statistical

analysis of the length of each dark state as well as how long the molecule fluoresces

before blinking to the dark state again. The blinking kinetics of 26 molecules have

been analyzed. The fluorescence intensity of each molecule was analyzed for a

background fluorescence value when the molecule was assumed to be non-

fluorescent. Below this threshold the molecule is termed "off" and the amount of

time it remains off before blinking on again is the off time. Likewise, a threshold

was set for each molecule when it was determined to be fluorescing. The fluorescent

times have been termed the "on" times. The on and off times for all of the PyY

molecules and PyY/CB7 complexes of each sample type have been collected and

plotted in Figure 6.15. There are many short blink times and few long blink times,

whether as on times or off times. Though it seems the on times are more likely to

have extended durations, this may be an experimental bias, because a molecule that

was non-fluorescent for more than 30 seconds was deemed photobleached.
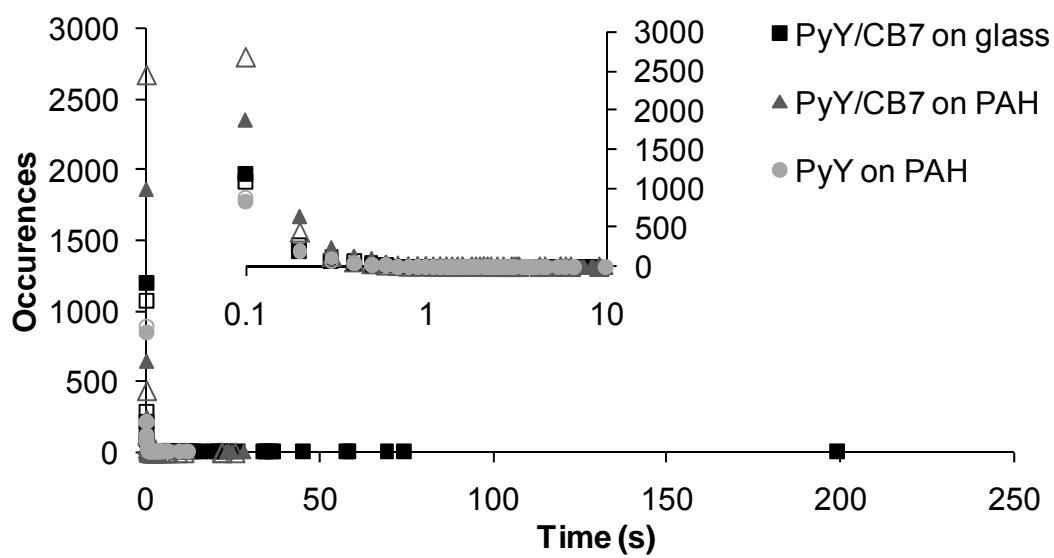
Figure 6.15 – On and off times of the PyY and PyY/CB7 samples. On times are noted by solid symbols, off times by open symbols. Each sample type has a different shape; PyY/CB7 on glass (■), PyY/CB7 on PAH (▲), and PyY on PAH (●). Inset shows a semi-log plot of the same data.

A better look at the differences between the samples is found in the semi-log plot, inset to Figure 6.15, and the normalized plot, Figure 6.16. If the semi-log plot presented linear data, all of the molecules would be expected to follow the same relaxation process to go from the excited state through a single dark state to the ground state. However, in the semi-log plot, the data is not linear. So, either multiple processes are involved for the different molecules or there is heterogeneity in the sample which affects the blinking.
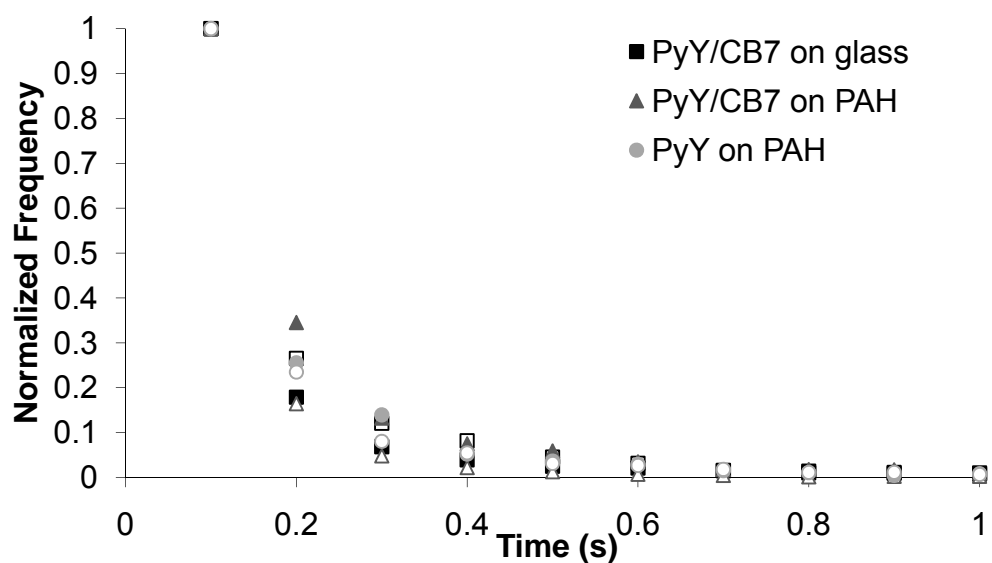
Figure 6.16 – PyY and PyY/CB7 blinking times. On times are noted by solid symbols, off times by open symbols. Each sample type has a different shape; PyY/CB7 on glass (■), PyY/CB7 on PAH (▲), and PyY on PAH (●).

Histograms of the blinking times for each PyY molecule or PyY/CB7 complex used for blinking analysis were fit with exponential decay functions parameters given in Tables 6.5, 6.6, and 6.7 for PyY on PAH, PyY/CB7 on PAH and PyY/CB7 on glass, respectively. The data for each molecule were sufficiently fit by single exponential decay curves, demonstrating that only one type of excited state is relaxing to the dark state for each molecule and each molecule seems to have one dark state that relaxes to the ground state.

Table 6.5 – Exponential Decay Fitting Parameters for Blinking Kinetics of PyY Molecules on PAH

$$f(x) = A_1 e^{-k_1 t}$$

Molecule	k_{on} (s^{-1})	A_{on}	R^2	k_{off} (s^{-1})	A_{off}	R^2	# of blinks
A	7.454	162.5	0.994	21.81	731.8	0.999	374
B	8.328	99.09	0.960	18.51	122.7	0.974	89
C	9.490	94.41	0.976	19.64	99.13	0.959	68
D	10.45	123.6	0.975	21.81	123.8	0.969	86
E	15.69	91.67	0.908	17.44	137.1	0.988	103
F	16.02	286.3	0.975	11.61	167.4	0.954	92
G	18.41	1013.	0.996	12.43	159.1	0.984	212
H	18.90	477.3	0.998	9.303	146.0	0.901	336

PyY on PAH seems to have a wide variety of blinking kinetics. There is a small distinction between molecules that have a smaller value of k_{on} or k_{off}, those of 12 and less, and those with a larger k_{on} or k_{off}. The larger k_{on} correlates to a greater number of short on times, with few on times of longer duration, which indicates a fast transition from the on state to the off state. As blinking is strongly influenced by the local environment of PyY,[8,9] differences in the transition rate could indicate localized differences in charge density of the PAH around the PyY molecules.[11] The dark state is speculated to be either a triplet state or a charge transfer state of PyY. It is reasonable to suggest that formation of a charge transfer state could be influenced significantly by the charge distribution in the environment around the PyY, due to the electrolytic nature of PAH. The charge transfer state has a positive charge on the center ring of the xanthene moiety, Figure 6.7, which would be stabilized by

negative charges in the environment provided by the chloride ions.[1] However, at pH 7, PAH should have some positive charges, which would not help to stabilize the charge transfer state of PyY. PyY molecules with large k_{off} values may be due to a mostly unstable charge transfer state or simply the triplet state. PAH was intended to provide an uncharged surface to immobilize PyY. However, it seems the local differences in charge and the presence of the chloride counter ion may be affecting PyY dark states, increasing the heterogeneity of the system.

Table 6.6 – Exponential Decay Fitting Parameters for Blinking Kinetics of PyroninY/CB7 complexes on PAH

Complex	k_{on} (s^{-1})	A_{on}	R^2	k_{off} (s^{-1})	A_{off}	R^2	# of blinks
I	2.338	13.75	0.8842	26.48	131.4	0.9964	50
J	2.997	22.02	0.8939	34.66	305.3	0.9977	70
K	9.451	575.3	0.9960	21.36	715.0	0.9986	389
L	10.05	2616	0.9940	17.18	7717	0.9988	1826
M	10.16	290.1	0.9885	16.82	854.6	0.9995	200
N	10.48	96.19	0.9470	25.58	407.0	0.9908	172
O	12.12	326.9	0.9889	16.85	548.3	0.9948	443
P	12.30	33.73	0.9014	18.61	24.81	0.9584	18
Q	15.25	223.0	0.9947	19.44	313.1	0.9934	210
R	15.41	134.7	0.9686	30.59	152.3	0.9896	48

There seem to be two distinct k_{on} values from the exponential decay fittings of the on time histograms of individual PyY/CB7 complexes on PAH, Table 6.6. Though the values near 2 have a lower R^2 for their individual exponential fittings,

this can be attributed to the emission transients having few short on times and does not seem to be an indication of poor data quality. Significant from PyY/CB7 on PAH data is the fact that the number of blinking events does not seem to affect the blinking kinetics. For example, a molecule with few blinking events, such as molecule P, had similar k_{on} and k_{off} values to molecules with more than 200 blinking events. Therefore, whether the complex is short-lived and blinks fewer times, or long-lived and blinks many times, the blinking kinetics seem to be consistent. This consistency in blinking kinetics suggests that PyY and PyY/CB7 do not have a correlation between their blinking kinetics and survival lifetime. This may allow shorter-lived molecules to be used for kinetics studies, but the longer-lived molecules still provide more data to increase confidence in the results. It is unknown whether the smaller k_{off} values or larger k_{off} values are associated with the suggested relaxation mechanisms. However, it is possible that the triplet state correlates to a range of k_{off} values and the charge transfer state is responsible for a different range of k_{off} values. It is expected that a molecule that has a single exponential decay constant relaxes to the ground state from a single non-fluorescent species.

Table 6.7 – Exponential Decay Fitting Parameters for Blinking Kinetics of PyY/CB7 Complexes on Glass

Complex	k_{on} (s^{-1})	A_{on}	R^2	k_{off} (s^{-1})	A_{off}	R^2	# of blinks
S	11.20	196.5	0.9750	14.66	297.7	0.9888	109
T	11.67	278.8	0.9910	11.59	296.3	0.9748	158
U	14.71	455.6	0.9894	12.76	373.1	0.9850	168
V	15.72	389.0	0.9860	15.66	385.8	0.9728	137
W	16.93	160.3	0.9752	12.86	131.1	0.9770	165
X	19.99	250.2	0.9914	10.19	97.62	0.9604	185
Y	22.11	274.1	0.9935	16.32	168.0	0.9692	165
Z	22.16	1208.	0.9935	12.47	521.8	0.9855	674

The range of k_{off} values for PyY/CB7 complexes on glass, Table 6.7, are less than the range of k_{off} values for PyY/CB7 complexes on PAH. Smaller k_{off} values result from longer off times, which could indicate greater stability of the dark state. It is possible that the negatively charged glass surface, or partial negative charge of the CB7 cavity portal is stabilizing the positive charge on the xanthene ring of the PyY charge transfer state when PyY/CB7 complexes are directly on the glass surface. Common k_{on} values for PyY/CB7 complexes on PAH and on glass support the possibility of the PyY/CB7 complexes undergoing the same relaxation mechanisms to transition from the on state to the off state.

As with the intensity enhancement, analysis of PyY and PyY/CB7 blinking kinetics indicate CB7-complexation may affect the photophysics of PyY to a small extent, but not substantially. PyY molecules have average values of k_{on} and k_{off}

between the average values for the PyY/CB7 complexes, summarized in Table 6.8. The blinking heterogeneity of individual PyY molecules and PyY/CB7 complexes, as indicated by the large standard deviations, gives an indication of interactions between the PAH and dye molecules even in the presence of CB7. Therefore, PyY is probably incompletely complexed or experiencing dynamic motions even when encapsulated by CB7.

Table 6.8 – Summary of Blinking Activity

Sample Type	Average k_{on}	Average k_{off}
PyY on PAH	13 ± 5	17 ± 5
PyY/CB7 on PAH	10 ± 4	23 ± 6
PyY/CB7	17 ± 4	13 ± 2

The average values were obtained by averaging the fittings for the representative molecules of each sample type.

The two rate constants, k_{on} and k_{off}, are unrelated as k_{on} is the rate of a photoinduced process, and k_{off} is the rate constant of a natural relaxation process. As indicated by the variety of rate constants for the blinking processes, both going from the on state to the off state, k_{on}, and from the off state to the on state, k_{off}, there are probably multiple non-fluorescent species of PyY involved in each sample. Given that CB7 does not affect the photophysics of PyY much, it is likely that the same non-fluorescent species are involved in all three samples. The two non-fluorescent species suggested are 1) a charge transfer state from the excited state, PyY^*_{CT}, Figure 6.17A, and 2) a triplet state, ^3PyY, Figure 6.17B. Since the blinking kinetics of each molecule was well-fit by single exponential decays, it is expected that each PyY
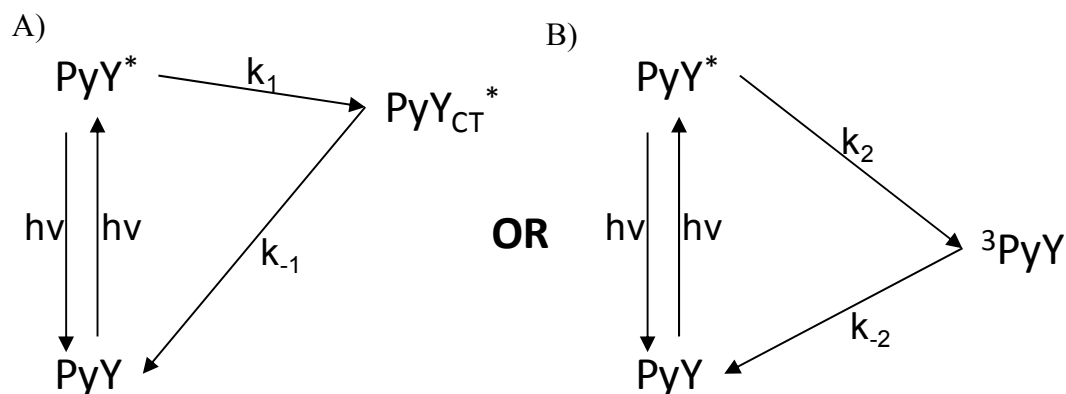
Figure 6.17 – Schematics of possible PyY radiative and non-radiative relaxation pathways, including A) a charge transfer state, or B) a triplet state

molecule or PyY/CB7 complex transitioned to the same dark state each time it blinked. As is detailed by Reija, et al. the amine groups on PyY are capable of non-planar conformations, causing PyY to adopt the non-fluorescent charge transfer (CT) state,[1] suggested above. It is possible that PyY/CB7 can undergo this movement in the volume available within CB7, as well as uncomplexed PyY molecules. Though little is known about PyY photophysics in the literature, it seems reasonable from knowledge of other xanthene dyes that PyY can non-radiatively relax to a triplet state through intersystem crossing from the singlet excited state.[11] However, other xanthene dyes such as rhodamines do not usually blink as often as PyY. It is possible that PyY is able to transition to the charge transfer state more easily than rhodamines due to less steric hindrance for a negatively charged moiety to stabilize the positive charge on the xanthene ring, which could allow PyY to blink more often. Since k_{on} is smaller for PyY and PyY/CB7 on PAH as compared to the PyY/CB7 complexes on glass, the presence of PAH seems to lead to longer on times and slower transitions, k_1 and k_2, to the dark states. The k_{off} values for PyY molecules

and PyY/CB7 complexes on PAH are larger due to shorter off times and faster transitions, k_{-1} and k_{-2}, to the on states, which demonstrates that the dark state is not stabilized as well when PAH is present. Though the samples with PAH have these tendencies, the large standard deviations of k_{on} and k_{off} in the presence of PAH tell of much greater heterogeneity than the PyY/CB7 on glass. Again, it seems the presence of CB7 does not impact the photophysics of PyY very much.

6.5 CONCLUSIONS

Pyronin Y/CB7 complexes show different effects of complexation on the fluorescence of the dye molecules. The PyY/CB7 complexes fluoresce at higher intensities than PyY molecules, especially when PAH does not compete with the complexation by CB7. The photostability enhancement due to CB7-complexation is even more significant. An increase in photostability indicates the charge transfer state has been stabilized, reducing the likelihood of photodegradation. Since quantum efficiency is defined as the number of times the emitting molecule undergoes radiative decay out of all the times it is excited ($\varphi = $ photons$_{emitted}$/photons$_{absorbed} = k_{rad}/ \; k_{rad} + k_{non-rad}$), and the amount of photons emitted by PyY has increased upon complexation with CB7, it is expected the quantum yield has increased. However, it has been shown that CB7-complexation does not seem to affect the photophysics of PyY significantly, except to extend the survival lifetime of PyY.

6.6 REFERENCES

1.   Reija, B.; Al-Soufi, W.; Novo, M.; Tato, J. V., Specific Interactions in the Inclusion Complexes of Pyronin Y and B with β-Cyclodextrin. *J. Phys. Chem. B* **2005**, 109, (4), 1364-1370.

2.   Montes-Navajas, P.; Corma, A.; Garcia, H., Complexation and Fluorescence of Tricyclic Basic Dyes Encapsulated in Cucurbiturils. *ChemPhysChem* **2008**, 9, (5), 713-720.

3.   Schiller, R. L.; Lincoln, S. F.; Coates, J. H., The Inclusion of Pyronine Y by β- and γ-Cyclodextrin. *J. Chem. Soc., Faraday Trans. 1* **1987**, 83, (11), 3237-3248.

4.   Nau, W. M.; Mohanty, J., Taming fluorescent dyes with cucurbituril. *Int. J. Photoenergy* **2005**, 07, 133-141.

5.   Asimov, M. M.; Bushuk, B. A.; Senyuk, M. A.; Stupak, A. P.; Rubinov, A. N., Some Features of Formation of an Inclusion Complex of β-Cyclodextrin with Rhodamine 6G. *J. Appl. Spectrosc.* **1999**, 66, (5), 697-700.

6.   Hamai, S.; Sasaki, K., Investigation of the Formation of Inclusion Complexes between Rhodamine 6G and Cyclodextrins by Means of Capillary Electrophoresis Using Poly(vinyl sulfate). *J. Inclusion Phenom. Macrocyclic Chem.* **2003**, 45, (1-2), 19-25.

7.   Mohanty, J.; Nau, W. M., Ultrastable rhodamine with cucurbituril. *Angew. Chem., Int. Ed. Engl.* **2005**, 44, (24), 3750-3754.

8.   Clifford, J. N.; Bell, T. D. M.; Tinnefeld, P.; Heilemann, M.; Melnikov, S. M.; Hotta, J.-i.; Sliwa, M.; Dedecker, P.; Sauer, M.; Hofkens, J.; Yeow, E. K. L., Fluorescence of Single Molecules in Polymer Films: Sensitivity of Blinking to Local Environment. *J. Phys. Chem. B* **2007**, 111, (25), 6987-6991.

9.   Cannone, F.; Chirico, G.; Bizzarri, A. R.; Cannistraro, S., Quenching and Blinking of Fluorescence of a Single Dye Molecule Bound to Gold Nanoparticles. *J. Phys. Chem. B* **2006**, 110, (33), 16491-16498.

10.   Vogelsang, J.; Kasper, R.; Steinhauer, C.; Person, B.; Heilemann, M.; Sauer, M.; Tinnefeld, P., A Reducing and Oxidizing System Minimizes Photobleaching and Blinking of Fluorescent Dyes. *Angew. Chem., Int. Ed. Engl.* **2008**, 47, (29), 5465-5469.

11.   Zondervan, R.; Kulzer, F.; Orlinskii, S. B.; Orrit, M., Photoblinking of Rhodamine 6G in Poly(vinyl alcohol): Radical Dark State Formed through the Triplet. *J. Phys. Chem. A* **2003**, 107, (35), 6770-6776.

12.   Wu, C.; Bull, B.; Szymanski, C.; Christensen, K.; McNeill, J., Multicolor Conjugated Polymer Dots for Biological Fluorescence Imaging. *ACS Nano* **2008**, 2, (11), 2415-2423.

13.   Biju, B.; Micic, M.; Hu, D.; Lu, H. P., Intermittent Single-Molecule Interfacial Electron Transfer Dynamics. *J. Am. Chem. Soc.* **2004**, 126, (30), 9374-9381.

14.   Mitani, Y.; Shimada, A.; Koshihara, S.; Fukuhara, K.; Kobayashi, H.; Kotani, M., Role of adsorbed water in diffusion of rhodamine 6G on glass surface. *Chem. Phys. Lett.* **2006**, 431, (1-3), 164-168.

15.   Al-Soufi, W.; Reija, B.; Novo, M.; Felekyan, S.; Kuhnemuth, R.; Seidel, C. A. M., Fluorescence Correlation Spectroscopy, a Tool to Investigate Supramolecular Dynamics: Inclusion Complexes of Pyronines with Cyclodextrin. *J. Am. Chem. Soc.* **2005**, 127, (24), 8775-8784.

16.   Yakshe, K. Senior Thesis. University of Oklahoma, Norman, OK, 2007.

17.   Moore, J. L. Host-Guest Complexation of Cationic Xanthene Dyes with Cucurbit[7]uril. University of Oklahoma, Norman, 2008.

18.   Arys, S.; Jonas, A. M.; Laschewsky, A.; Legras, R.; Mallwitz, F., Layered Polyelectrolyte Assemblies. In *Supramolecular Polymers, Second Edition*, Ciferri, A., Ed. Taylor & Francis, Inc.: 2005; pp 651-710.

Chapter VII

Comparison of R6G and R6G/CB7 Complex Photostability in Solution Phase, Alcogel Monolith and Hydrogel Monolith at Bulk Concentrations

7.1 CHAPTER ABSTRACT

The ability of complexation by cucurbit[7]uril (CB7) to enhance rhodamine 6G (R6G) fluorescence was found to be interrupted when R6G and CB7 were encapsulated within alcogel and hydrogel monoliths. R6G/CB7 complexes did not have significantly enhanced photostability in the alcogel and hydrogel matrices, as compared to R6G molecules in the same matrices. This is in direct opposition to the solution behavior of CB7 complexation, which is known to prolong fluorescence emission of cationic dye molecules, including R6G. This work adds to the understanding of CB7 complexation of R6G as a dynamic interaction, which can be interrupted.

The alcogel and hydrogel analogs of R6G and CB7-complexed R6G were compared to solution phase R6G molecules and R6G/CB7 complexes in terms of ability to enhance the fluorescent properties of the dye. Examining the emission spectra with respect to intensity and peak position, showed the interactions with each of the matrices have influenced the emission intensity, as well as the photostability of the dye molecule and complexed dye. As R6G interacted with the matrices, λ_{max}^{em} shifted, indicating a shift in absorbance toward the excitation light wavelength. CB7 seemed to increase the survival lifetime by a factor of two for R6G in both the

solutions and hydrogels, however, the addition of CB7 to the alcogel did little to enhance the fluorescence of R6G as compared to the other samples. Each sample type, solution, alcogel, or hydrogel had a characteristic initial emission peak wavelength and underwent a hypsochromic shift of different amounts. The hypsochromic shift is indicative of electronic interactions between R6G molecules, or between R6G and the alcogel or hydrogel matrix. The hydrogels were found to be superior hosts for R6G fluorescence with the addition of CB7 further enhancing the lifetime, without decreasing emission intensity appreciably. However, the hydrogels displayed a large amount of scattered light, which may have affected the photostability measurements.

7.2 INTRODUCTION

In the 1980s solid-state laser media became a popular development.[1] Advantages of using solid-state media for dye lasers include providing a compact medium and simplified replacement of the laser medium.[1] Development of better solid-state lasers has continued by working to improve the arrangement of the solid-state laser apparatus,[1, 2] as well as the lasing material[3]. Solgel silicates are a popular solid-state matrix to encapsulate lasing dyes.[4]

Optimizing interactions between the dye and matrix has been integral to improving the solid-state dye laser systems. Use of inorganic host materials such as those obtained by the solgel process trap the molecules within the matrix, which reduces both mobility and dimerization of dye molecules, improving both quantum yield and photostability. Other efforts to covalently bond dye molecules to the

inorganic matrix[5, 6] have doubled the lifetime of a laser by improving the photostability of the covalently bonded dyes.

Improving the photostability of dye lasers requires reduction of photodegradation of the dye molecules. Work to define the pathways that lead to photodegradation has also tried to limit those pathways by deoxygenation,[7, 8] doping singlet oxygen quenchers into the host,[9, 10] or controlling the diffusion of the dyes.[8] This work has been successful demonstrating increased photostability with singlet oxygen quenchers, but did not observe enhancement with triplet state quenchers.[10]

The versatility of the solgel silicate structure allows varying quantities of water to be incorporated into the matrix. Structures with less water are referred to as alcogels, while structures with large quantities of water are called hydrogels. Many hydrogels have been composed of polymers,[11-13] though others have incorporated calixarenes,[14], cucurbiturils,[15] and other supramolecular structures.[16] Hydrogel systems have been studied for their ability to absorb and release guest molecules,[17, 18] and incorporate surfactants. Hydrogels are also useful as hosts to investigate motion of macromolecules and how they interact with guest molecules.[19, 20] Incorporating dye complexes into monolithic silica alcogel and silica hydrogel structures could be a useful way to extend the macromolecular complexes to new applications, including long-lived, bright solid-state dye lasers. The larger pore size of hydrogels as compared to alcogels presents an environment that may allow greater molecular motion while retaining some of the photostability of solid-state systems.

The monolith research in this chapter adds to the understanding of interactions between matrices and dye complexes discussed within the context of thin films in earlier chapters. A previous comparison of thin films and monoliths found thin film and monolith solgel materials presented similar environments for the guest molecules.[21] However, the comparison only looked at different thicknesses of the same gel composition. Since interactions between guest molecules and the silicate environment are known to determine dye properties,[22-25] differences between gel compositions can affect dye emission properties. The surrounding environment around a noncovalent complex has also been shown to affect how well the dye molecule is complexed due to the addition of salts[26-28] or different solvents.[29] Changing the water content of the solgel silicates may affect the ability of CB7 to complex dye molecules.

Building on the progress we have made in the previous chapters, that utilized cucurbit[7]uril-complexed dye molecules, in this chapter we present monolithic materials with R6G and CB7-complexed R6G. Included are both silica alcogel and silica hydrogel monoliths. This work provides a comparison of solution phase, alcogel and hydrogel systems to probe how the different environments affect dye photostability and emission spectra. A model dye and dye complex were used to allow the transfer of knowledge accumulated through alcogel investigations to hydrogel systems. Bulk dye concentrations of rhodamine 6G (R6G) and CB7-complexed R6G were used to establish a detailed comparison of the systems with a commonly used dye and a dye-complex of interest as guests within optical materials.

151

7.3 MATERIALS AND METHODS

99.9+% tetraethyl orthosilicate (TEOS), 99.+% tetramethyl orthosilicate (TMOS), spectrophotometric grade 95% ethanol and 85 wt % phosphoric acid were purchased from Sigma-Aldrich. Hydrochloric acid was purchased from Fisher Chemicals. Rhodamine 6G (R6G) was purchased from Molecular Probes. Cucurbit[7]uril (CB7) was synthesized as adapted from literature and was provided by Dr. Halterman at the University of Oklahoma. All chemicals were used without further purification. Deionized water was obtained by purification through a Millipore system to at least 18Ω before use.

2.1 mL samples of R6G (1.2 x 10^{-5} M final concentration) and R6G with CB7 (1.2 x 10^{-5} M R6G and 5.3 x 10^{-5} M CB7) were prepared (1) in aqueous solution, (2) in solution with TEOS alcogel and (3) in solution with TMOS hydrogel. Solution samples were pipetted into polypropylene cuvettes and sealed with quartz slides and vacuum grease to prevent evaporation during the course of the experiments. Alcogel samples began as a solution of 1.411 mL TEOS, 800 μL H$_2$O, and 2.817 mL ethanol at a ratio of 3.5:2:7 by volume mixed with 15.6 μL 0.01 phosphoric acid and sonicated for 2 hours. The alcogel solution was then divided and pipetted into two cuvettes before adding 13.89 μL of aqueous R6G solution (1.8 x 10^{-3} M) or 125 μL of R6G/CB7 solution (13.89 μL of 1.8 x 10^{-3} M R6G and 111.12μL of 1 mM CB7 in water). The TMOS hydrogel solution of 562.5 μL TMOS and 120 μL deionized water was mixed with 11.25 μL 0.01 M hydrochloric acid and sonicated for 20 minutes in an ice bath. Then ten volumes of pH 7 phosphate buffer (1850 μL) were

152

added to 185 μL solgel in a polypropylene cuvette. The final addition was either R6G (13.89 μL of 1.8 x 10^{-3} M in water) or R6G/CB7 solution (13.89 μL of 1.8 x 10^{-3} M R6G in water and 111.12μL 1 mM CB7). Once the alcogel and hydrogel solutions were pipetted into polypropylene cuvettes and the dye solution added, the cuvettes were sealed by using vacuum grease to affix quartz slides to the open end of the cuvettes. Sealing the cuvettes limited evaporation during gelation and while the samples were heated by the UV lamp.

The monoliths described in this chapter were not dried, but were allowed to gel without interference. Though gelation occurs at different rates for alcogels and hydrogels all samples were allowed to rest the same amount of time before UV exposure was begun. Once the silicate gels had set for 1 week they no longer appeared to move as fluids in their covered cuvettes.

The 1 week aged samples were irradiated with UV light (20 W, Daigger 2812C) suspended 4.5 cm above the cuvettes for extended periods through the quartz slides. The quartz slides were used to minimize any change in humidity within the samples, while allowing UV light to pass to the sample. The materials utilized require the samples to be irradiated only through the quartz slide.

Bulk fluorescence measurements were made on a Shimadzu RF-5301 PC Spectrofluorophotometer with excitation wavelength 480 nm and emission measured from 488 nm to 675 nm, with excitation and emission slit widths set at 1.5 nm and spectra measured at medium speed.

7.4 RESULTS AND DISCUSSION

7.4.1 Determining Optimal Excitation Wavelength

Though R6G absorbs best near 520 nm,[30] it was not possible to achieve quality emission spectra for the alcogel and hydrogel samples with excitation light near the absorption maximum. The scattering of the excitation light by the hydrogels, and to a lesser extent the alcogels, overlaps substantially with the R6G emission peak when the samples are excited at 514 nm as seen in Figures 7.1 and 7.2. R6G in the alcogel sample, Figure 7.1, does not seem to exhibit any shift in the emission peak position upon UV exposure. However, the peak area is difficult to quantify when the scattered light peak overlaps the emission peak and maintains a high intensity, while the R6G emission is decreasing in intensity. This makes it difficult to compare samples and determine the effects of CB7-complexation within different matrices.
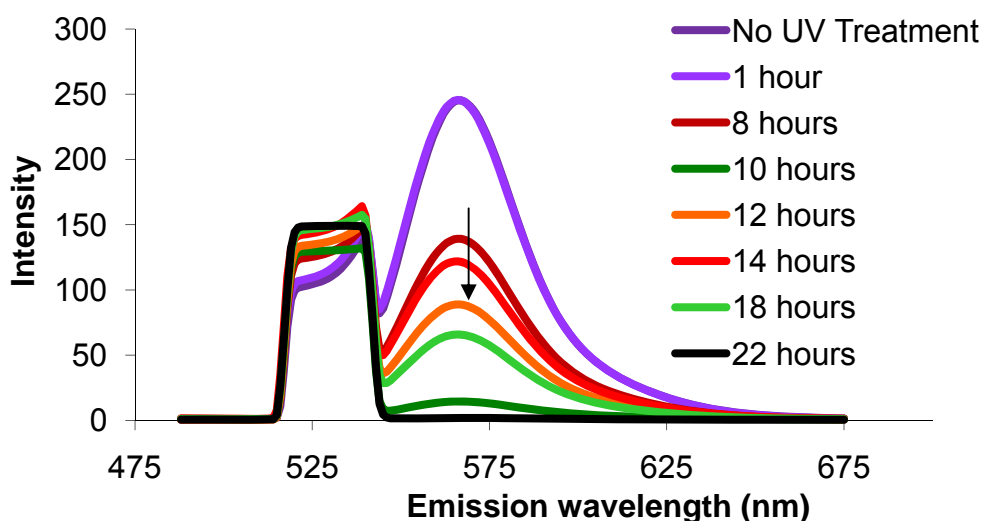
Figure 7.1 – R6G in alcogel, excited at 514 nm. The arrow indicates the spectral progression with increasing UV exposure.
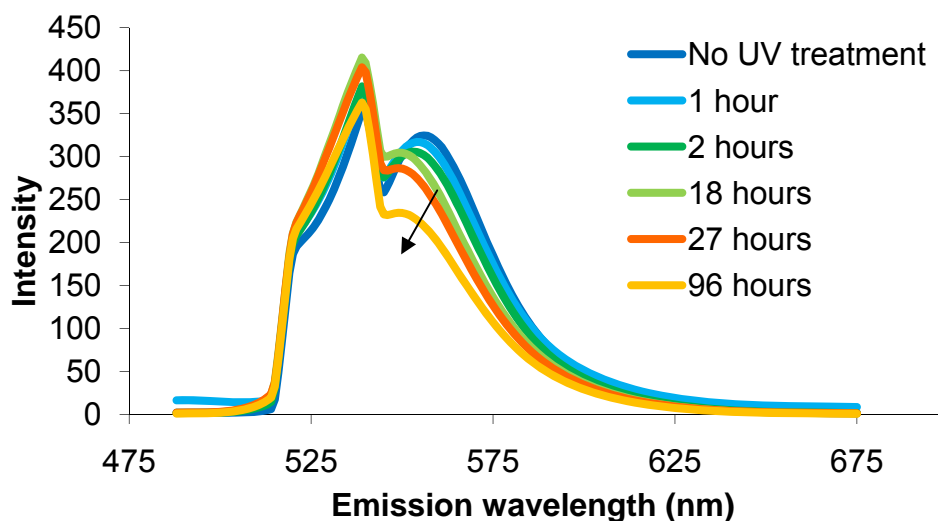
Figure 7.2 – R6G in hydrogel, excited at 514 nm. The arrow indicates the spectral progression with increasing UV exposure.

In the hydrogel sample, as the R6G emission peak shifts to shorter wavelengths during the UV exposure, Figure 7.2, the emission peak overlaps the scattered light peak to a greater extent. This overlap interferes with an accurate measure of the emission intensity of R6G, as well as a clear determination of the peak position. In Figure 7.3, R6G/CB7 in a hydrogel demonstrates the same blue shift in emission peak maximum as R6G in the hydrogel.
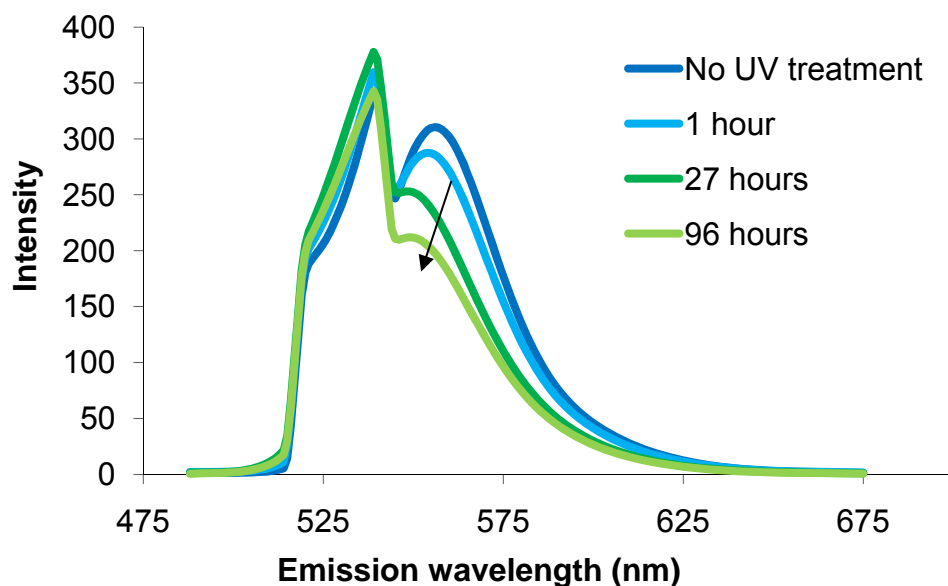
Figure 7.3 – R6G/CB7 in hydrogel, excited at 514 nm. The arrow indicates the spectral progression with increasing UV exposure.

In order to remain close to the wavelength of maximum absorption, , for R6G and acquire emission spectra free of scattered light overlap, the hydrogels were tested for the best excitation wavelength, since the emission of R6G in the hydrogel samples had the most overlap with the scattered light peak. As seen in Figure 7.4, the hydrogel emission spectra were incrementally tested for the optimum excitation wavelength.
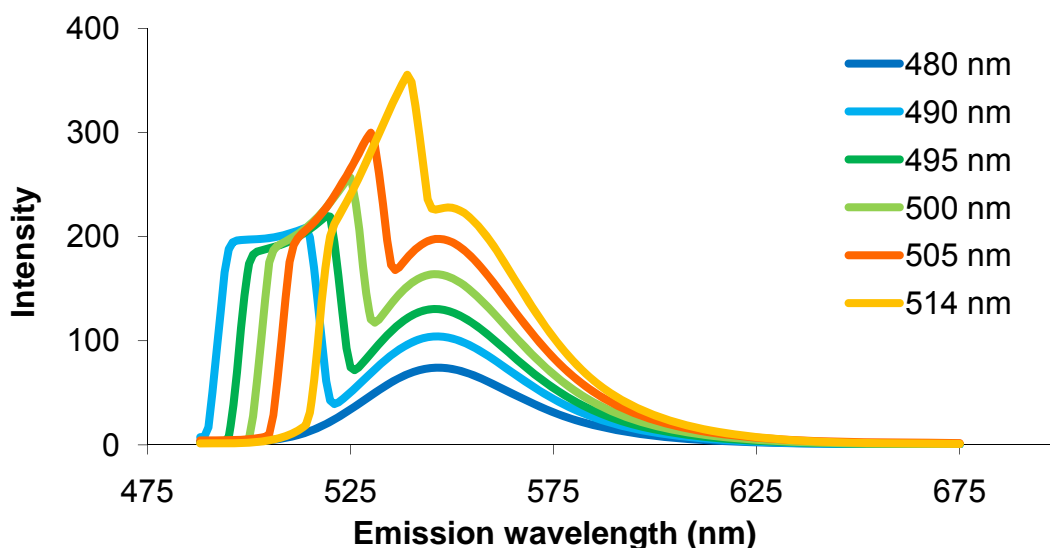
Figure 7.4 –Emission of R6G/CB7 in hydrogel with varied excitation wavelength (after 72 hours of UV exposure).

The optimal hydrogel sample excitation wavelength was determined after 72 hours of UV exposure. Since, the R6G emission peak shifts hypsochromically, toward the scattered light peak, in the hydrogels it was necessary to determine what wavelength of excitation light would allow the minimum overlap of scattered excitation light with R6G emission after the R6G emission had shifted. The peak position continues its hypsochromic shift to 544 nm, as will be shown later, however, the scattered light signal is still far removed from the R6G emission peak. In Figure 7.4, the scattered light peak has moved beyond the observation range using 480 nm excitation, allowing the intensity to reach the baseline level on the left side of the spectrum.

Changing the excitation wavelength reduces the intensity of the R6G emission, as well as reducing the scattered light overlap. This was expected as the

excitation light was moved away from the wavelength of maximum absorbance for R6G, λ_{max}^{abs}. R6G/CB7 in hydrogel shows exactly this behavior, Figure 7.4. Use of excitation light closest to λ_{max}^{abs} shows R6G emission with the highest emission intensity.

7.4.2 R6G IN SOLUTION

As a solution of R6G is exposed to UV light, both the emission intensity and emission peak wavelength, λ_{max}^{em}, of R6G experience changes, Figure 7.5. A bulk concentration of R6G in an aqueous solution undergoes a two-stage decay process in its emission intensity while exposed to UV light as seen by plotting the maximum intensity and λ_{max}^{em} of each measurement, Figure 7.6. Parameters for the exponential changes in emission intensity and λ_{max}^{em} for R6G in solution are summarized in Table 7.1, section 7.4.4. The first 2 hours of UV exposure do not cause any decrease in R6G emission intensity. After the initial 2 hours, the intensity decays exponentially over the next 86 hours, with a decay constant of 24 hr. The slight initial increase is most likely due to reducing the number of low-fluorescent aggregates of R6G in the solution as R6G adsorbs to the cuvette surface.[31, 32]
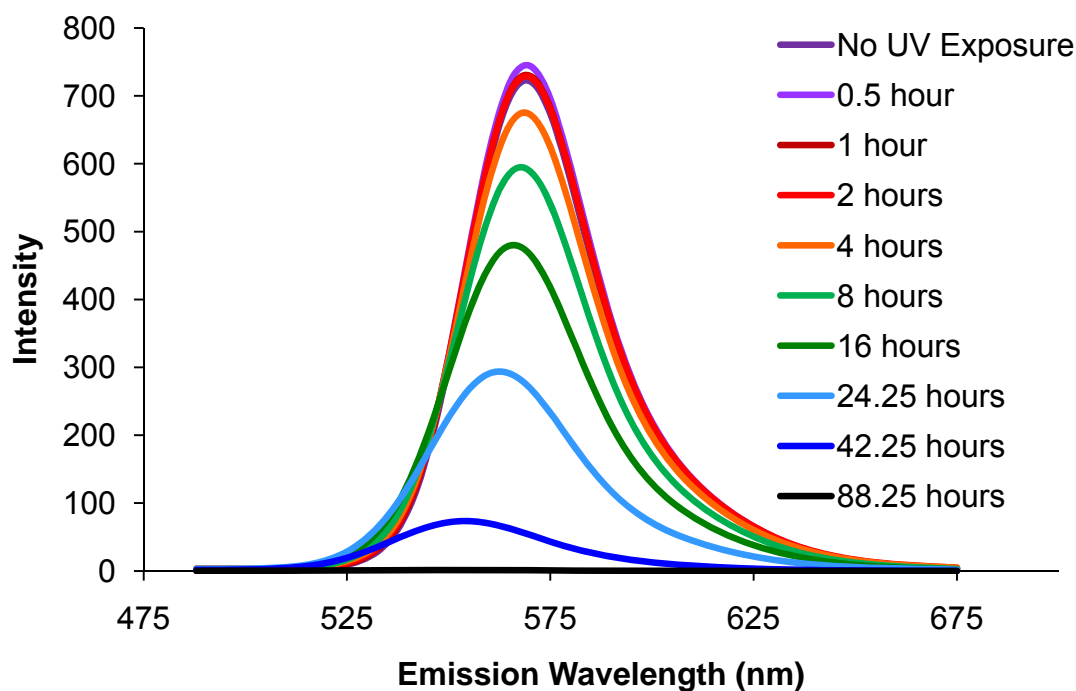
Figure 7.5 – Emission spectra of bulk R6G in solution. 480 nm excitation light.

Xanthene dyes, including rhodamines, typically aggregate at concentrations above 200 μM.[33] Though the solutions have R6G concentrations at just 12 μM, some aggregation is possible even at this low concentration. The low concentration of R6G may explain why there is not a large intensity increase as the aggregates break apart. Aggregation provides multiple non-radiative relaxation pathways for the dye molecules, which reduces the fluorescence emission.[34] In addition, the exciton/exciton quenching can be reduced by a decrease in the R6G concentration in solution due to non-specific adsorption to the surface of the cuvette.[31] By reducing the number of non-radiative pathways, the fluorescence emission intensity of the sample increases.[35] This is seen during the initial two hours of UV exposure. The exponential decay in intensity is due to photobleaching the R6G monomers.
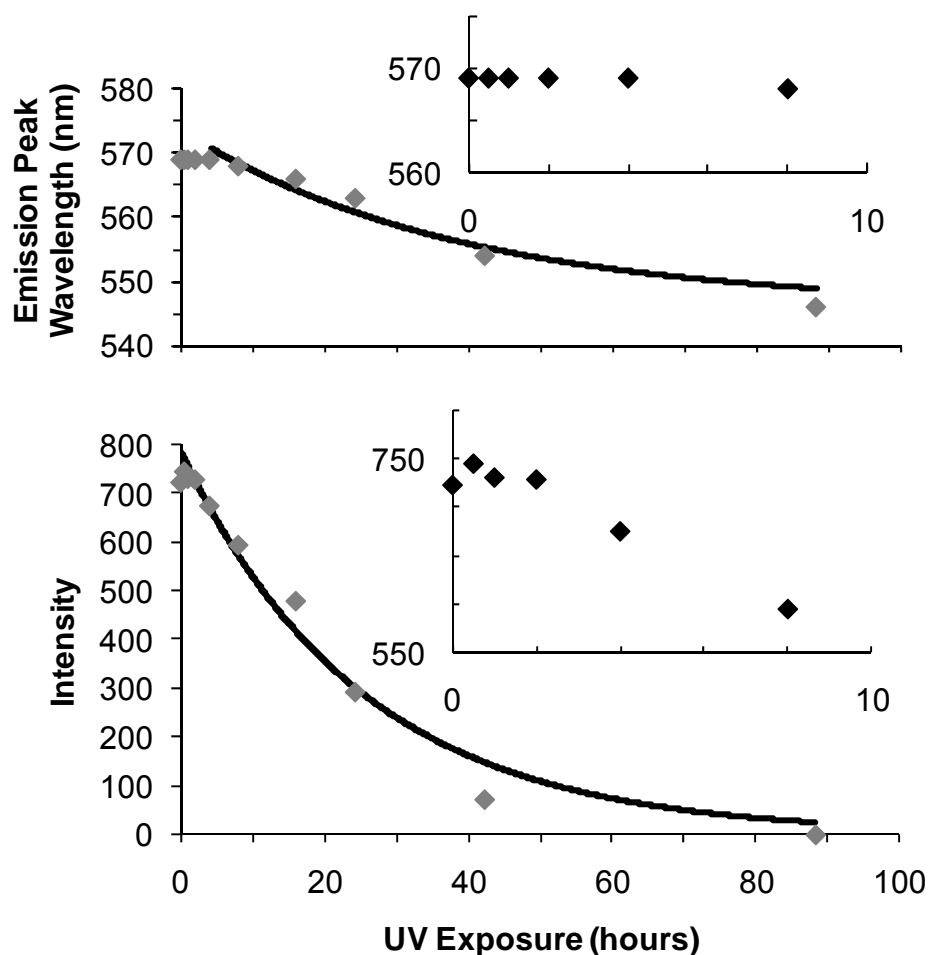
Figure 7.6 – Shift in λ_{max}^{em} and decrease in intensity of R6G emission in bulk solution, while excited at 480 nm. Insets are expansions of data points from the first 10 hours of UV exposure. Exponential decay fittings are in black.

The emission peak position also has two characteristic behaviors. The peak of R6G emission is at 569 nm for the first 4 hours of UV exposure. Then, λ_{max}^{em} blue shifts exponentially to 546 nm, with a decay constant of 60 hr nm^{-1}. Since R6G is the only molecule emitting in this sample, the change in emission wavelength is due to a change in R6G. The original form of R6G will be referred to as R6G$_A$ and the new form of R6G will be referred to as R6G$_B$. Aggregates of R6G are known to

emit at longer wavelengths than R6G monomers.[36] If the blue shift occurred only during the intensity increase, disaggregation may have caused this shift, however, the shift does not occur during the increase in emission intensity. The change occurring with R6G is unidirectional and may be due to a light-induced process, but the process is uncertain.

It seems that the R6G emission peak shift occurs at the same time as the decay in emission intensity. The emission peak does not shift initially, when the intensity is mostly stable. However, the peak begins to shift as the intensity decays. Normalization of the two decays gives exponential decay constants for the spectral shift and the intensity decay of 39.4 hr and 22.4 hr, respectively. If the two changes were due to the same cause, most likely photobleaching, the decay constants might be the same, assuming similar quantum efficiencies of $R6G_A$ and $R6G_B$. Photobleaching is a first-order kinetics process, which should give a first-order decay. Though there are multiple processes occurring, the photobleaching of $R6G_A$, transformation of $R6G_A$ to $R6G_B$, and photobleaching of $R6G_B$, the single exponential decay of the emission intensity is characteristic of first-order decay due to photobleaching. The difference between the emission wavelength of $R6G_A$ and $R6G_B$ is not enough to distinguish 2 peaks from the emission spectra. If the emission peaks from the two species were far enough apart to be well-resolved, the emission due to each species would be clearly differentiable at all points during the experiment allowing determination of the rates of decay for $R6G_A$ and $R6G_B$. The formation of $R6G_B$ does not seem to prolong the emission of R6G significantly, as

would be indicated by a biexponential decay of the emission intensity. $R6G_A$ and $R6G_B$ may have different extinction coefficients and quantum yields yielding different intensities at each wavelength. Without being able to determine the quantum efficiencies of $R6G_A$ and $R6G_B$, the single exponential decay of intensity still may indicate similar photostability of $R6G_A$ and $R6G_B$ in solution.

7.4.3 R6G/ CB7 IN SOLUTION

The emission of CB7-complexed R6G decays over the course of the UV exposure, Figure 7.7, similar to the uncomplexed R6G in solution. The emission of R6G in solution with CB7 (R6G/CB7) undergoes a two-part intensity change upon exposure to UV light. Initially, the emission intensity is constant, Figure 7.8. However, once it begins to decay, after 4 hours of UV exposure, the intensity decay is exponential, with a decay constant of 38 hr.

The λ_{max}^{em} for R6G/CB7 exhibits a similar two-stage process. First, λ_{max}^{em} for R6G/CB7 is at 570 nm and remains stable for approximately 8 hours of UV exposure. Then it shifts exponentially to 550 nm with a decay constant of 60 hr nm^{-1}, where it appears to stop shifting. Parameters for the exponential changes in emission intensity and λ_{max}^{em} for R6G/CB7 in solution are summarized in Table 7.1.

Again, the change in emission peak wavelength indicates a change in R6G/CB7. The wavelength of $R6G_A$/CB7 emission is the same as $R6G_A$ in solution, but the wavelength of $R6G_B$/CB7 emission is not as blue-shifted as $R6G_B$ in solution. Whereas some cationic dye complexes with CB7 emit at shorter wavelengths,[37] R6G seems to emit at slightly longer wavelengths when complexed by CB7.[38] CB7-

complexation shifts both the λ_{max}^{abs} and λ_{max}^{em} of R6G in a manner consistent with

specific interactions between R6G and a less polar environment.[38, 39]
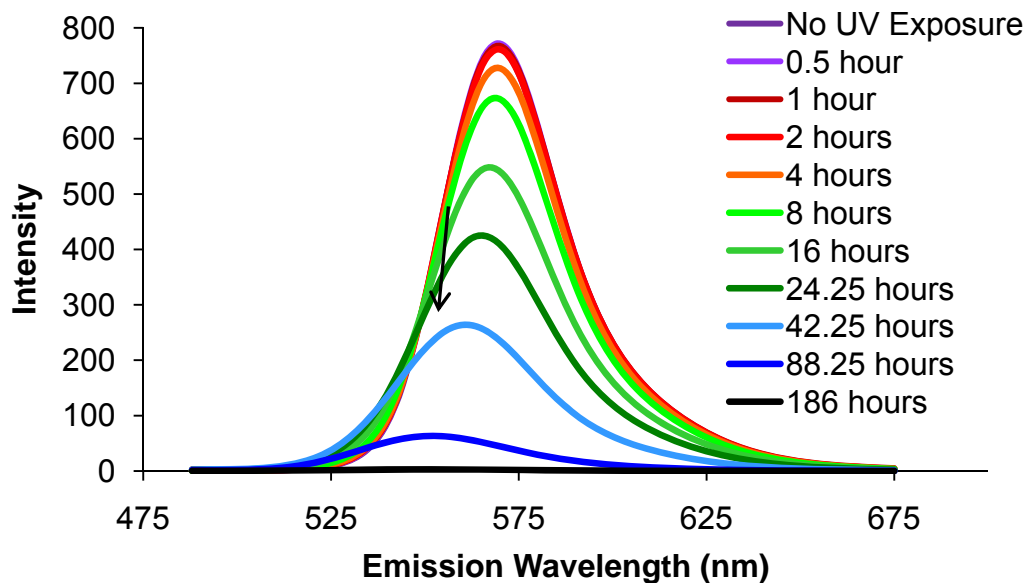
Figure 7.7 – R6G/CB7 in solution, excitation at 480 nm. The arrow shows the
direction of spectral progression with UV exposure time.
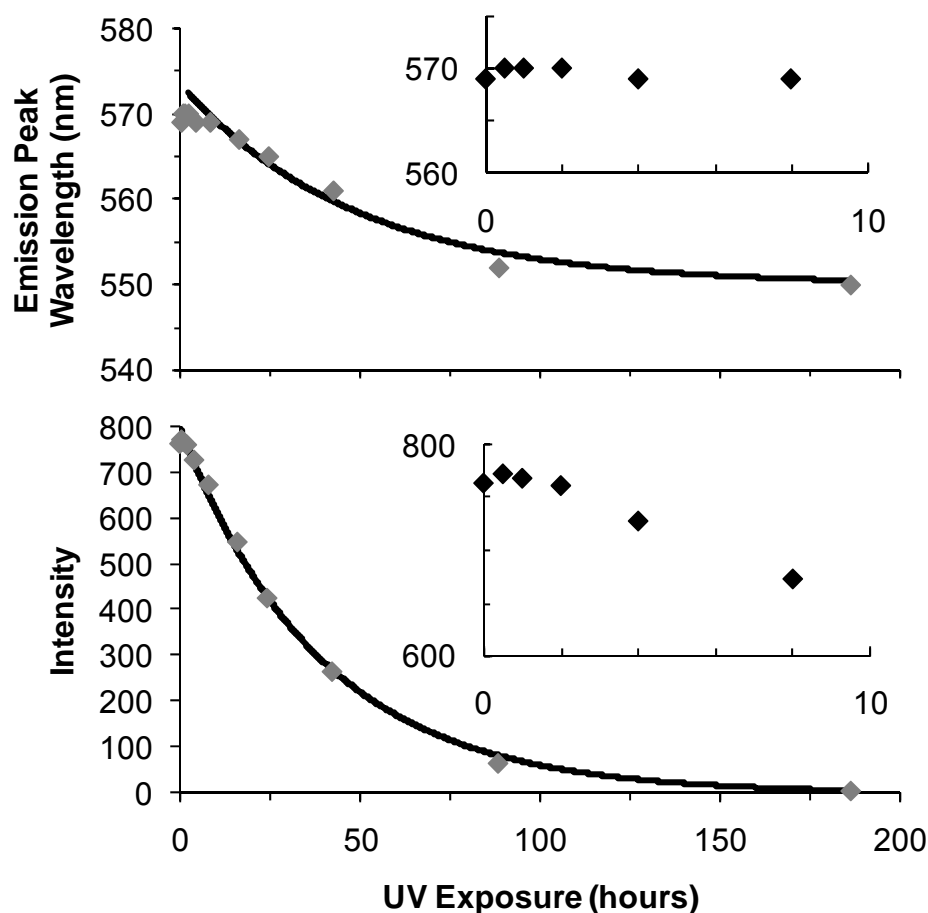
Figure 7.8 – Emission peak shift and intensity decay for R6G/CB7 in solution, excitation at 480 nm. Insets are expansions of data points from the first 10 hours of UV exposure. Exponential decay fittings are in black.

The timing of emission intensity change correlates well to the timing of the hypsochromic shift of the R6G/CB7 signal. Each property demonstrates a first portion with little change followed by an exponential change. The 17 nm change in R6G/CB7 λ_{max}^{em} indicates a similar change in R6G$_A$/CB7 to the R6G$_B$/CB7 species, as with R6G in solution. The similarity in timing of emission intensity decay and spectral shift to emission by R6G$_B$/CB7 indicates that the change from R6G$_A$/CB7 to R6G$_B$/CB7 and the photobleaching process may be occurring simultaneously.

However, normalization of the two decays gives exponential decay constants for the spectral shift and the intensity decay of 56.6 hr and 35.6 hr, respectively. Again, if the two changes were due to the same cause, photobleaching, the decay constants might be the same, assuming similar quantum efficiencies of $R6G_A$/CB7 and $R6G_B$/CB7. Light-induced emission intensity decay and the change in emitting species may be unrelated processes.

7.4.4 COMPARISON OF SOLUTIONS

There are at least two features that show differences between the R6G/CB7 solution and the solution with R6G alone. The first is the extension of time until R6G/CB7 is no longer emitting a measurable amount as compared to R6G. The blue shift of R6G/CB7 λ_{max}^{em} was also less extensive and shifted later than R6G.

The duration of R6G/CB7 emission is twice that of R6G in solution. This can be seen from the exponential decay constants of the fittings for the normalized emission intensity data. The normalized intensities of R6G and R6G/CB7 have decay constants of 22.4 hr and 35.6 hr, respectively. The R6G/CB7 solution emission intensity decays more slowly. The addition of CB7 is expected to reduce the interactions between R6G molecules. Quenching of fluorescence by other R6G molecules, whether monomers or aggregates, can occur non-radiatively by electron exchange or coulombic interaction as the fluorescence of one R6G molecule is absorbed by another R6G molecule. Therefore, photobleaching of R6G/CB7 in solution is expected to be slower than R6G in solution.

Table 7.1 – Fitting Parameters of Exponential Changes for R6G and R6G/CB7 in Solution[*] (Figures 7.6 and 7.8)

	τ (hrs)	A (a.u.)	y_0	R^2	Time range fit
R6G Intensity	24± 3 (hrs)	810 ± 40	0	0.981	2 to 88.25 hrs
R6G/CB7 Intensity	38 ± 1 (hrs)	815 ± 9	0	0.999	2 to 186 hrs
R6G spectral shift	60 ± 30 (hrs nm⁻¹)	37 ± 8	536 ± 10 nm	0.983	8 to 88.25 hrs
R6G/CB7 spectral shift	60 ± 10 (hrs nm⁻¹)	24.5± 2	548 ± 2 nm	0.985	8 to 186 hrs
	τ (hrs)	Maximum	Minimum	R^2	Time range fit
Normalized R6G intensity	22.4	853	0	0.977	4 to 88.25 hrs
Normalized R6G/CB7 intensity	35.6	848	0	0.999	8 to 186 hrs
Normalized R6G shift	39.4	579	542	0.997	16 to 88.25 hrs
Normalized R6G/CB7 shift	56.6	573	548	0.985	8 to 186 hrs

[*]using $f(x) = Ae^{-\frac{t}{\tau}} + y_0$, where A is a factor related to the intensity, τ is the decay constant and y_0 is the y-intercept, which indicates the final wavelength for spectral shift fittings. Normalization fittings used $f(x) = e^{-\frac{t}{\tau}}$, with the maximum and minimum values also being fit.

The emission peak position is interesting for both the timing of the shift and the extent of shift. The peak begins to shift at 2 hours of UV exposure for the R6G solution, while the R6G/CB7 solution emits at the same wavelength until 4 hours of UV exposure. It seems complexation with CB7 delays the change from R6G$_A$/CB7 to R6G$_B$/CB7 slightly as compared to the R6G$_A$ to R6G$_B$ change, though the

normalized data does not have significantly different decay constants, 39.4 hr for R6G and 56.6 hr for R6G/CB7.

The extent of spectral shift is less for R6G/CB7 as compared to R6G in solution. The R6G emission spectrum blue shifts a total of 20 nm over the course of the experiment, while the R6G/CB7 solution shifts 17 nm. A smaller shift in peak position points to less change in R6G/CB7. The transformation from R6G$_A$/CB7 to R6G$_B$/CB7 seems to be less significant than the change from R6G$_A$ to R6G$_B$. Since the spectral shift does not occur during the time when the emission intensity is increasing due to fewer aggregates in solution, the spectral shift should not be connected with disaggregation. The final λ_{max}^{em} is at the wavelength of the R6G monomer, accepted to be near 547 nm.[36] Some R6G$_A$ seems to photobleach before the R6G$_B$ species begins to form, since the emission intensity begins to decay before λ_{max}^{em} changes. However, R6G/CB7 undergoes both changes simultaneously, as indicated by the coincident decrease in emission intensity and peak shift. This possible progression is detailed in Figure 7.9. In region 1 of Figure 7.9, R6G$_A$ represents the monomers and aggregates present. Region 2 corresponds to the time when some R6G has adsorbed to the glass surface. By reducing the R6G concentration in solution, the solution aggregation decreases, increasing the emission intensity. λ_{max}^{em} begins to change as R6G$_A$ transforms to R6G$_B$. Region 3 corresponds to photobleaching of the remaining R6G$_A$ and R6G$_B$ monomers, while λ_{max}^{em} continues to shift to λ_{max}^{em} of R6G$_B$.
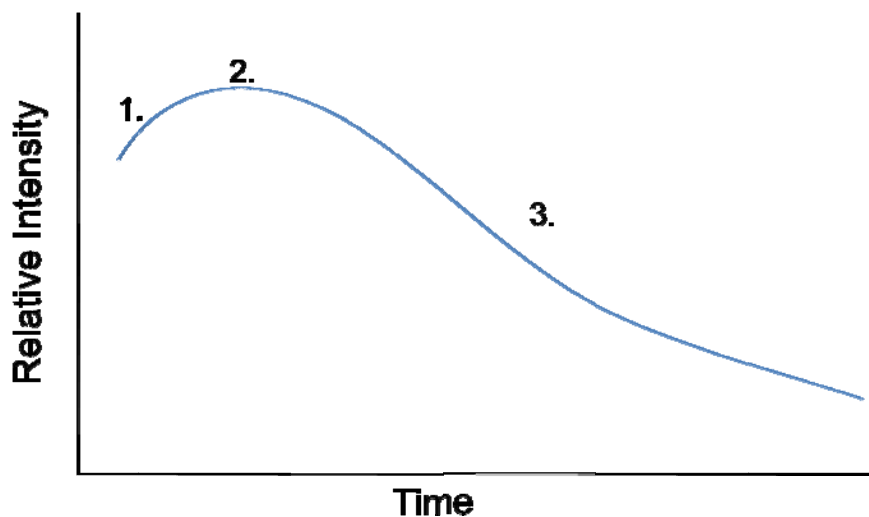
Figure 7.9 – Progression of R6G emission in solution

Though only the final   of R6G$_B$ seems to be the emission wavelength of

R6G monomers, it is not likely there are substantial quantities of aggregates

throughout the UV exposure. Besides a change in aggregation, another possibility is

that R6G forms a complex during the UV exposure period. R6G$_B$ could be a

complex with the polystyrene of the cuvette. However, detection of an

R6G/polystyrene complex is unlikely since the concentration of molecules affected

would be low.

7.4.5 R6G IN ALCOGEL

The alcogel monoliths remain optically clear throughout the experiment. A

small water layer formed on the upper surface of the alcogel, but there was not any

obvious shrinking. The emission progression for R6G in an alcogel monolith during

UV exposure, Figure 7.10, shows obvious differences from the solution phase R6G

molecules. There are two separate increases in emission intensity, separated by an

extreme drop in intensity. However, an R6G$_B$ species seems to form in the alcogels as well, as indicated by a blue shift in the emission peak. This may be the same type of R6G$_B$ species as indicated in the solutions, however, λ_{max}^{em} is altered by interactions with the local environment.
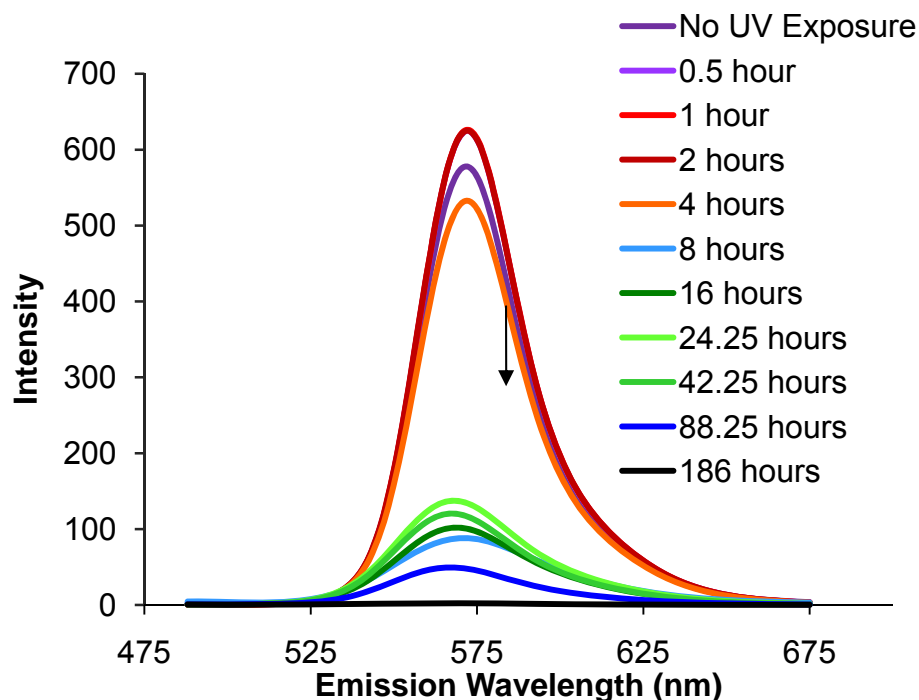
Figure 7.10 - R6G in alcogel, excitation at 480 nm. The arrow shows the direction of spectral progression with UV exposure time.

The emission intensity of R6G in the alcogel monolith, Figure 7.11, increases slightly (approximately 8%) over the first 2 hours of UV exposure, then plummets to only 15% of the original intensity in the next 6 hours of UV exposure. Parameters for the exponential changes in emission intensity and λ_{max}^{em} for R6G in alcogel are summarized in Table 7.2. The first decrease in intensity was followed by another small increase and then a slow decay.

The emission peak position of R6G in an alcogel monolith displays a single exponential shift from its original position at 572 nm to the final λ_{max}^{em} at 567 nm, changing with an exponential decay constant of 11.6 hr nm^{-1}. The change in λ_{max}^{em} in the alcogel monolith seems to correlate to the times when the intensity decays, before the intensity increases again. At the time in the experiment when the R6G first begins to decrease in emission intensity with a normalized decay constant of 60.2 hr, the emission peak begins to shift hypsochromically with a normalized decay constant of 13.2 hr. The second intensity increase seems occur at the end of the peak shift. It is possible that the coincidental timing indicates that R6G$_B$ has a higher quantum efficiency which causes the intensity decay to be slower than the peak shift. Figure 7.12 shows a schematic of the progression of R6G in alcogel emission changes. In region 1 the number of aggregates is reduced, increasing the intensity. Within region 2 photobleaching of R6G$_A$ is rapid while λ_{max}^{em} begins to shift. Region 3 corresponds to continued formation of R6G$_B$. At the beginning of region 4 the formation of R6G$_B$ has completed; λ_{max}^{em} does not shift further. During region 5, any remaining R6G$_A$ and R6G$_B$ are photobleached.
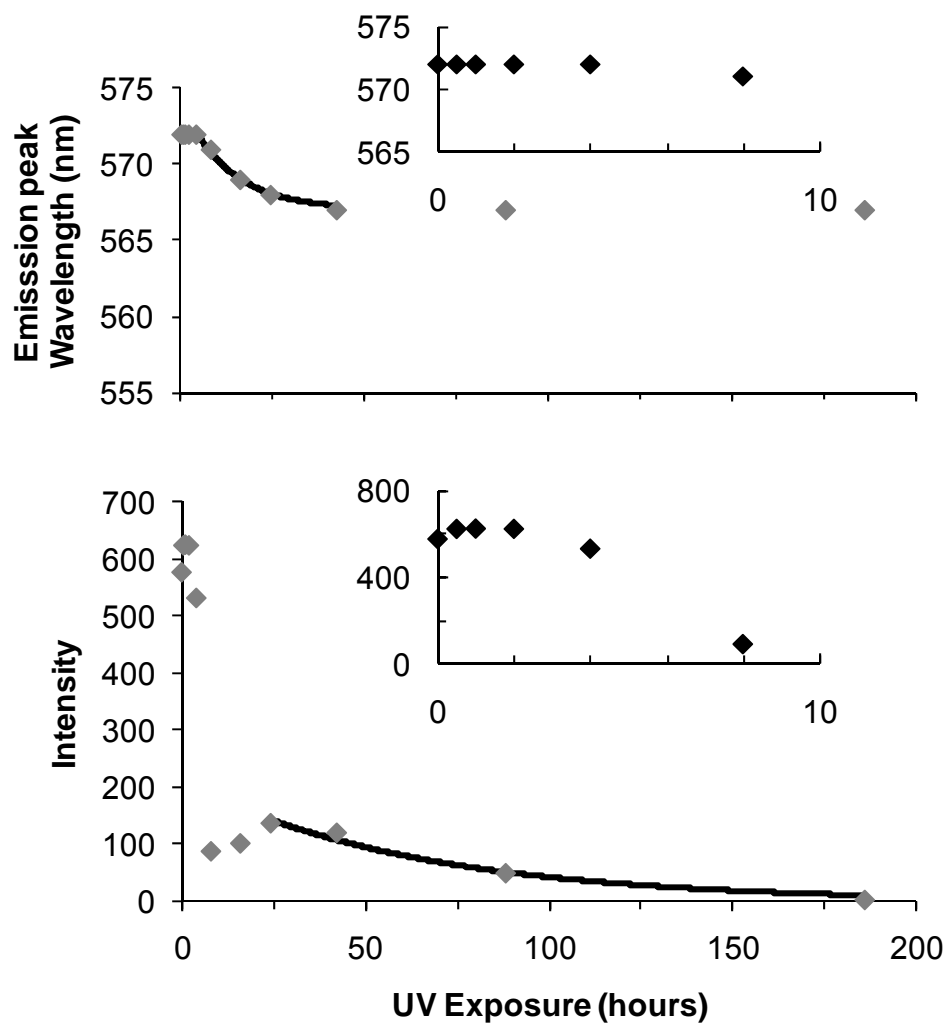
Figure 7.11 - Emission peak shift and intensity decay for R6G in alcogel. Insets are expansions of data points from the first 10 hours of UV exposure. Exponential decay fittings are in black.
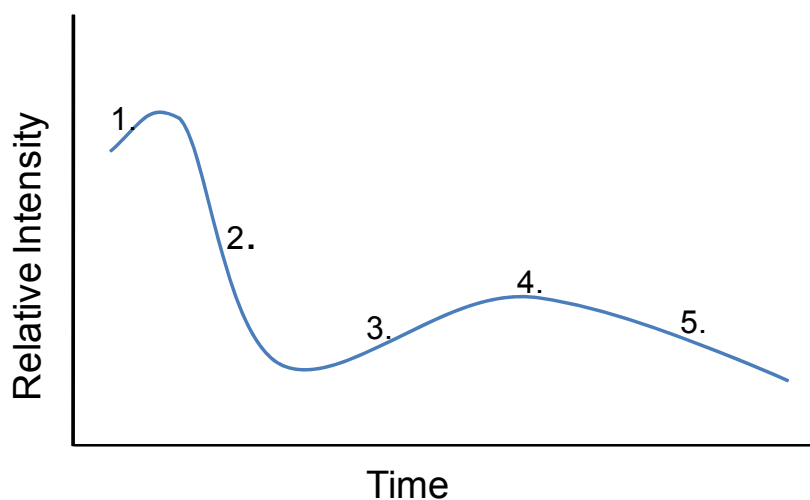
Figure 7.12 – Progression of R6G emission in alcogel

It is possible the first increase in intensity is due to a reduction in the number of less-fluorescent aggregates as in the solutions, while the second intensity increase is due to interactions with the alcogel. Aging of an alcogel is known to change λ_{max}^{em} of dye molecules[40] by changing the solvent composition around the molecules. Initially, as the aggregation of R6G$_A$ decreases, the remaining R6G$_A$ molecules will become more fluorescent. If R6G$_A$ photobleaches quickly to yield the fast intensity decay, it seems R6G$_B$ photobleaches much more slowly yielding a long-tailing intensity decay. As the alcogel ages, R6G$_B$ forms and emits at a shorter wavelength. The corresponding λ_{max}^{abs} for R6G$_B$ would also be at a shorter wavelength. R6G$_B$ would then absorb the excitation light better than R6G$_A$, yielding an increase in emission intensity as well.

Table 7.2 – Fitting Parameters for the Exponential Decay of R6G and R6G/CB7 Emission Intensity and Emission Peak Shift in Alcogels (Figures 7.11 and 7.14)

Sample	τ	A (a.u.)	y_0	R^2	Time range fit
R6G in Alcogel Intensity	60 ± 10 (hrs)	210 ± 30	0	0.977	24 to 186 hrs
R6G/CB7 in Alcogel Intensity	50 ± 10 (hrs)	180 ± 20	0	0.965	16 to 186 hrs
R6G in Alcogel Spectral Shift	11.6 ± 0.8 (hrs nm^{-1})	8.1 ± 0.5	566.9 ± 0.07 nm	0.997	8 to 42 hrs
R6G/CB7 in Alcogel Spectral Shift	12 ± 1 (hrs nm^{-1})	8.1 ± 0.5	566.9 ± 0.1 nm	0.997	8 to 42 hrs
	τ (hrs)	Maximum	Minimum	R^2	Time range fit
Normalized R6G intensity	60.2	220	0	0.976	24 to 186 hrs
Normalized R6G/CB7 intensity	41.9	186	0	0.963	16 to 186 hrs
Normalized R6G shift	13.2	575 nm	567 nm	0.999	8 to 42 hrs
Normalized R6G/CB7 shift	13.2	575 nm	567 nm	0.999	8 to 42 hrs

*using $f(x) = Ae^{-\frac{t}{\tau}} + y_0$, where A is a factor related to the intensity, τ is the inverse of the decay constant and y_0 is the y-intercept, which indicates the final wavelength for spectral shift fittings. Normalization fittings used $f(x) = e^{-\frac{t}{\tau}}$, with the maximum and minimum values being fit also.

7.4.6 R6G/CB7 IN ALCOGEL

When R6G/CB7 is encapsulated by an alcogel monolith, it seems the emission of R6G/CB7, Figure 7.13, responds to UV exposure similarly to R6G in an alcogel. The emission intensity presents three stages within the progression, Figure 7.14. The first was a stable intensity for the first 2 hours of UV exposure. Then, the intensity drops sharply to 15% of the original intensity. The intensity then briefly increases by 44% followed by the R6G emission intensity decaying at a much slower rate. Parameters for the exponential changes in emission intensity and λ_{max}^{em} for R6G/CB7 in alcogel are summarized in Table 7.2.
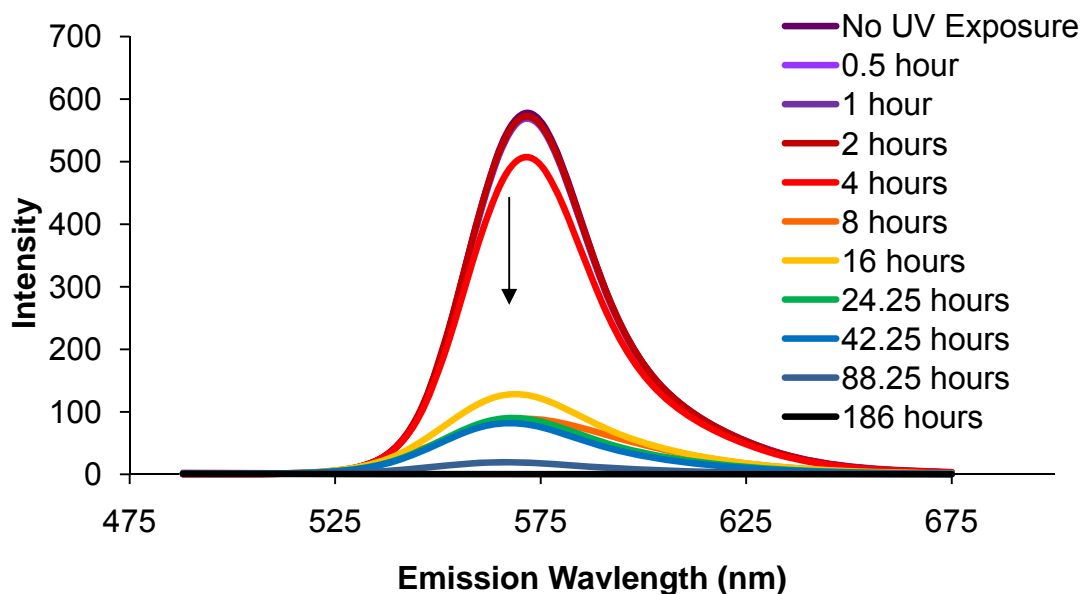
Figure 7.13 - R6G/CB7 in alcogel, excitation at 480 nm. The arrow shows the direction of progression with UV exposure time.
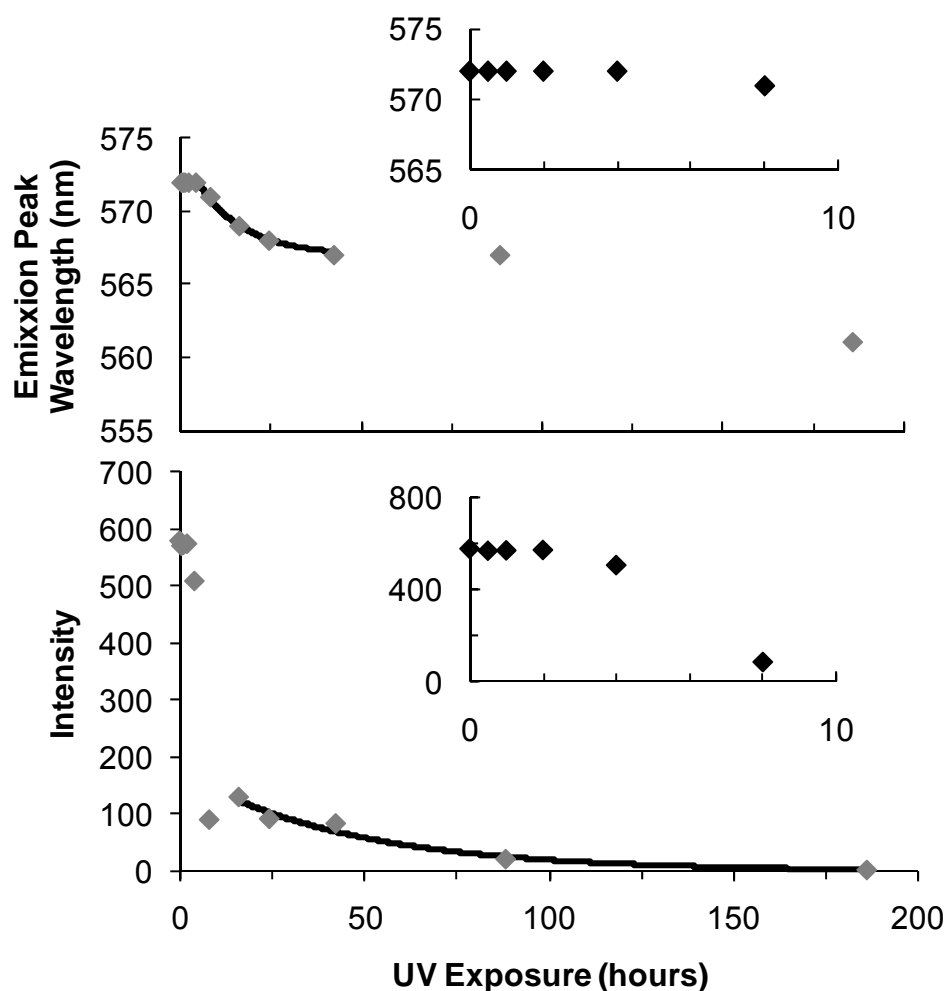
Figure 7.14 – Emission peak shift and intensity decay for R6G/CB7 in alcogel.
Insets are expansions of data points from the first 10 hours of UV exposure.
Exponential decay fittings are in black.

The peak position of R6G/CB7 emission also shows a three-part progression,

Figure 7.14. For the first 4 hours of UV exposure, λ_{max}^{em} is at 572 nm. Over the next

38 hours λ_{max}^{em} blue shifts exponentially to 567 nm, with a decay constant of 12 hr

nm^{-1}. Finally, λ_{max}^{em} seems to be stable at 567 nm, until the last measurement at 561

nm.

The correlation between the emission intensity and the wavelength shift seems minimal for this sample. Though the two properties each have 3 main parts, the timing of the changes do not correspond well with each other. However, it is possible that the increase in intensity near 16 hours of UV exposure correlates to the greatest shift in wavelength. This agrees with the interpretation of the R6G in alcogel progression that the second intensity peak is due to better absorption of excitation light by R6G$_B$, increasing the emission intensity as well.

As with R6G in alcogel, R6G/CB7 in an alcogel monolith seems to have two fluorescent R6G/CB7 species. R6G$_A$/CB7 decays rapidly due to photobleaching, while R6G$_B$/CB7 seems to be formed more slowly. The emission intensity of R6G$_B$/CB7 peaks after much of R6G$_A$/CB7 decays and requires much longer to photobleach. The full R6G/CB7 progression is described in Section 7.4.7. Though the addition of CB7 changes the timing, the progression remains the same as R6G in alcogel, except for the initial intensity increase experienced by R6G in alcogel. It seems CB7 has protected R6G from aggregation; therefore R6G/CB7 in alcogel does not undergo the disaggregation intensity change as R6G in alcogel.

7.4.7 COMPARISON OF ALCOGELS

R6G in the two alcogels responded to UV exposure with similar progressions. The shifts of λ_{max}^{em} for both R6G in alcogel and R6G/CB7 in alcogel were almost identical. The shapes of the emission intensity progressions have the same features: an initial high intensity, a sharp drop, followed by a small increase

and then a much slower decay. The differences between R6G and R6G/CB7 in the alcogels are evident in the extent and timing of the changes.

Though the overall emission intensity progression was similar for R6G and R6G/CB7 in alcogel, a couple differences are apparent. Both samples had nearly constant emission intensities at the beginning, but the R6G in alcogel monolith did have a small increase in intensity after the first 30 minutes of UV exposure. The lack of this increase due to R6G deaggregation when CB7 was present is most likely because CB7 protects R6G from aggregating by encompassing part of the dye molecules.[41] The intensity increase after the initial drop for the R6G/CB7 in alcogel sample was earlier than the same increase for the R6G in alcogel, peaking at 16 hours of UV exposure. The R6G in alcogel also displayed the intensity increase after the initial decay, Figure 7.15, but was much more gradual with the peak near 25 hours of UV exposure. CB7 seems to have increased the rate of formation of $R6G_B$/CB7 in the alcogel. Since complexation between CB7 and R6G is dynamic, it is possible that CB7 has encouraged different interactions between R6G and the alcogel pore surface. The final decay in emission intensity was exponential, Table 7.2, using only the data points after the final intensity increase for the exponential fittings. The exponential decay is due to photobleaching of any remaining $R6G_A$ or $R6G_A$/CB7 as well as $R6G_B$ and $R6G_B$/CB7. Unlike the solutions, this portion of the alcogel samples had a faster decay rate of the emission intensity of $R6G_B$/CB7 as compared to $R6G_B$, 41.9 hr and 60.2 hr for the normalized fittings. The R6G/CB7 in alcogel emission intensity decayed faster than R6G in alcogel both before and after

the secondary intensity increase, Figure 7.15. As the alcogel thin film seemed to

interrupt interactions between R6G and CB7 that enhanced photostability, chapter 5,

a similar interaction may occur in the alcogel monolith. If there is a competition

between CB7 and the alcogel pore surface to complex with R6G, neither would be

able to protect the dye from photobleaching as well as when R6G is complexed

strongly by either the alcogel or CB7 alone.
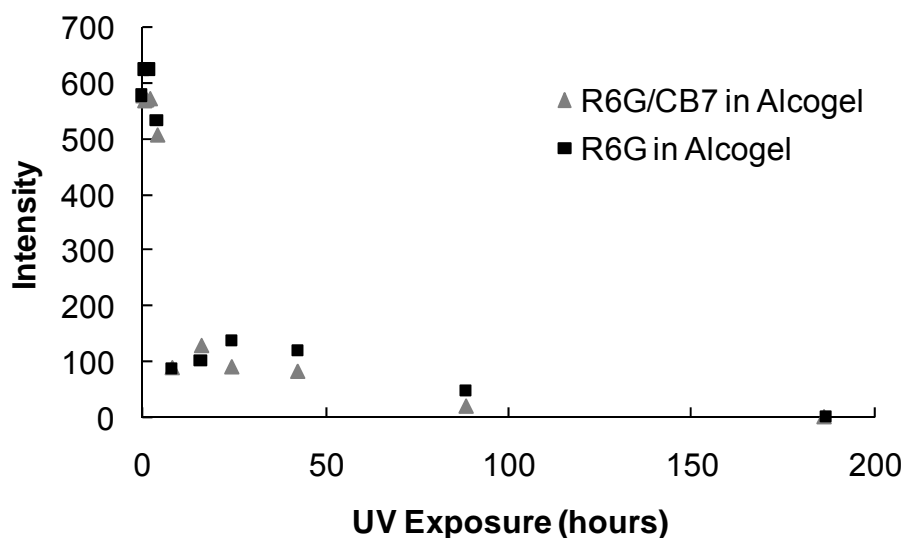
Figure 7.15 – Comparison of alcogel emission intensity progressions.

The last λ_{max}^{em} data point of R6G/CB7 shows a difference in shift compared to

R6G in the alcogels. The timing, magnitude and exponential decay of the

hypsochromic shifts are nearly identical, until the last data point at 186 hours of UV

exposure, Figures 7.11 and 7.14. The emission intensity at 186 hours is nearly

negligible in both alcogel samples, but a shift in λ_{max}^{em} in the R6G/CB7 in alcogel

indicates a possible R6G$_C$/CB7 species. It is possible that the R6G/CB7 in alcogel

sample possesses a less intense or smaller population of a third species that is

overshadowed earlier in the measurement by R6G$_A$/CB7 and R6G$_B$/CB7. The

intensity is low due to a small population of R6G/CB7 complexes still emitting. This

R6G$_C$/CB7 species may be a population of strongly complexed R6G/CB7, which is

unperturbed by the alcogel matrix, since CB7-complexed R6G is known to be blue-

shifted from R6G emission and has a higher photostability.[31] The full progression of

R6G/CB7 in alcogel is diagrammed in Figure 7.16. In region 1, the peak intensity

and λ^{em}_{max} do not change. Region 2 corresponds to the decrease in intensity as

R6G$_A$/CB7 photobleaches and the beginning of the shift of λ^{em}_{max}. Again, R6G$_B$/CB7

is likely due to interactions with the aging alcogel. In regions 3 and 4, the λ^{em}_{max} is

again constant, indicating no change in emitting species (R6G$_B$/CB7). Region 4

corresponds to photobleaching of any remaining R6G$_A$/CB7 as well as R6G$_B$/CB7.

Region 5 indicates a sudden shift in λ^{em}_{max}, a possible R6G$_C$/CB7, which may have

been present as a small population the entire time, or product of R6G$_A$/CB7 or

R6G$_B$/CB7.
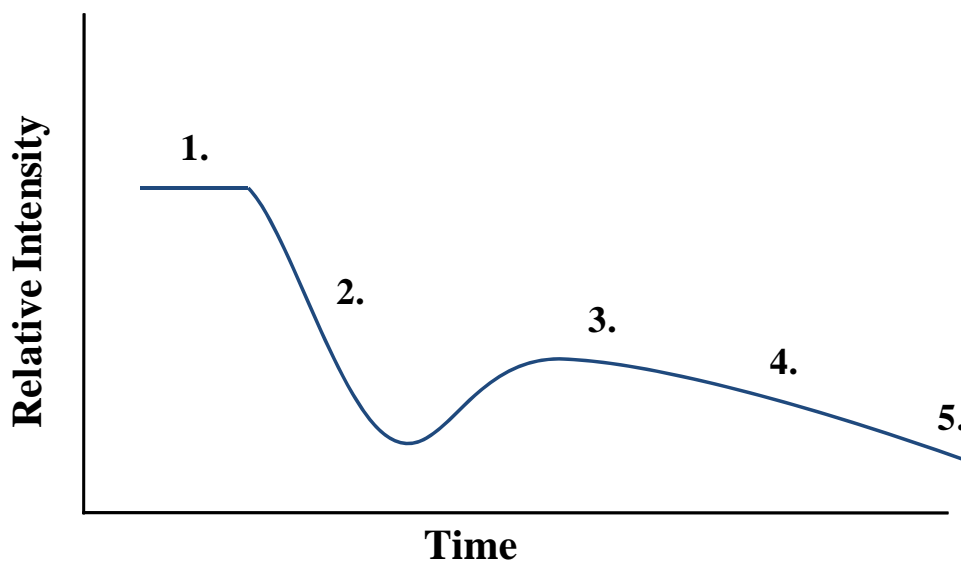
Figure 7.16 – Progression of R6G/CB7 emission in alcogel monolith

The similarity of the progressions of R6G and R6G/CB7 emission in alcogels indicates an interaction between the alcogel and R6G, whether CB7 is present or not. It seems that the addition of CB7 does not increase the photostability of R6G when it is in an alcogel monolith as was also found in chapter 5 for the alcogel thin film. However, the increased rate of decay of R6G/CB7 as compared to R6G indicates that CB7 does affect the photostability of R6G in alcogel monoliths. Alcogels have been shown to stabilize the fluorescence emission of encapsulated dyes when they are fixed to the surface of the matrix. Therefore, the increased rate of decay with CB7 present may be due to destabilizing the dye-matrix interactions. This is plausible as both CB7 and the alcogel matrix rely on electrostatic attractions of the cationic dye with electronegative regions on the CB7 cavity portal or unreacted hydroxyl groups of the alcogel. This competition between CB7 and the alcogel to complex with the R6G could reduce the photostability of the R6G/CB7 complexes as compared to R6G in alcogel, as indicated by the faster decay in emission intensity in the R6G/CB7 in alcogel sample.

7.4.8 R6G IN HYDROGEL

The hydrogels were initially clear when pipetted into cuvettes, but became cloudy during UV exposure. There was not any obvious shrinking away from the cuvette walls and only a thin liquid layer formed on the upper surface of the hydrogel monoliths. The liquid layer is presumed to be water or buffer excluded from the hydrogel.

R6G encapsulated by a hydrogel monolith had much higher emission intensity, Figure 7.17, than either the solutions or alcogels at the same dye concentration, despite large amounts of scattered light from the cloudy appearance of the hydrogel. The emission of R6G in hydrogel maintained a high signal to noise ratio for the extended duration of UV exposure. The emission intensity of R6G in hydrogel changed in three stages, Figure 7.18. First, R6G displayed a 15.9 % increase in emission intensity over the first 25 hours of UV exposure. Then, a plateau was reached and maintained for approximately 50 hours of UV exposure. Finally, the intensity decayed exponentially, with a decay constant of 450 hr, over the next several weeks.
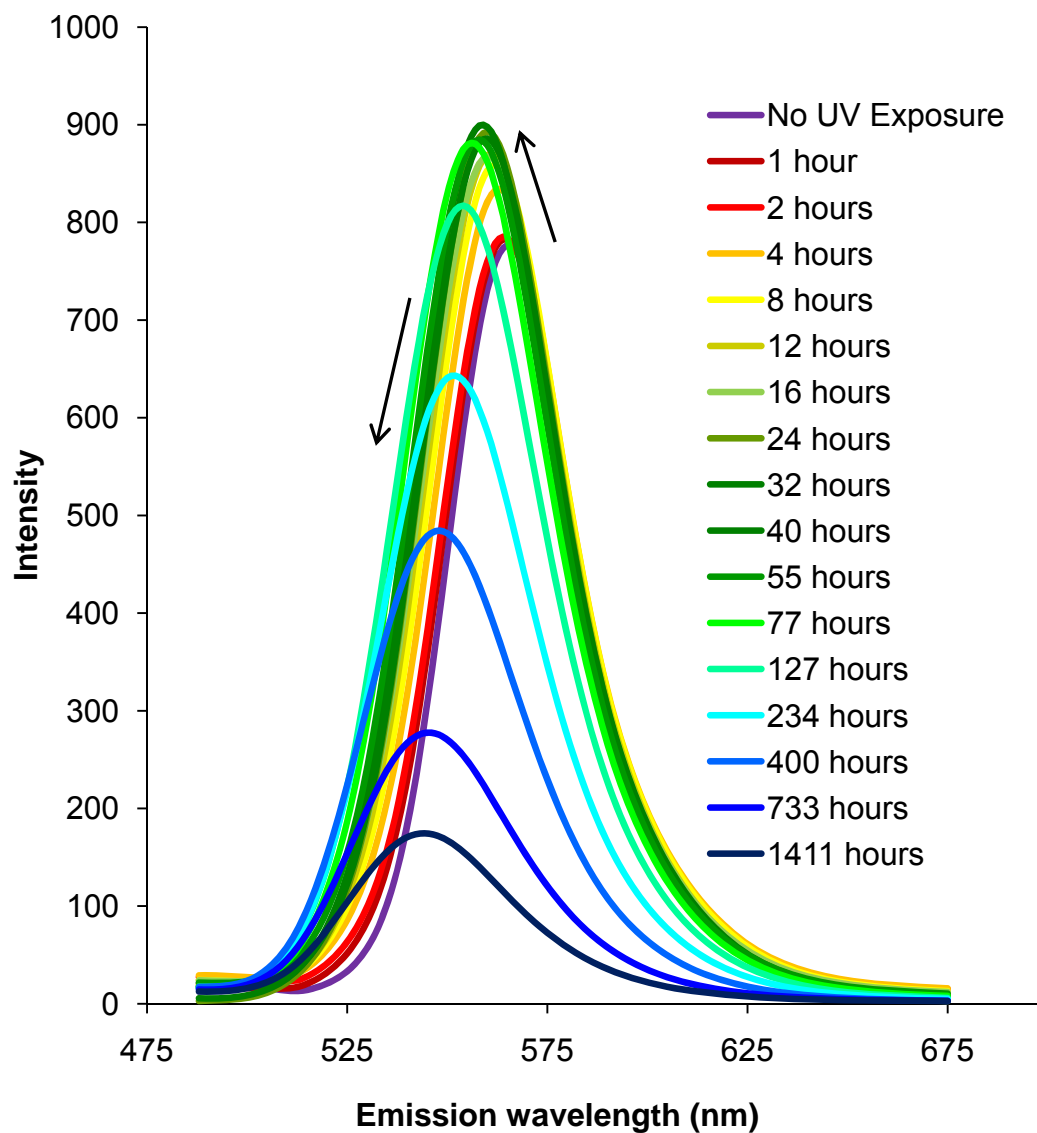
Figure 7.17 - R6G in hydrogel, excitation at 480 nm. Arrows show direction of spectral progression with increasing UV exposure time.
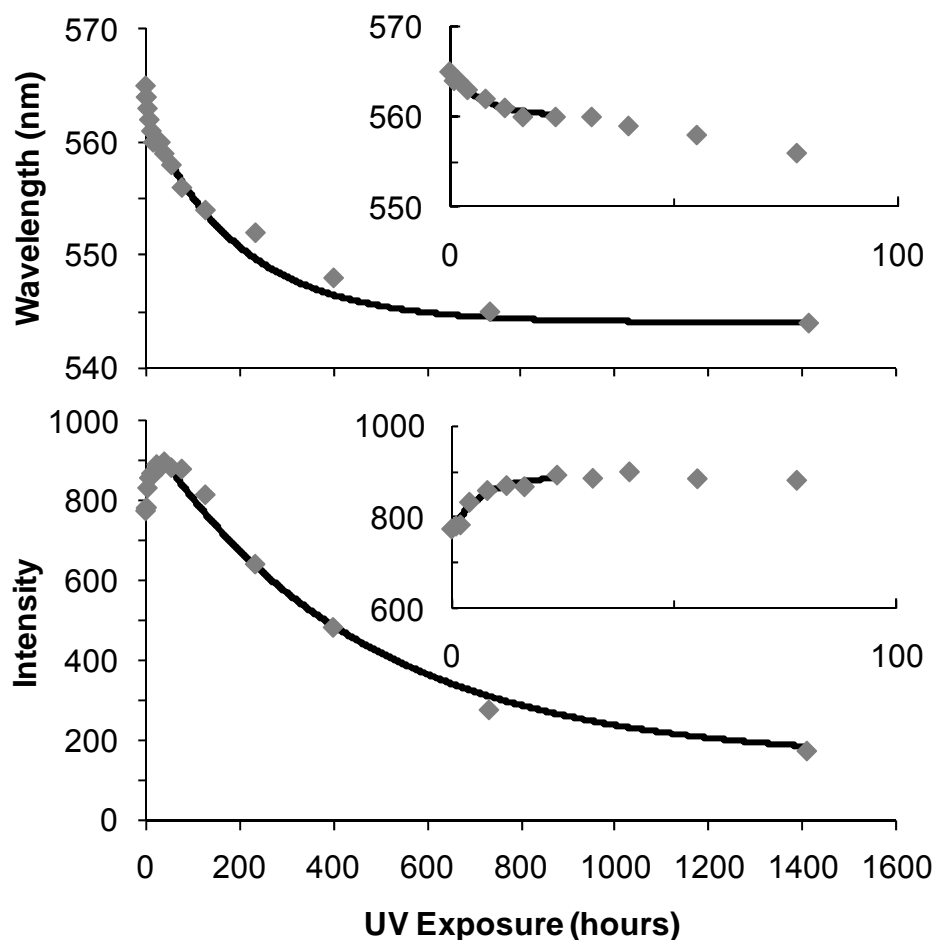
Figure 7.18 - R6G in hydrogel, excited at 480 nm, shift in emission peak and intensity decay with UV exposure. Insets are expansions of data points from the first 100 hours of UV exposure. Exponential fittings are shown in black.

The shift in λ_{max}^{em} also progressed in three stages, Figure 7.18, an initial hypsochromic shift, a time period without any notable shift and another more significant hypsochromic shift. The initial exponential shift (decay constant 16 hr nm^{-1}) of 5 nm occurred during the first 16 hours of UV exposure. The emission peak did not shift further for the next 14 hours of UV exposure. The final 25 nm hypsochromic shift occurred over the next 56 days exponentially, with a decay constant of 270 hr nm^{-1}.

The emission peak shifts correlate well to the three stages of intensity change. When the emission intensity was increasing the peak position underwent an initial shift. When the intensity had reached a plateau, the emission peak did not shift. The final decay of the intensity and the greatest hypsochromic shift correspond to the same time interval of UV exposure and with similar normalized rate constants 510 hr and 270 hr, respectively. Parameters for the exponential changes in emission intensity and λ_{max}^{em} for R6G in hydrogel are summarized in Table 7.3.

The initial increase in intensity is most likely due to a change in the λ_{max}^{abs} and λ_{max}^{em} when R6G$_B$ complexes with the hydrogel matrix. Strong interactions between the hydrogel matrix and some R6G$_A$ molecules lead to less motion of the R6G$_A$ molecules. Strong interactions affect the electronic structure of the dye, forming R6G$_B$. This is likely analogous to the effect that occurs with aging of alcogels. As λ_{max}^{em} is shifting towards the excitation light, it can be assumed the absorption spectrum of R6G$_B$ is also shifted closer to the excitation light, as had been discussed with the alcogels. It is highly likely the excitation light is now closer to λ_{max}^{abs} for R6G$_B$ than it was for R6G$_A$. This will cause an increase in emission intensity as the molecules are better able to absorb the excitation light. In this case, a clear correlation between peak shift and intensity change is expected. Though the times of change were not exactly the same, they differ by only one measurement increment.

Table 7.3 – Fitting Parameters of Exponential Changes in Emission of R6G in Hydrogel (Figure 7.18)

Exponential	τ	A (a.u.)	y_0	R^2	Time range fit
Intensity increase	7 ± 2 (hrs)	120 ± 10	890 ± 10	0.958	0 to 23.6 hrs
Initial spectral shift	16 ± 8 (hrs nm^{-1})	7 ± 2	558 ± 2 nm	0.987	0 to 23.6 hrs
Intensity decay	450 ± 50 (hrs)	870 ± 30	120 ± 30	0.995	39 to 1411 hrs
Final spectral shift	270 ± 30 (hrs nm^{-1})	17.2 ± 0.7	544.0 ± 0.6 nm	0.991	32 to 1411 hrs
	τ (hrs)	Maximum	Minimum	R^2	Time range fit
Normalized intensity decay	510	989 (a.u.)	82 (a.u.)	0.994	39 to 1411 hrs
Normalized final shift	270	561 nm	544 nm	0.991	32 to 1411 hrs

*using $f(x) = Ae^{-\frac{t}{\tau}} + y_0$, where A is a factor related to the intensity, τ is the decay constant and y_0 is the y-intercept, which indicates the final wavelength for spectral shift fittings; the increasing intensity function used: $f(x) = y_{max} - Ae^{-\frac{t}{\tau}}$, where y_0 is the peak intensity. Normalization fittings used $f(x) = e^{-\frac{t}{\tau}}$, with the maximum and minimum values being fit also.

7.4.9 CB7 – COMPLEXED R6G IN HYDROGEL

The extended duration of R6G emission in hydrogel is seen in the presence of CB7 also, Figure 7.19. The highest emission intensity for R6G/CB7 in hydrogel is not as high as R6G in hydrogel. The R6G/CB7 in hydrogel had a similar amount of scattered light as R6G in hydrogel during UV exposure. This is not expected to be a

product of UV exposure, but may be due to aging of the samples since it was not apparent early in the experiment.
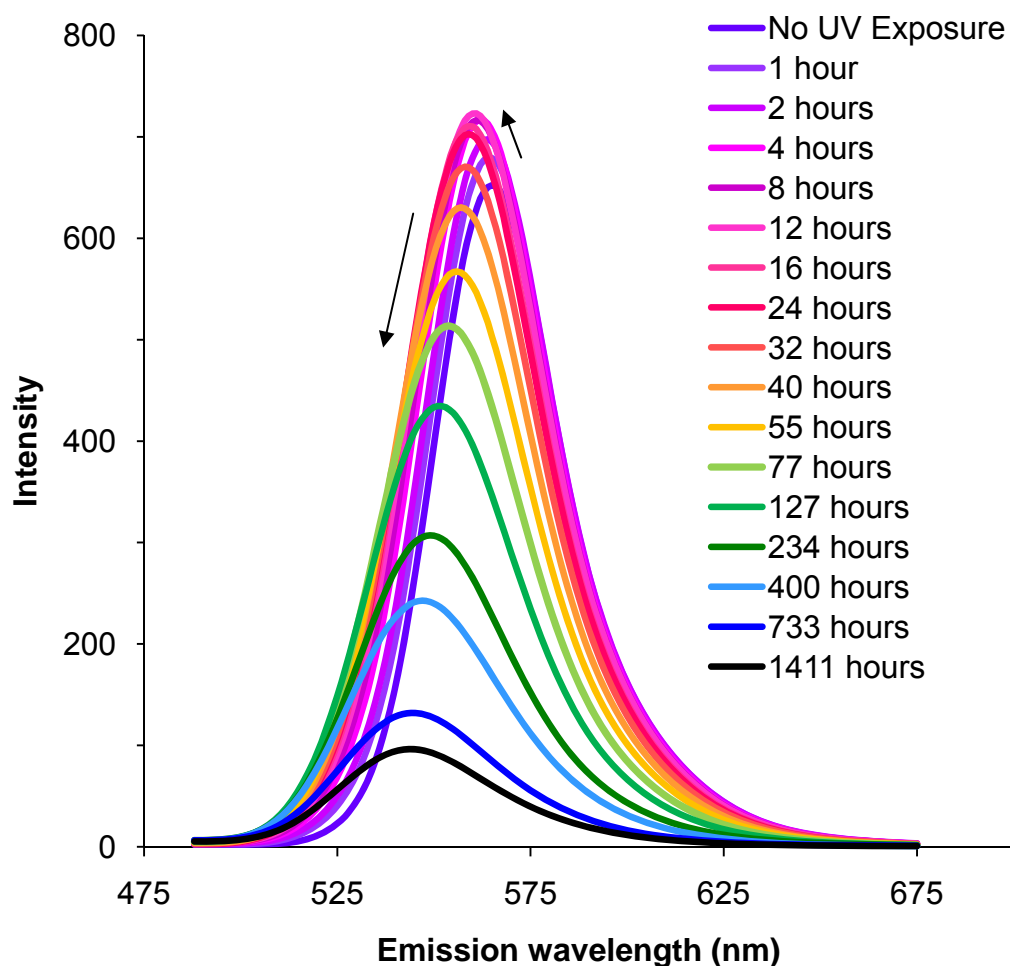
Figure 7.19 - Emission spectra of R6G/CB7 in hydrogel, excited at 480 nm. The arrows show the spectral progression with increasing UV exposure time.

R6G/CB7 in hydrogel has an increasing emission intensity with the initial UV exposure, which then decays exponentially, Figure 7.20. The initial increase in intensity is 10.9 % of the original intensity. After the initial increase, the intensity level plateaus for 8 hours of UV exposure before it begins to decay. The third stage is an exponential decay with a decay constant of 190 hr.
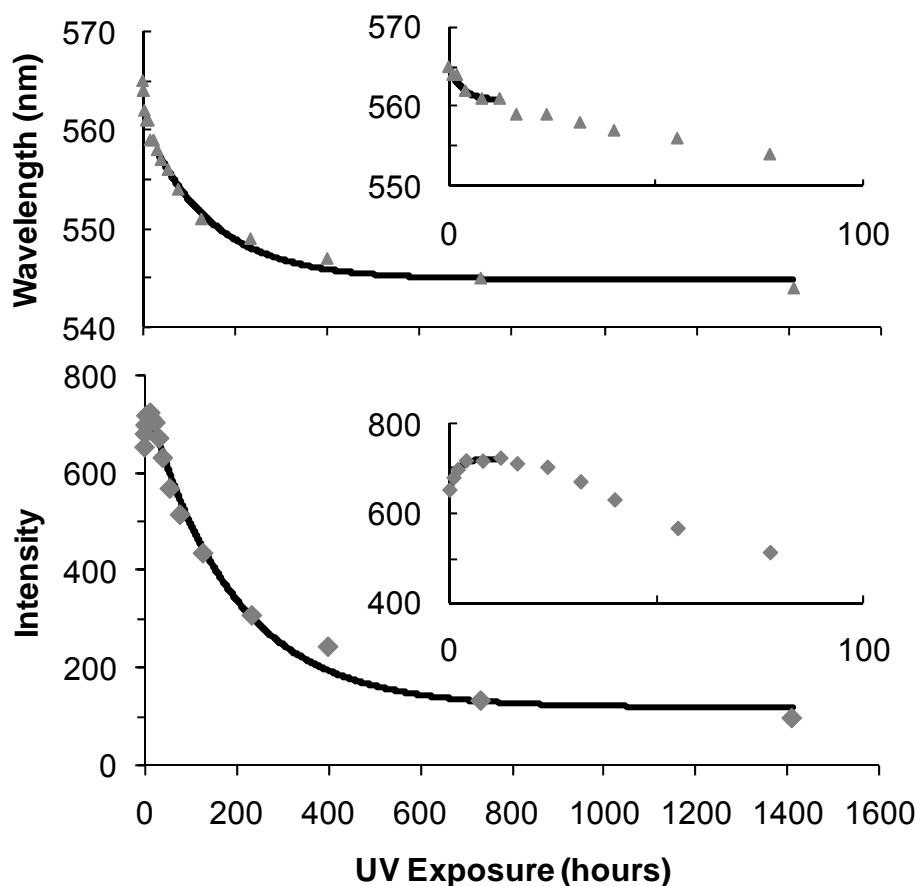
Figure 7.20 - R6G/CB7 in hydrogel, excited at 480 nm, shift in emission peak wavelength and intensity change with UV exposure. Insets are expansions of the first 100 hours of UV exposure. Exponential fittings are shown in black.

The emission peak shifts gradually over the course of the measurements, Figure 7.20. Initially λ_{max}^{em} is at 565 nm, and then the peak undergoes a hypsochromic shift to shorter wavelength, pausing shortly at 561 nm before shifting on to shorter wavelengths. Parameters for the exponential changes in emission intensity and λ_{max}^{em} for R6G/CB7 in hydrogel are summarized in Table 7.4.

Table 7.4 – Fitting Parameters of Exponential Changes in Emission of R6G/CB7 in Hydrogel (Figure 7.20)

	τ	A (a.u.)	y	R^2	Time range fit
Intensity increase	1.8 ±0.2 (hrs)	70 ± 4	721 ± 2	0.991	0 to 12.3 hrs
Initial spectral shift	3.17 ±0.4 (hrs nm^{-1})	4.3 ±0.2	561.0 ±0.2 nm	0.997	0 to 12.3 hrs
Intensity decay	190 ± 20 (hrs)	636 ±20.0	121 ±17.7	0.991	12.3 to 1411 hrs
Biexponential intensity decay	70 ± 30, 400 ± 100 (hrs)	300 ± 100, 400 ± 100	80 ± 20	0.998	12.3 to 1411 hrs
Final spectral shift	140 ± 20 (hrs nm^{-1})	16.3 ±0.7	545.0 ±0.5 nm	0.986	12.3 hrs to 1411 hrs
	τ (hrs)	Maximum	Minimum	R^2	Time range fit
Normalized intensity decay	193	752 (a.u.)	115 (a.u.)	0.992	24 to 1411 hrs
Normalized shift	137	562 nm	544 nm	0.999	24 to 1411 hrs

*using $f(x) = Ae^{-\frac{t}{\tau}} + y_0$, where A is a factor related to the intensity, τ is the decay constant and y_0 is the y-intercept, which indicates the final wavelength for spectral shift fittings; the increasing intensity function used: $f(x) = y_{max} - Ae^{-\frac{t}{\tau}}$, where y_0 is the peak intensity. Normalization fittings used $f(x) = e^{-\frac{t}{\tau}}$, with the maximum and minimum values being fit also.

The progression of R6G/CB7 in a hydrogel, Figure 7.21, has the same features as the R6G in hydrogel, differing only in timing and extent of changes. The shifts in R6G/CB7 in hydrogel λ_{max}^{em} correspond with the intensity changes. The final exponential changes in shift and intensity have normalized decay constants of 137 hr and 193 hr, respectively. In region 1 of Figure 7.21 the intensity is increasing and the hypsochromic shift is apparent. This initial shift is likely due to the aging of

the hydrogel. At the plateau in intensity, region 2, the λ^{em}_{max} does not shift much. When the intensity is decaying, region 3, the λ^{em}_{max} changes exponentially. It is difficult to tell if there are 2 or 3 species of R6G and R6G/CB7 in the hydrogels. However, it seems the plateau may indicate a stable species, R6G$_{AB}$, either intermediate to R6G$_A$ and R6G$_B$, or a separate entity. However, since the plateau is short-lived, only 2 species will be referred to in this text. The decay in intensity is expected to be due to photobleaching any remaining R6G$_A$ or R6G$_B$. The accompanying shift in λ^{em}_{max} is either a continuation of the initial shift, or another change, possibly due to interactions with the hydrogel matrix. It is possible the extended duration of R6G and R6G/CB7 emission in the hydrogels has allowed observation of further hydrogel aging that was not observed with the alcogels.
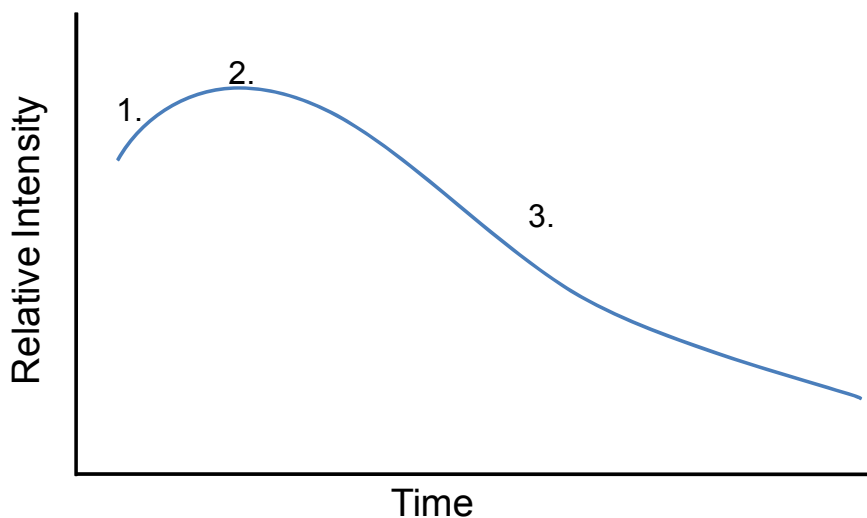

Figure 7.21 R6G emission progression in hydrogel monolith

7.4.10 COMPARISON OF HYDROGELS

There are differences between R6G/CB7 in hydrogel and R6G in hydrogel. However, the differences in R6G and R6G/CB7 emission in the hydrogels are mostly in the extent of change, or timing of the changes. Though λ_{max}^{em} for both hydrogel emission peaks shift the same magnitude, there is a clear inflection in which λ_{max}^{em} of the R6G in hydrogel stops shifting for 16 hours of UV exposure, and then continues to shift. The inflection in λ_{max}^{em} shift is much less obvious for R6G/CB7 than for R6G in hydrogels.

Secondly, both hydrogel samples increase in emission intensity before the emission intensity decreases. However, the R6G in hydrogel sample demonstrates a 15.9 % increase in fluorescence intensity, while the R6G/CB7 in hydrogel sample only increases by 10.9 %. In a repeated trial, with a brighter UV lamp, the λ_{max}^{em} did not shift as much before the photobleaching of R6G outpaced the shift, yielding smaller values of the initial emission intensity increase, 8.91% for R6G in hydrogel and 5.78% for R6G/CB7 in hydrogel. This suggests that formation of $R6G_B$ is a slower process than photobleaching of $R6G_A$ and may be an independent process that is not photo-induced. The ratio of intensity increase in R6G in hydrogel to the increase in R6G/CB7 in hydrogel was consistently 1.5: 1. The difference may be due to slower formation of $R6G_B$/CB7 as compared to $R6G_B$, or less $R6G_B$/CB7 is being formed than $R6G_B$ regardless of photobleaching of $R6G_A$. The initial intensity increase is due to blue shift in absorption and emission spectra of $R6G_B$ and $R6G_B$/CB7 as compared to $R6G_A$ and $R6G_A$/CB7. This increase may be less when

CB7 is present, because CB7 may be reducing the ability of R6G to complex fully with the matrix, as was suggested with the alcogels.

Finally, the correlation between the duration each sample remains at its highest intensity and the corresponding lack of λ_{max}^{em} shift is clear. In R6G/CB7 in hydrogel, the intensity plateau is shorter lived, only 8 hours of UV exposure, leading to an earlier decay in intensity. The spectral shift is almost continuous through the short amount of time that the intensity has peaked. However, with R6G in hydrogel, the peak intensity plateaus for 53 hours of UV exposure, corresponding to a longer-lived inflection in the emission peak shift.

The R6G in hydrogel system gives the best evidence of two types of emitting molecules, Figure 7.21. $R6G_A$ is shorter-lived, but emits immediately at the beginning. $R6G_B$ seems to be longer-lived, but forms during the course of the experiment. It is in the clear inflection point of this sample that we can see $R6G_A$ has decayed either due to photobleaching or changing to $R6G_B$. The emission intensity of $R6G_B$ is increasing, which is due to the increased overlap of the absorption spectrum of $R6G_B$ with the excitation light. It is not possible to distinguish between the decay of each species of R6G as the increasing $R6G_B$ emission overlaps with the decay of $R6G_A$ emission and $R6G_A$ may continue to decay long after $R6G_B$ has formed. However, by fitting the emission of R6G as a combination of the first emission spectrum (before UV exposure) and the final emission spectrum (1411 hours of UV exposure), each of the measurements can be related to a weighted sum of the spectra, Figure 7.22 for R6G and Figure 7.23 for

R6G/CB7. This method of splitting the spectra emphasizes the effect of photobleaching. Because the final spectrum collected is at a lower intensity than the initial, due to photobleaching, the scaling factor for the final spectrum is greater than one for the majority of the plot. By fitting the decrease of $R6G_A$ emission with an exponential function, Table 7.5, it seems the $R6G_A$/CB7 emission decays more rapidly than $R6G_A$ in the hydrogels. Likewise, the $R6G_B$/CB7 emission increases more rapidly than R6G in the hydrogels. These changes agree with the rates of emission intensity increases, initial spectral shifts, emission intensity decays and final spectral shifts, Tables 7.3 and 7.4, all pointing to faster changes in the presence of CB7.
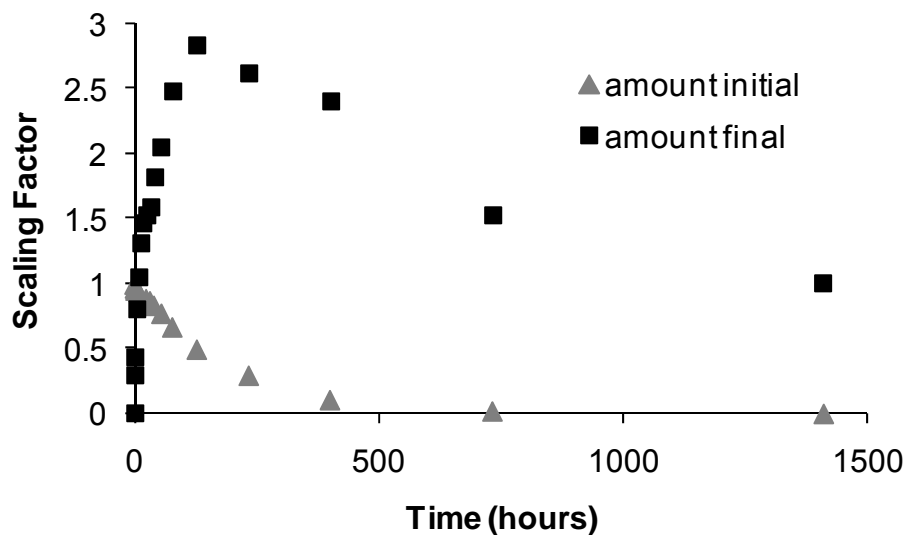
Figure 7.22 – R6G in hydrogel emission spectra as a function of the first and last spectra measured.
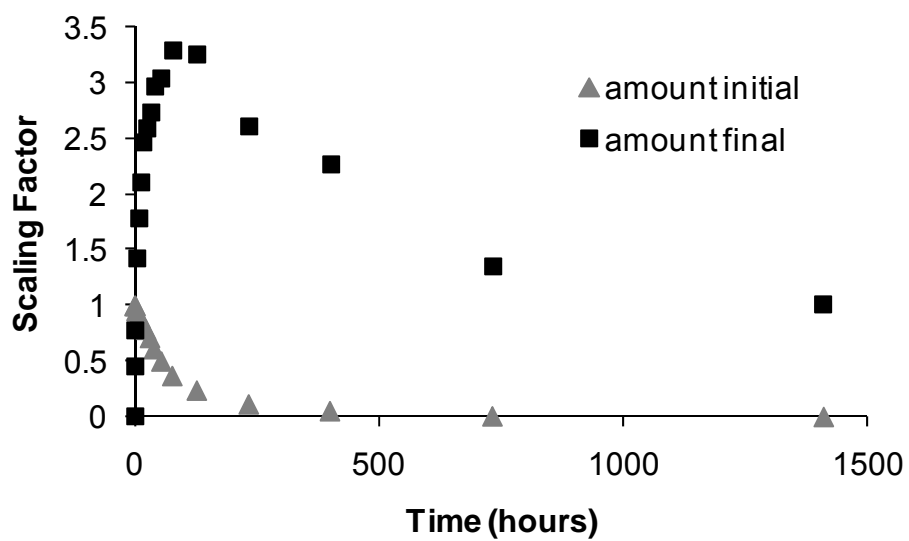
Figure 7.23 – R6G/CB7 in hydrogel emission spectra as a function of the first and last spectra measured.

Table 7.5 – Rise of R6G$_B$ and Decay of R6G$_A$ in Hydrogels

	τ (hours)	A	y	R^2	Time Range Fit
R6G$_B$ in Hydrogel (rise)	34 ± 8	2.4 ± 0.2	2.7 ± 0.2	0.946	0 to 127 hrs
R6G$_A$ in Hydrogel (decay)	200 ± 10	1.00 ± 0.02	0	0.997	All data
R6G$_B$/CB7 in Hydrogel (rise)	10 ± 1	2.8 ± 0.1	3.0 ± 0.1	0.979	0 to 77.25 hrs
R6G$_A$/CB7 in Hydrogel (decay)	77 ± 8	0.98 ± 0.05	0	0.995	All data
	τ (hours)	Maximum	Minimum	R^2	Time Range Fit
Normalized R6G$_B$ in Hydrogel (rise)	38	2.9	0.29	0.937	0 to 127 hrs
Normalized R6G$_A$ in Hydrogel (decay)	197	0.98	0	0.997	All data
Normalized R6G$_B$/CB7 in Hydrogel (rise)	11.7	3.1	0.34	0.978	0 to 77 hrs
Normalized R6G$_A$/CB7 in Hydrogel (decay)	82	1	0.021	0.997	All data

[*]using $f(x) = Ae^{-\frac{t}{\tau}} + y_0$, where A is a factor related to the intensity, τ is the decay constant and y_0 is the y-intercept, which indicates the final wavelength for spectral shift fittings; For the increasing intensity function τ and A are appropriately negative and y_0 is the peak intensity. Normalization fittings used $f(x) = e^{-\frac{t}{\tau}}$, for the decay and $f(x) = 1 - e^{-\frac{t}{\tau}}$, with the normalization maximum and minimum values being fit also.

7.4.11 COMPARISON OF SOLUTIONS AND MONOLITHS

Table 7.6 – Comparison of Sample Shift and Intensity Change

Sample	initial λ (nm)	final λ (nm)	initial intensity	high intensity	Time (hours)[1]
R6G in water	569	546	723	745	88
R6G/CB7 in water	569	550	763	772	186
R6G in alcogel	572	567	578	625	186
R6G/CB7 in alcogel	572	561	578	578	186
R6G in hydrogel	565	544	777	900	4354[4]
R6G/CB7 in hydrogel	565	544	652	723	913[2], 7684[3]; 2057[4]

[1]The duration of UV exposure to photobleach sample to background levels; [2]One R6G species of a biexponential decay; [3]Second R6G species of a biexponential decay; [4] Time required if only one species is considered, a single exponential decay. The preferred fit is listed first for the hydrogel samples

All of the samples displayed a clear hypsochromic shift over the duration of UV exposure; this has been referred to as a change from R6G$_A$ as the emitting species to R6G$_B$. R6G and R6G/CB7 in each matrix seem to have a characteristic λ_{max}^{em} initially, 569 nm in solution, 572 nm in alcogel and 565 nm in hydrogel. However, comparing the emission of R6G to the emission of R6G/CB7, the final λ_{max}^{em} was not the same for the solutions or alcogels, Table 7.6. The addition of CB7 to the samples does not consistently cause a greater or lesser spectral shift, when comparing the R6G and R6G/CB7 emissions in different matrices. R6G/CB7 in solution experiences less of a spectral shift than R6G in solution; however, R6G/CB7 in alcogel experiences a greater spectral shift than R6G in alcogel. And in the hydrogels, CB7 did not alter the shift in λ_{max}^{em}.

The difference in the identity of R6G$_B$ or R6G$_B$/CB7 in each matrix undoubtedly is impacting the λ_{max}^{em} shift. In solution, disaggregation of R6G is suggested to cause the initial change in emission intensity, but the cause of R6G$_B$ formation is uncertain, though possibly light-induced. In the alcogels, the dye materials disaggregate initially, but interactions with the aging alcogel matrix are suggested to cause the change forming R6G$_B$, with some competition between the alcogel and CB7 for complexation of R6G. In the hydrogels, R6G is still interacting with the silicate matrix, but seems to behave more like the solutions as the final wavelengths are shifted similarly to the solutions. Though the aging of the silicate matrix is likely a cause of R6G$_B$ formation, the exponential change from R6G$_A$ to R6G$_B$ indicates the process may still be light-induced.

The emission intensities of the R6G in the solution samples did increase slightly over the initial intensities within the first half hour of UV exposure. The increase in intensity is larger than the random error of the measurement and is highly reproducible. R6G in alcogel increased in emission intensity some within the first hour of UV exposure, similar to the solutions. This initial increase is likely due to disaggregation of aggregates. The emission intensity of R6G/CB7 in alcogel did not increase due to CB7 protecting R6G from the initial aggregation. The significant difference in emission intensity increase comes with the hydrogel samples. The R6G/CB7 in hydrogel sample peaked in intensity at 12.3 hours, whereas the R6G in hydrogel sample continued to increase until 39 hours of UV exposure. As the intensity increase correlates to peak shift, this elongated increase in intensity is an

indication of the slow process of change in the hydrogels. The slow process is understandable, considering the amount of light that is scattered by the hydrogels, reducing the excitation intensity received by R6G and R6G/CB7 in the hydrogels. In spite of the high scattered light of the hydrogel matrix, R6G and R6G/CB7 still had the highest initial emission intensity, which may indicate stronger protection of R6G within the hydrogel. The higher pH expected within the hydrogel matrix as compared to the alcogel may leave a greater percentage of the silanol groups deprotonated. This could cause the hydrogel to complex with R6G more strongly than the alcogel, which showed competition between the matrix and CB7 to complex R6G.

The greatest difference between the R6G emissions in different environments, whether solution or silicate matrix, is the amount of time required to photobleach the sample, Table 7.6. The solution samples showed a clear dependence on the presence of CB7. The CB7-complexed R6G in solution displayed an extended survival lifetime.[31, 41] The R6G/CB7 solution sample photobleached at nearly the same rate as R6G/CB7 in alcogel (35.6 hr R6G/CB7 in solution, 41.9 hr R6G/CB7 in alcogel, using normalized data). However, R6G/CB7 in alcogel decayed in emission intensity faster than R6G in alcogel (60 hr R6G in alcogel). Based on photostability, the amount of protection offered by CB7 in solution seems also to be provided by the alcogel. The electrostatic interactions between CB7 and R6G are similar to those between R6G and the alcogel matrix. Likewise, the mechanism of protection provided by CB7 is by limiting dynamic motion of R6G,

similar to the protection offered by the alcogel matrix. For these two examples it seems that CB7 and the alcogel may be reducing dye-dye interactions and protecting the dye from interacting with the solvent, reducing both aggregation (by providing small pockets for single R6G molecules to reside in) and the possibility of collisions with other molecules whether dye or solvent. Reducing aggregation and collisions between R6G molecules reduces the possibility of exciton/exciton annihilation, allowing R6G and R6G/CB7 to have a higher quantum yield.

R6G and R6G/CB7 in hydrogel, continued to emit after extended UV exposure, longer than the solutions and alcogels, by months. The full time required for the hydrogel samples to photobleach to background values (0.5 % of the initial intensity) was calculated by fitting the intensity decay with an exponential decay function. The emission intensity data for both R6G in hydrogel and R6G/CB7 in hydrogels were initially fit using single exponential decays. Though the emission of R6G in hydrogel was fit using a single exponential decay function ($R^2 = 0.995$) giving the time to photobleach as 4354 hours (or 181 days), as shown in Table 7.5, a single exponential function was inadequate for the R6G/CB7 in hydrogel. The single exponential decay for R6G/CB7 in hydrogel projected a time to photobleach of 2057 hours, which seems to be an abrupt ending to an otherwise extended emission, since there is still substantial emission at 1400 hours. The R6G/CB7 in hydrogel was fit much better with a biexponential decay function ($R^2 = 0.998$), especially the last few data points which were not fit well by a single exponential function. Fitting a biexponential function to the R6G/CB7 in hydrogel intensity data clearly shows a

short-lived R6G/CB7 species and a much longer-lived species of R6G/CB7. It is possible that complexation of R6G was more complete by the hydrophobic cavity of CB7 in a hydrogel having many polar water molecules surrounding the CB7. The doubled survival lifetime of R6G/CB7 in hydrogel indicates CB7 would provide greater protection to R6G in the hydrogel. In contrast, the silicate structure of the alcogel seems to compete with CB7 for complexation of R6G using unreacted silanol groups to interact with R6G and interrupting the photostabilization of complexation by CB7. The extended duration of R6G and R6G/CB7 fluorescence in the hydrogel may also have been an effect of scattered light, reducing the amount of UV light reaching the dye molecules to photobleach them, a lower intensity of light will not photobleach the sample as quickly. The concentrations of $R6G_A$ and $R6G_B$ throughout the measurements are unknown due to photobleaching of $R6G_A$, photobleaching of $R6G_B$, formation of $R6G_B$, and reduction in the amount of $R6G_A$. Because there are multiple simultaneous changes, determination of whether $R6G_A$ or $R6G_B$ is a brighter or more photostable form of R6G is beyond the scope of the current investigation.

7.5 CONCLUSIONS

Incorporating CB7-complexed R6G into silica alcogel and hydrogel monoliths looks to be a promising means to developing photolytically stable optical materials. Enhanced photostability and maintained high emission intensities for R6G are apparent with CB7-complexation. However, through this study of solution,

199

alcogel and hydrogel monoliths, there were several competing interactions with the dye molecules.

The formation of R6G$_B$ and R6G$_B$/CB7 seem to be partially related to photobleaching. In the solutions, the cause of the change from R6G$_A$ and R6G$_A$/CB7 to R6G$_B$ and R6G$_B$/CB7 is unknown, but is likely not due to changing aggregation at the concentrations of dye used. In the alcogels, it is speculated that the R6G$_B$ or R6G$_B$/CB7 species is a product of R6G and R6G/CB7 interacting with the silicate pore surface as the alcogel ages. The interactions may be enhanced by the presence of light. In the hydrogels, the high water content seems to slow formation of R6G$_B$ and R6G$_B$/CB7 as well as photobleaching of R6G$_B$ and R6G$_B$/CB7 fluorescence. However, the high amount of scattered light by the hydrogel makes the rate of emission intensity change uncertain. The formation of R6G$_B$ and R6G$_B$/CB7 in the hydrogels is speculated to be due to similar interactions with the silicate as with the alcogel, possibly photo-induced, but with slower kinetics due to the higher water content reducing interactions between R6G and the silicate matrix.

Interactions between R6G and the silicate matrix and between R6G and CB7 had longer lasting effects than initial intensity changes. Both the alcogel and hydrogel were able to sustain R6G fluorescence longer than the solution. The attraction of R6G to the silica matrix continues to reduce the effect of CB7-complexation, as it had been demonstrated in the single molecule work, chapter 5. The emission peak shifts for all systems seem to present the possibility of having two or more emitting species of R6G. As one species decays, the peak shifts to the

wavelength of the remaining component. Overall, the silicate matrix stabilized the

emission properties of R6G and R6G/CB7 better than aqueous solution. Likewise,

R6G and R6G/CB7 seemed to be more photostable in the hydrogel than in alcogel,

but the hydrogel also possessed the most scattered light.

7.6 REFERENCES

1.   Hybrid Organic-Inorganic Solid-State Dye Laser Glasses. In *Photonic Glasses*, Gan, F.; Xu, L., Eds. World Scientific Publishing: Singapore, 2006.

2.   Oki, Y.; Maeda, M., Development and application of integrated solid-state dye lasers. In *Recent Developments in Lasers and their Applications*, Vasa, N. J., Ed. Research Signpost: Kerala, India, 2006.

3.   Ishchenko, A. A., Photonics and molecular design of dye-doped polymers for modern light-sensitive materials. *Pure Appl. Chem.* **2008**, 80, (7), 1525-1538.

4.   Reisfeld, R.; Weiss, A.; Saraidarov, T.; Yariv, E.; Ishchenko, A. A., Solid-state lasers based on inorganic-organic hybrid materials obtained by combined sol-gel polymer technology. *Polym. Adv. Technol.* **2004**, 15, (6), 291-301.

5.   Suratwala, T.; Gardlund, Z.; Davidson, K.; Uhlmann, D. R.; Bonilla, S.; Peyghambarian, N., Photostability of Silylated Coumarin Dyes in Polyceram Hosts. *J. Sol.-Gel Sci. Technol.* **1997**, 8, (1-3), 973-978.

6.   Canva, M.; Dubois, A.; Georges, P. M.; Brun, A.; Chaput, F.; Ranger, A.; Boilot, J.-P., Perylene, pyrromethene and grafted rhodamine-doped xerogels for tunable solid state laser. *Proc. SPIE-Int. Soc. Opt. Eng.* **1994**, 2288, 298-309.

7.   Rahn, M. D.; King, T. A.; Gorman, A. A.; Hamblett, I., Photostability enhancement of Pyrromethene 567 and Perylene Orange in oxygen-free liquid and solid dye lasers. *Appl. Opt.* **1997**, 36, (24), 5862-5871.

8.   Faloss, M.; Canva, M.; Georges, P.; Brun, A.; Chaput, F.; Boilot, J.-P., Toward millions of laser pulses with pyrromethene- and perylene-doped xerogels. *Appl. Opt.* **1997**, 36, (27), 6760-6763.

9.   Ahmad, M.; Rahn, M. D.; King, T. A., Singlet oxygen and dye-triplet-state quenching in solid-state dye lasers consisting of Pyrromethene 567–doped poly-methyl methacrylate. *Appl. Opt.* **1999**, 38, (30), 6337-6342.

10.   King, T. A.; Ahmad, M.; Gorman, A.; Hamblett, I.; Rahn, M. D., Dye-triplet-state and singlet-oxygen quenching effects in solid state dye lasers. *Proc. SPIE-Int. Soc. Opt. Eng.* **2000**, 3929, 145-153.

11.   Mitala, J. J.; Michael, A. C., Improving the performance of electrochemical microsensors based on enzymes entrapped in a redox hydrogel. *Anal. Chim. Acta* **2006**, 556, (2), 326-332.

12.   Allcock, H. R.; Phelps, M. V. B.; Barrett, E. W.; Pishko, M. V.; Koh, W.-G., Ultraviolet Photolithographic Development of Polyphosphazene Hydrogel Microstructures for Potential Use in Microarray Biosensors. *Chem. Mater.* **2006**, 18, (3), 609-613.

13.   Watanabe, M.; Akahoshi, T.; Tabata, Y.; Nakayama, D., Molecular Specific Swelling Change of Hydrogels in Accordance with the Concentration of Guest Molecules. *J. Am. Chem. Soc.* **1998**, 120, (22), 5577-5578.

14.   Zhu, W.; Gou, P.; Zhu, K.; Shen, Z., Synthesis, Extraction, and Adsorption Properties of Calix[4]arene-poly(ethylene-glycol) Crosslinked Polymer. *J. Appl. Polym. Sci.* **2008**, 109, (3), 1968-1973.

15.   Hwang, I.; Jeon, W. S.; Kim, H.-J.; Kim, D.; Kim, H.; Slvapalam, N.; Fujita, N.; Shinkai, S.; Kim, K., Cucurbit[7]uril: A Simple Macrocyclic, pH-Triggered Hydrogelator Exhibiting Guest-Induced Stimuli-Responsive Behavior. *Angew. Chem., Int. Ed. Engl.* **2007**, 46, 210-213.

16.   Yamaguchi, S.; Yoshimura, I.; Kohira, T.; Tamaru, S.-i.; Hamachi, I., Cooperation between Artificial Receptors and Supramolecular Hydrogels for Sensing and Discriminating Phosphate Derivatives. *J. Am. Chem. Soc.* **2005**, 127, (33), 11835-11841.

17.   Jensen, M.; Birch Hansen, P.; Murdan, S.; Frokjaer, S.; Florence, A. T., Loading into and electro-stimulated release of peptides and proteins from chondroitin 4-sulphate hydrogels. *Eur. J. Pharmaceut. Sci.* **2002**, 15, (2), 139-148.

18.   Mangione, M. R.; Giacomazza, D.; Cavallaro, G.; Bulone, D.; Martorana, V.; Biagio, P. L. S., Relation between structural and release properties in a polysaccharide gel system. *Biophys. Chem.* **2007**, 129, 18-22.

19.   Kosto, K. B.; Deen, W. M., Hindered convection of macromolecules in hydrogels. *Biophys. J.* **2005**, 88, (1), 277-286.

20.   Murakata, T.; Sato, K.; Nakamura, I.; Hujishima, K.; Higuchi, T.; Sato, S., Interaction between gel framework of SiO_2 or TiO_2 hydrogel and incorporated surfactants and $Ru(bpy)_3^{2+}$. *J. Chem. Eng. Jpn.* **2002**, 35, (10), 938-943.

21.   Subbiah, S.; Mokaya, R., Transparent thin films and monoliths synthesized from fullerene doped mesoporous silica: evidence for embedded monodispersed C_{60}. *Chem. Commun.* **2003**, (1), 92-93.

22.   del Monte, F.; Levy, D., Formation of Fluorescent Rhodamine B J-Dimers in Sol−Gel Glasses Induced by the Adsorption Geometry on the Silica Surface. *J. Phys. Chem. B* **1998**, 102, (41), 8036-8041.

23.   Ferrer, M. L.; del Monte, F.; Levy, D., Microviscosities at the Porous Cage of Silica Gel−Glasses and Ormosils through Fluorescence Anisotropy. *J. Phys. Chem. B* **2001**, 105, (45), 11076-11080.

24.   Gilliland, J. W.; Yokoyama, K.; Yip, W. T., Effect of Coulombic Interactions on Rotational Mobility of Guests in Sol-Gel Silicate Thin Films. *Chem. Mater.* **2004**, 16, (20), 3949-3954.

25.   Zhou, Y.; Yip, W. T., Balance between Coulombic Interactions and Physical Confinement in Silica Hydrogel Encapsulation. *J. Phys. Chem. B* **2009**, 113, (17), 5720-5727.

26.   Mezzina, E.; Cruciani, F.; Pedulli, G. F.; Lucarini, M., Nitroxide Radicals as Probes for Exploring the Binding Properties of the Cucurbit[7]uril Host. *Chem. – Eur. J.* **2007**, 13, (25), 7223-7233.

27.   Marquez, C.; Huang, F.; Nau, W. M., Cucurbiturils: Molecular Nanocapsules for Time-Resolved Fluorescence-Based Assays. *IEEE Trans. Nanobiosci.* **2004**, 3, (1), 39-45.

28.   Ong, W.; Kaifer, A. E., Salt Effects on the Apparent Stability of the Cucurbit[7]uril-Methyl Viologen Inclusion Complex. *J. Org. Chem.* **2004**, 69, (4), 1383-1385.

29.   Liu, Y.; Li, C.-J.; Guo, D.-S.; Pan, Z.-H.; Li, Z., A Comparative Study of Complexation of b-Cyclodextrin, Calix[4]arenesulfonate and Cucurbit[7]uril with Dye Guests: Fluorescence Behavior and Binding Affinity. *Supramol. Chem.* **2007**, 19, (7), 517-523.

30.   Ammer, F.; Penzkofer, A.; Weidner, P., Concentration-dependent fluorescence behaviour of oxazine 750 and rhodamine 6G in porous silicate xerogel monoliths. *Chem. Phys.* **1995**, 192, 325-331.

31.   Moore, J. L. Host-Guest Complexation of Cationic Xanthene Dyes with Cucurbit[7]uril. University of Oklahoma, Norman, 2008.

32.   Meech, S. R.; Yoshihara, K., The Photoreaction of a Rhodamine 6G Monolayer Adsorbed on Quartz Studied by Surface Second Harmonic Generation. *Photochem. Photobiol.* **1991**, 53, (5), 627-632.

33.   Tajalli, H.; Gilania, A. G.; Zakerhamidi, M. S.; Moghadamb, M., Effects of surfactants on the molecular aggregation of rhodamine dyes in aqueous solutions. *Spectrochim.ica Acta, Part A* **2009**, 72, (4), 697-702.

34.	Martinez, V. M.; Arbeloa, F. L.; Prieto, J. B.; Arbeloa, I. L., Characterization of Rhodamine 6G Aggregates Intercalated in Solid Thin Films of Laponite Clay. 2 Fluorescence Spectroscopy. *J. Phys. Chem. B* **2005**, 109, (15), 7443-7450.

35.	Kasha, M.; Rawls, H. R.; El-Bayoumi, M. A., The exciton model in molecular spectroscopy. *Pure Appl. Chem.* **1965**, 11, (3-4), 371-392.

36.	Monte, F. d.; Mackenzie, J. D.; Levy, D., Rhodamine Fluorescent Dimers Adsorbed on the Porous Surface of Silica Gels. *Langmuir* **2000**, 16, (19), 7377-7382.

37.	Mohanty, J.; Bhasikuttan, A. C.; Nau, W. M.; Pal, H., Host-guest complexation of neutral red with macrocyclic host molecules: Contrasting pKa shifts and binding affinities for cucurbit[7]uril and b-cyclodextrin. *J. Phys. Chem. B* **2006**, 110, (10), 5132-5138.

38.	Nau, W. M.; Mohanty, J., Taming fluorescent dyes with cucurbituril. *Int. J. Photoenergy* **2005**, 07, 133-141.

39.	Reija, B.; Al-Soufi, W.; Novo, M.; Tato, J. V., Specific Interactions in the Inclusion Complexes of Pyronin Y and B with β-Cyclodextrin. *J. Phys. Chem. B* **2005**, 109, (4), 1364-1370.

40.	Gupta, R.; Mozumdar, S.; Chaudhury, N. K., Effect of ethanol variation on the internal environment of sol-gel bulk and thin films with aging. *Biosens. Bioelectron.* **2005**, 21, (4), 549-556.

41.	Mohanty, J.; Nau, W. M., Ultrastable rhodamine with cucurbituril. *Angew. Chem., Int. Ed.Engl.* **2005**, 44, (24), 3750-3754.

Chapter VIII

Conclusion

This work aimed to develop novel materials to better explore the capabilities of solgel silicates to host dye molecules for optical materials. Two features of the solgel silicates were investigated: thickness control and ability to host non-covalent macromolecular complexes. Expanding on the versatility of silica solgel by incorporating solgel into PEM thin films and incorporating CB7-complexed dye molecules into solgel materials has addressed the goals of this thesis work.

Use of PEM thin films as a scaffold system provided a new means of thickness control of silica solgel materials. Thickness control afforded by PEM thin films is on the nanometer scale and seems to be a system that could be adapted to silicates with a variety of guest molecules. This research determined the resulting film composed of solgel and the polyelectrolyte film is a hybrid film that has well-intercalated phases. Guest molecules interact with both portions of the composite film. Though thickness control was achieved, and porosity and charge density of the solgel film were maintained, the silica solgel does not act as a separate entity, but instead works cooperatively with the PEM scaffold to hold guest dye molecules.

CB7-complexed xanthene dyes, R6G and PyY, were combined with a matrix to yield optical materials with both enhanced photostability due to immobilization and increased emission intensity due to complexation. Incorporating the CB7-complexed dyes changed the emission properties of the dye complexes markedly, giving evidence of changes in the complex. By encapsulating R6G/CB7 complexes

in silica solgel matrices, the ability of CB7 to enhance the emission of R6G was reduced. Single-molecule measurements of R6G/CB7 complexes on glass demonstrated how CB7 is capable of protecting dye molecules from interactions with the environment and aggregation, leading to higher photostability. CB7-complexation also increases the emission intensity of R6G. These properties of CB7-complexation were previously known from solution studies. However, incorporation of R6G/CB7 complexes into silica solgel seems to negate the enhancement due to CB7-complexation. Competition between the silicate surface and CB7 for complexation of R6G does not allow R6G to experience the increased emission intensity or photostability of R6G/CB7 on glass. A similar competition also seems to be present when PyY/CB7 complexes were immobilized on a PAH monolayer. PyY/CB7 complexes on PAH seem to experience half of the enhancement due to CB7-complexation as compared to PyY/CB7 complexes on glass. The differences between interactions with the silicate and the PAH surface seem to be due to the better size compatibility of PyY with CB7, which may strengthen the complexation. However, less physical confinement to the immobilization matrix may also aid PyY/CB7 complexation. In contrast, CB7 complexes incorporated within the solgel silicate matrix experience the physical confinement of the matrix pores which could hinder the complex from a preferred conformation.

The R6G/CB7 work reveled changing emission intensity, possibly due to a changing extent of complexation. Though R6G is known to emit at multiple

intensities, complexation with CB7 increases the likelihood of multiple intensities and number of intensity levels observed for each R6G/CB7 complex. Analysis of the blinking kinetics of PyY and PyY/CB7 indicates that CB7-complexation does not significantly impact the photophysical characteristics of individual PyY molecules. Therefore, the photostability enhancement is likely a physical protection not due to interactions between the electronic structure of PyY and CB7.

Complexation with CB7 led to longer-lived, bright dye molecules. This approach is capable of being employed with cationic dye molecules and has varying levels of effectiveness depending on the specific size, shape and charge distribution of the dye. Further enhancement upon encapsulation of CB7-complexed dye molecules may be possible with a suitable matrix. In thin films and monolithic structures, charged substrates seem to interfere with the complexation of dyes by CB7. Clean coverglasses and hydrogels seemed to have the best characteristics to host dye complexes with enhanced dye molecule emission intensity and photostability. Future research might utilize CB7-complexed dyes incorporated into neutral silicates, which would maintain separation between dye molecules, but not interfere with the intermolecular attractions between the dye and CB7.